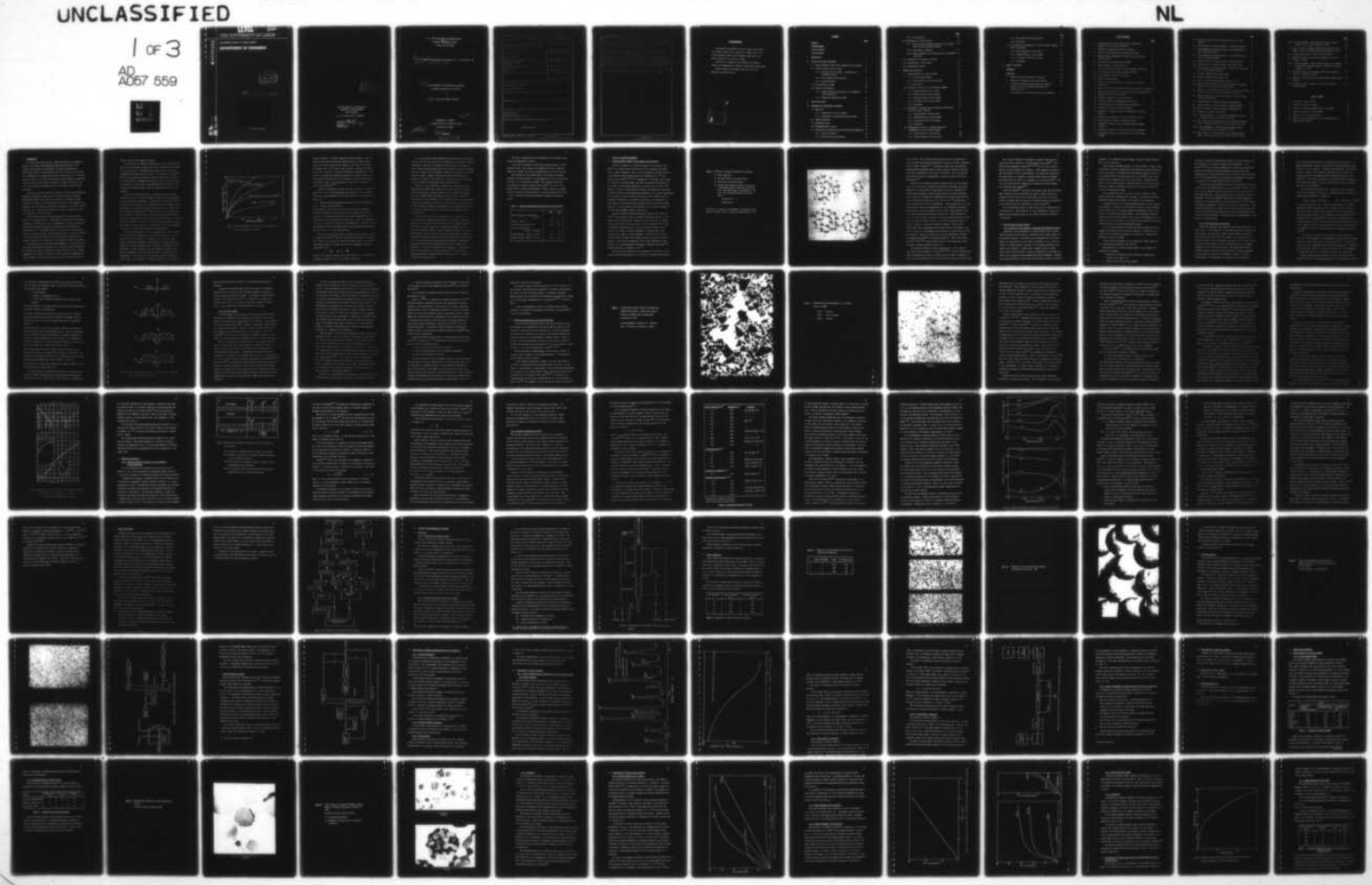
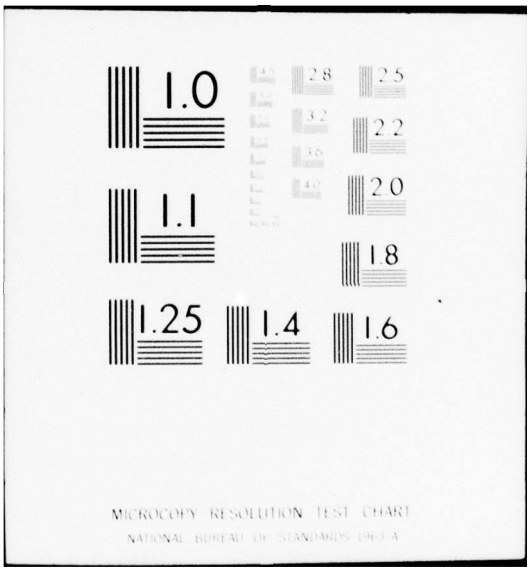
AD-A057 559 HOULDSWORTH SCHOOL OF APPLIED SCIENCE LEEDS (ENGLAND)--ETC F/G 11/2
THE DEVELOPMENT OF THE MECHANICAL STRENGTH OF REACTION-BONDED S--ETC(U)
APR 78 A J MOULSON, P LONGLAND DA-ERO-75-G-078

UNCLASSIFIED NL

1 OF 3
AD A057 559




1.0
1.1
1.25
1.4
1.6
2.8
2.5
3.2
2.2
3.6
2.0
4.0
1.8
MICROCOPY RESOLUTION TEST CHART
NATIONAL BUREAU OF STANDARDS 1963-A

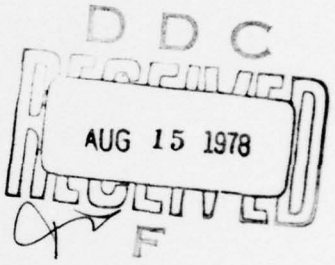
LEVEL II

THE UNIVERSITY OF LEEDS

AD A057559

HOULDSWORTH SCHOOL OF APPLIED SCIENCE

DEPARTMENT OF CERAMICS



78 08 15 041

AD No.
DDC FILE COPY

DDC
RECEIVED
AUG 15 1978
F

THE DEVELOPMENT OF THE MECHANICAL STRENGTH OF REACTION-BONDED SILICON NITRIDE

by A.J. Moulson and P. Longland

APRIL 1978

This document has been approved for public release and sale; its distribution is unlimited.

U.S. Army Research and Development Group

Agreement No. DAERO-75-G-078

Control No. 531-12943

Final Report. Covering Period 1st October 1975 - 31st December 1976

THE DEVELOPMENT OF THE MECHANICAL STRENGTH OF REACTION-BONDED SILICON NITRIDE.

by

A.J. Moulson and P. Longland

Department of Ceramics

Houldsworth School of Applied Science,

University of Leeds.

199 p.

APRIL 1978

410807

410807

UNCLASSIFIED
SECURITY CLASSIFICATION OF THIS PAGE (When Data Entered)

R&D 2235

REPORT DOCUMENTATION PAGE		READ INSTRUCTIONS BEFORE COMPLETING FORM
1. REPORT NUMBER	2. GOVT ACCESSION NO.	3. RECIPIENT'S CATALOG NUMBER
4. TITLE (and Subtitle) THE DEVELOPMENT OF THE MECHANICAL STRENGTH OF REACTION BONDED SILICON NITRIDE		5. TYPE OF REPORT & PERIOD COVERED 6. PERFORMING ORG. REPORT NUMBER
7. AUTHOR(s) DR. A. J. MOULSON		8. CONTRACT OR GRANT NUMBER(s)
9. PERFORMING ORGANIZATION NAME AND ADDRESS DEPARTMENT OF CERAMICS UNIVERSITY OF LEEDS LEEDS U.K.		10. PROGRAM ELEMENT, PROJECT, TASK AREA & WORK UNIT NUMBERS
11. CONTROLLING OFFICE NAME AND ADDRESS U.S. ARMY R&S GROUP BOX 65 FPO NY 09510		12. REPORT DATE 13. NUMBER OF PAGES
14. MONITORING AGENCY NAME & ADDRESS(If different from Controlling Office)		15. SECURITY CLASS. (of this report) 15a. DECLASSIFICATION/DOWNGRADING SCHEDULE

16. DISTRIBUTION STATEMENT (of this Report)

APPROVED FOR PUBLIC RELEASE

DISTRIBUTION UNLIMITED

17. DISTRIBUTION STATEMENT (of the abstract entered in Block 20, if different from Report)

18. SUPPLEMENTARY NOTES

19. KEY WORDS (Continue on reverse side if necessary and identify by block number)

SILICON NITRIDES
REACTION BONDING
STRENGTH OF SINTERED COMPACTS

20. ABSTRACT (Continue on reverse side if necessary and identify by block number)

PLEASE SEE OVER

DD FORM 1 JAN 73 1473 EDITION OF 1 NOV 65 IS OBSOLETE

UNCLASSIFIED
SECURITY CLASSIFICATION OF THIS PAGE (When Data Entered)

The report describes research aimed at furthering understanding of the nature and mechanism of development of the bond in RBSN. The project formed a part of an overall programme aimed at securing control of the microstructure of RBSN and, in consequence, over the mechanical properties of the ceramic.

The study embraced three grades of starting silicon powder: a specially prepared high purity powder (99.99% Si), a similar powder contaminated with Fe ($\sim$ 10 ppm Fe), and a commercial powder ($\sim$98% Si; 0.5% Fe; 1.5% AL).

Sonic Young's modulus was determined at stages throughout the nitriding reaction for all three powders and the data correlated with microstructural observations. In the case of the high-purity silicon powder it was concluded that the bond forms as a result of the deposition of massive, vapour-formed, Si_3N_4, and that Si_3N_4 "whisker" formation played no part in the bonding process. It was also observed that RBSN made from the two higher purity powders had Young's modulus values significantly higher than commonly encountered.

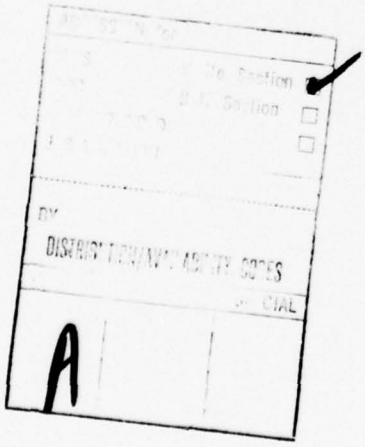
A 3-phase composite model developed by Cohen and Ishai satisfactorily described the rate of development of Young's modulus with extent of reaction.

ACKNOWLEDGMENTS

The authors are grateful to the U.S. Army R and D Group for financial support for a period of 15 months, and to the Science Research Council for a research studentship (P.L.) which extended over a period of 2 years.

The help of colleagues of the academic and technical staffs of the Department of Ceramics is gratefully acknowledged.

Special thanks are extended to Miss S.H. Toon for typing and secretarial help.



78 08 15 041

CONTENTS

		Page
	ABSTRACT	
	ACKNOWLEDGMENTS	
	LIST OF FIGURES	
	LIST OF TABLES	
1.	INTRODUCTION	1
2.	REVIEW OF RELEVANT LITERATURE	7
	2.1 Crystallographic forms of the compound silicon nitride	7
	2.2 Reaction-bonded silicon nitride	10
	2.2.1 Formation of the ceramic; technology and background science	10
	2.2.2 The nitrogen/silicon reaction	12
	2.2.3 Impurity effects	16
	2.3 Microstructure of RBSN	19
	2.4 Mechanical properties	27
	2.4.1 General principles relating to the strength of brittle materials	27
	2.4.2 Mechanical properties of RBSN	31
3.	AIMS OF THE STUDY	41
4.	APPARATUS AND EXPERIMENTAL PROCEDURE	44
	4.1 Materials	44
	4.1.1 Preparation of silicon powders	44
	4.1.2 Production of spheroidized silicon powder	44
	4.2 Powder compaction	47
	4.3 Nitriding furnace	50
	4.4 Thermogravimetric balance	53
	4.5 Techniques for studying phase morphology and composition	55
	4.5.1 Optical microscopy	55
	4.5.2 Scanning electron microscopy	55

		Page
4.5.3	X-ray analysis	55
4.6	Measurement of Young's Modulus	56
4.6.1	Dynamic Young's Modulus determined by an electrostatic drive and detection method	56
4.6.2	Electrostatic apparatus	59
4.6.3	Sample preparation and identification of resonance conditions	61
4.7	Determination of modulus of rupture	62
4.8	Determination of bulk density	62
4.9	Microhardness testing	62
5.	RESULTS AND DISCUSSION	63
5.1	Characterization of silicon powders	63
5.1.1	Silicon powder purity	63
5.1.2	Powder particle size and structure	64
5.1.3	Discussion	67
5.2	Nitridation kinetics of silicon powder compacts	68
5.2.1	Washed Monsanto silicon powder	68
5.2.2	Washed Monsanto silicon spheres	70
5.2.3	Unwashed Monsanto silicon powder	70
5.2.4	Koch-Light 99.9% silicon powder	73
5.2.5	Discussion	73
5.3	Development of Young's Modulus during the nitridation of silicon powder compacts	73
5.3.1	Washed Monsanto silicon powder	75
5.3.2	Unwashed Monsanto silicon powder	77
5.3.3	Koch-Light 99.9% silicon powder	77
5.3.4	Discussion	77
5.4	Development of modulus of rupture during the nitridation of silicon powder compacts	99
5.4.1	Washed Monsanto silicon powder	99
5.4.2	Unwashed Monsanto silicon powder	99

Page

5.4.3 Koch-Light 99.9% silicon powder 99

5.4.4 Discussion 104

5.5 Development of microstructure in silicon powder compacts during nitridation 105

5.5.1 Washed Monsanto silicon powder 105

5.5.2 Unwashed Monsanto silicon powder 112

5.5.3 Koch-Light 99.9% silicon powder 116

5.5.4 Discussion 122

6. GENERAL DISCUSSION 131

REFERENCES 143

APPENDICES 149

1. Dynamic mechanical behaviour of materials 149

2. Theory of electrostatic drive and detection 153

3. Relationship between volume fractions of silicon nitride, silicon and porosity with green and nitrided density 155

4 Microstructure of nitrided Monsanto silicon spheres. 158

LIST OF FIGURES

		Page
1.	Creep properties of two advanced nickel superalloys compared with two ceramic materials.	3
2.	Structure of alpha and beta-silicon nitride.	8
3.	Model for the nitridation of high purity silicon.	15
4.	Microstructural inhomogeneity caused by local melting of impurity phases.	20
5.	Representative photomicrograph of RBSN.	21
6.	Phase diagrams of Fe-Si and Al-Si.	26
7.	Solid-state diffusion model for the nitridation of silicon.	28
8.	High-temperature mechanical properties of RBSN.	36
9.	Flow diagram of aspects of the study.	43
10.	Spheroidizing apparatus.	46
11.	Spherical silicon produced under different experimental conditions.	48
12.	Spherical silicon produced under optimum experimental conditions.	49
13.	Green compact structures of isostatically pressed Monsanto and Koch-Light 99.9% silicon powders.	51
14.	Schematic diagram of nitriding apparatus.	52
15.	Schematic diagram of thermogravimetric balance.	54
16.	Diffractometer trace of RBSN using CuKα radiation.	57
17.	Calibration chart for alpha/beta content.	58
18.	Electrostatic apparatus for the determination of Young's Modulus.	60
19.	Aluminium-rich impurity in spherical Monsanto silicon.	65
20.	Grain structure of spherical Monsanto silicon.	66
21.	Nitridation kinetics of washed Monsanto silicon powder compacts.	69
22.	Nitridation kinetics of washed Monsanto silicon spheres.	71
23.	Nitridation kinetics of unwashed Monsanto silicon powder compacts.	72

Page

24. Nitridation kinetics of Koch-Light 99.9% silicon powder compacts. 74

25. Young's Modulus vs nitrided density, acid-washed Monsanto. 76

26. Young's Modulus vs nitrided density, acid-washed Monsanto with vacuum pretreatment. 78

27. Young's Modulus vs nitrided density, acid-washed Monsanto; effect of nitrogen pressure. 79

28. Young's Modulus vs nitrided density, unwashed Monsanto. 80

29. Young's Modulus vs nitrided density, Koch-Light 99.9%. 81

30. Young's Modulus vs nitrided density, comparison of Koch-Light 99.9% and acid-washed Monsanto. 83

31. Two-phase composite model after Ishai. 86

32. Two-phase composite model after Paul. 89

33. Silicon nitride-silicon-porosity, composite model. 92

34. Computed relationships between Young's Modulus and nitrided density, for a green density of 1900 kg m^{-3}. 95

35. Theoretical and experimental data (Young's modulus vs nitrided density), for Monsanto and Koch-Light powder compacts. 96

36. Dynamic Young's Modulus data for commercial RBSN's compared to the Koch-Light data. 98

37. Rupture modulus vs nitrided density, washed Monsanto. 100

38. Rupture modulus vs nitrided density, unwashed Monsanto. 101

39. Rupture modulus vs nitrided density, Koch-Light 99.9%. 102

40. Comparison of rupture modulus data. 103

41-48. Photomicrographs: acid-washed Monsanto powder compacts nitrided in 50 torr of nitrogen at 1370°C. 106-109

49. Phase composition of RBSN produced from acid-washed Monsanto powder; alpha and beta-silicon nitride content vs. time. 111

50-52. Photomicrographs: unwashed Monsanto powder compacts, nitrided in 50 torr of nitrogen at 1370°C. 113-114

53. Phase composition of RBSN produced from unwashed Monsanto powder; alpha and beta-silicon nitride content vs. time. 115

Page

54-60. Photomicrographs: Koch-Light 99.9% powder compacts, nitrided in 760 torr of nitrogen at 1370°C. 117-120

61. Phase composition of RBSN produced from Koch-Light 99.9% powder; alpha and beta-silicon nitride content vs. time. 121

62. Microhardness data for various silicon nitrides. 123

63. Nitridation model for pure silicon powder in 50 torr of nitrogen at 1370°C. 126

64,65. Photomicrographs: etched polished sections of unwashed Monsanto silicon powder compacts, nitrided in 50 torr of nitrogen at 1370°C. 128

66. Nitridation model for Koch-Light 99.9% silicon powder in 760 torr of nitrogen at 1370°C. 130

67. Scanning electron micrograph, washed Monsanto RBSN fracture surface. 135

68. Scanning electron micrograph, Koch-Light 99.9% RBSN fracture surface. 135

LIST OF TABLES

1. Properties of RBSN and HPSN. 6

2. Mechanical properties of RBSN. 33

3. Dependence of silicon compact density on pressure. 47

4. Chemical analysis of silicon powders. 63

5. Particle size of silicon powders. 64

6. Effect of vacuum pretreatment on the Young's Modulus of green silicon compacts. 75

1. INTRODUCTION

In recent years there has been a significant renewal of interest in ceramics as potential high-temperature engineering materials. This interest has developed in part because of economic considerations, particularly because of the increase in the cost of fuel oil, and in part as a consequence of a strong anti-pollution lobby in the U.S.A. For these reasons a number of automobile and gas-turbine manufacturers are examining the possibility of using ceramic components in engine construction, and also in the design and construction of an "all ceramic" vehicular type gas turbine.

The reason behind the interest in certain ceramics as high temperature engineering materials is their ability to retain a useful strength at temperatures higher than is the case for metals. The French military engineer, N.S. Carnot, first showed the efficiency of a heat engine to be dependent upon the difference between the temperatures of the heat 'source' and heat 'sink'. Expressed more simply, the hotter an engine runs, the more efficient is its use of fuel.

The gas-turbine engine has many advantages over the reciprocating engine for land-based vehicles. NASA studies indicate that a gas-turbine operating at 1650°C would be equal in performance to that of a present-day eight cylinder engine and obtain around fifty miles to the gallon of petroleum fuel[1]. In addition, turbines do not need to burn petroleum; they can be adapted to work on much lower grade fuels. A further advantage is that the better combustion obtained under the higher operating temperatures should lead to a reduction in the emission of exhaust pollutants.

The attainment of a 1650°C operating temperature is not possible with the metal alloys presently available, even the most resistant being prone to oxidation and creep at temperatures between 900°C and 1100°C. Ceramic components are, therefore, essential if higher operating temperatures are to be achieved. The creep properties of two nickel superalloys and two

ceramic materials are compared in Figure 1.

In addition to the technical advantages the use of ceramics offers, there are also important strategic and economic considerations relating to the raw materials. The superalloys currently used in gas-turbine construction are mainly alloys of Ni, Cr, Co, W and Mo and, except for the last, these metals come chiefly from the Soviet Union and nations of the Third World. Furthermore, the specific cost of unshaped superalloy ingots is of the order of ten times that of the elements of the candidate engineering ceramics, which are abundantly available to all countries.

For various reasons which will be enlarged upon later, silicon nitride and silicon carbide have emerged as the most promising ceramics for high temperature engineering. An indication of the current level of interest in these materials, particularly the nitrogen ceramics, may be gauged from the proceedings of the Hyannis Conference on "Ceramics for High Performance Applications".[1] This conference was reporting on the U.S. Government's "Advanced Research Projects Agency's (ARPA) Brittle Materials Design/High Temperature Gas Turbine Program", which is concerned with the building of a small 300 hp vehicular type gas turbine, entirely from ceramic materials, and also to demonstrate ceramic vanes operating at 1350°C in a 30 MW, 40,000 hp power generating turbine.

The direct replacement of a metal component with a ceramic copy is not in general successful because the mechanical properties of the two materials differ too widely. If ceramics are to be used as highly stressed engineering components, then principles of design specifically applicable to brittle materials must be adopted. The inherent lack of ductility of a ceramic material is a major factor to consider in the design of components; whilst brittleness implies resistance to creep deformation, it also means that local stresses cannot be relieved by plastic flow. The elimination of stress concentrations is therefore of

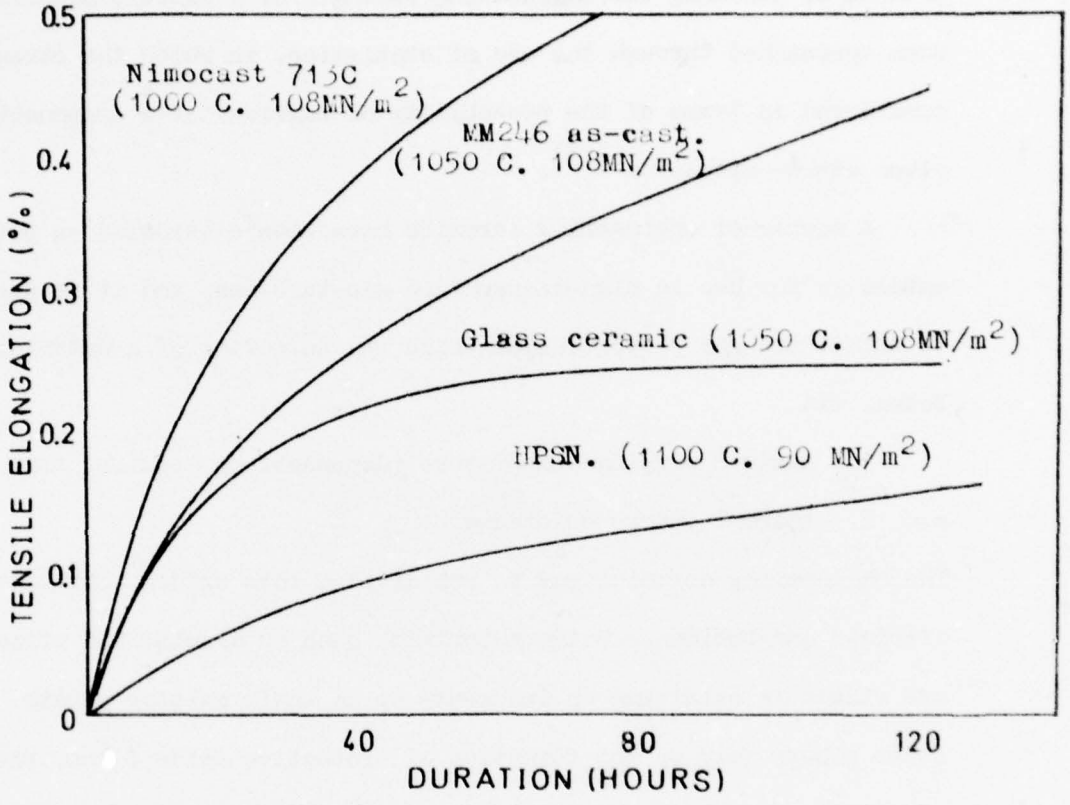


Fig.1. Creep properties of two nickel superalloys and two ceramic materials.

primary importance in ceramic component design philosophy. As well as stress concentrations arising from design features, inherent stress raisers are always present in the ceramic, in the form of cracks and inclusions, and it is the task of the materials' scientist to minimize the size and occurrence of these microstructural inhomogeneities. The problem of defining the engineering strength of a brittle material has been approached through the use of statistics, in which the strength is considered in terms of the probability of survival of a component in a given stress situation[2,3].

A number of engineering ceramics have been considered as potential materials for use in high-temperature gas-turbines, and it is possible to select two key properties on which the selection of a material can be based, viz.

1. maximum working temperature (dependent on required strength), and 2. thermal shock resistance.

The engineering ceramics may be sub-divided into oxides, carbides, nitrides and borides. Oxide materials, such as alumina and zirconia, are stable in oxidizing environments up to their melting points. The other groups rely on the formation of protective oxide films, principally of silica, for chemical stability at high temperatures. For this reason, the carbides, nitrides and borides which can be considered are limited to those of silicon, i.e. SiC, Si_3N_4 and SiB_6.

The first detailed investigation of thermal shock resistance was due to Glenny and Taylor[4,5] who used a fluidized bed technique to simulate the conditions in aircraft gas turbine nozzle guide vanes. Two indices measuring resistance to thermal shock have been suggested for brittle materials[6], viz:

$$R_1 = \frac{\sigma}{E\alpha} \quad \text{and} \quad R_2 = \frac{k\sigma}{E\alpha}$$

where σ is the tensile strength, E is Young's Modulus, α the coefficient of thermal expansion, and k is the thermal conductivity.

R_1 is applicable to rapid temperature cycling and R_2 to slow thermal cycling, and both indices indicate the importance of the thermal expansion coefficient. When used in conjunction with the results of Glenny and Taylor, these indices indicate that for gas turbine applications one must look for a ceramic with an expansion coefficient of less than $5 \times 10^{-6}/°C$. The data on oxide, carbide, nitride and boride ceramics have been examined by Godfrey[7], from which it is clear that silicon carbide and silicon nitride have outstanding thermal shock resistance.

While it is clear, both from an examination of property data and from published thermal shock results, that silicon carbide and silicon nitride are the only candidate materials for gas turbine applications, the choice between these two materials is not so clear. Godfrey[7] concludes that silicon nitride is to be preferred because of its superior thermal shock resistance. Testing of ceramic turbine components during the ARPA programme referred to previously has also suggested that silicon nitride has a greater resistance to severe impact and thermal shock conditions[8,9].

Both silicon nitride and silicon carbide can be fabricated by reaction-bonding, conventional sintering or hot-pressing. Hot-pressed materials are, in general, fully dense and have very high strength, but only relatively simple shapes can be fabricated by this route and finishing invariably involves expensive diamond machining. The reaction bonding route, while it leads to a material considerably less dense and mechanically weaker than that achieved by hot-pressing, is very flexible as far as component shape and dimensions are concerned. Components of very complex shape can be readily fabricated to close dimensional tolerances. Conventional, pressureless sintering, is a relatively new route for the fabrication of these materials[10,11], and only the reaction-bonded and hot-pressed forms of Si_3N_4 and SiC are commercially available at the present time.

The typical properties of reaction-bonded and hot-pressed silicon nitride are summarised in Table 1.

A new class of materials, known by the acronym "sialon", is also being developed. The "sialons" are composed of silicon, aluminium, oxygen and nitrogen, but reliable property data are not yet available.

The background to the present study is the extensive research programme currently pursued in the Department which has as its main aim the control of microstructure in RBSN. The knowledge accumulated concerning the nitriding of high purity silicon[12] is used in the present study to improve understanding of how the mechanical strength develops during the reaction-bonding of a silicon powder compact, with a view to optimising engineering properties through microstructure control.

Table 1: Physical and Mechanical Properties of RBSN and HPSN

	RBSN	HPSN
Thermal expansion coefficient. $10^{-6}K^{-1}$.	2.8	3.1
Density. $Mg.m^{-3}$.	2.5	3.2
Sublimation temperature. K.	2170	2170
Thermal conductivity. $W.m^{-1}K^{-1}$ at 1000 K.	4	16
Young's Modulus. $GN.m^{-2}$ at 300 K.	150	320
Rupture Modulus. $MN.m^{-2}$ at 300 K.	200	700

2. REVIEW OF RELEVANT LITERATURE

2.1 Crystallographic forms of the compound silicon nitride

During the formation of a reaction-bonded silicon nitride ceramic (RBSN), two crystal forms of silicon nitride are commonly encountered. The two forms, designated α and β, are both hexagonal and their existence was established nearly twenty years ago by Turkdogan et al.[13] and several other workers[14,15,16]. Subsequently, in the many studies aimed at improving the microstructure, and hence the engineering properties of the ceramic, it has become commonplace to refer to the α/β ratio of the material. There is little definite knowledge concerning the relationship between this ratio, microstructure and properties, but a general appreciation of the nature of the two crystal modifications, their stability and the conditions favourable to the growth of each form, is a prerequisite to a basic study of the microstructure and properties of the reaction-bonded material. For this reason a brief summary of the literature relating to the two crystallographic forms is given below.

The first structure determinations were carried out by Hardie and Jack[14] who established that the essential difference between α- and β-silicon nitride was that the c-dimension of the α-unit cell was approximately twice that of the β-unit cell. In the structure of the β-form, as proposed by Hardie and Jack, each silicon atom is situated at the centre of a slightly irregular tetrahedron of nitrogen atoms, each nitrogen being common to three tetrahedra. The structure can also be considered as being made up of puckered rings of Si_3N_4 units as shown in Figure 2. The structure parameters of the β-form, determined in this initial work, were subsequently confirmed by Ruddlesden and Popper[16] and more recently by Grieveson et al.[17].

During this early period it was a commonly-held view that α- and β-silicon nitride were respectively low and high temperature modifications

Fig. 2: Structure of alpha- and beta-silicon nitride.

a) Basic Si_4N_4 unit.

b) Beta-type layer of six basic units.

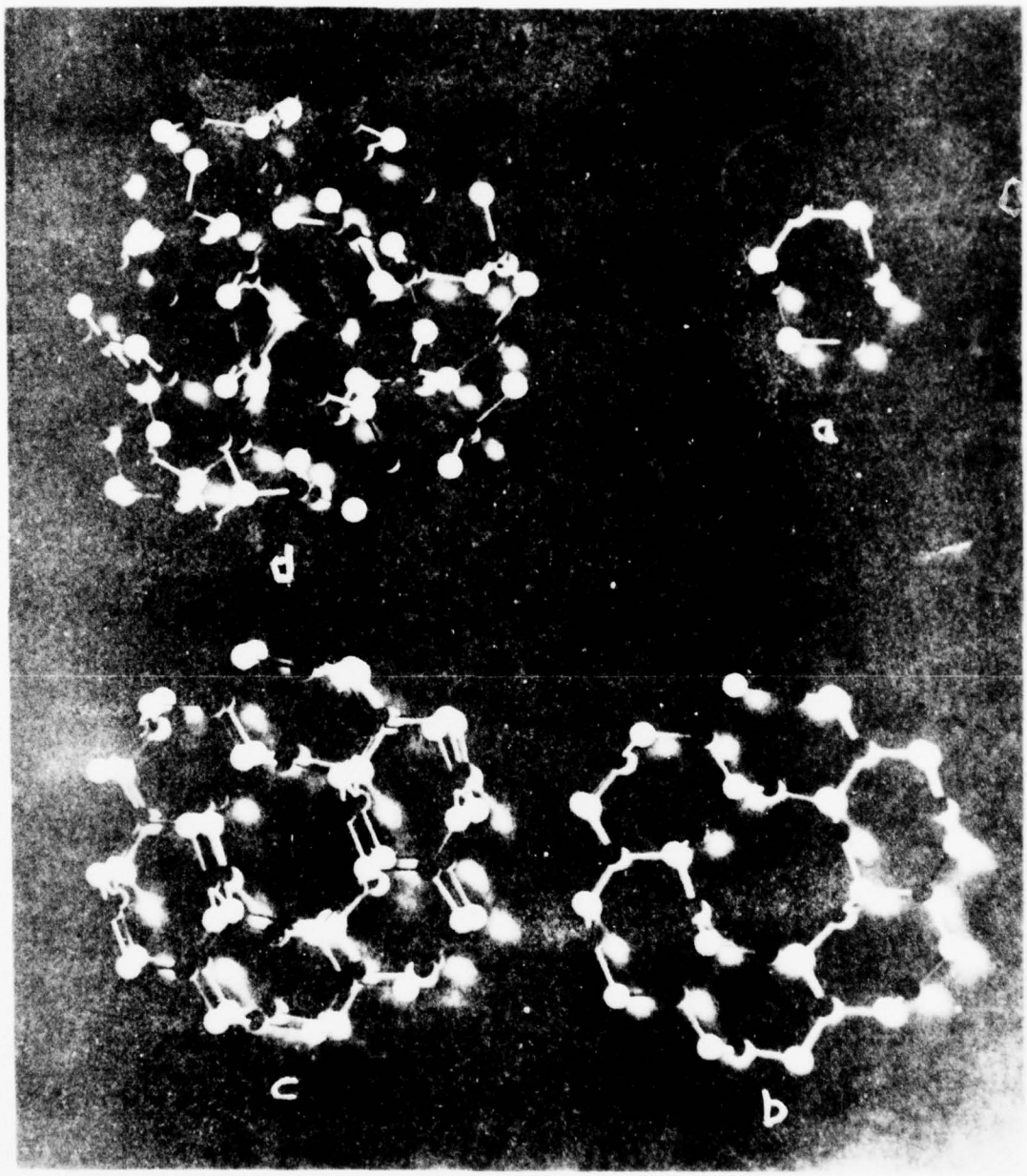
c) Beta-silicon nitride structure.

d) Alpha-silicon nitride structure, consisting of alternate layers of beta and a mirror of beta. The mirror layer is displaced by $\sim 4\text{Å}$ in a (110) direction relative to the beta layer.

Silicon atom - O

Nitrogen atom - O

Reproduced by courtesy of D.R. Messier, Army Materials and Mechanics Research Center, Watertown, Massachusetts, U.S.A.


a
d
c
b

of the nitride. This viewpoint arose from the observation that when α-silicon nitride was heated at temperatures in excess of 1500°C a conversion to the β-crystal occurred[13]. Supporting evidence came from reaction-bonded material development work in which a general observation was that at reaction temperatures in the range of 1250-1300°C, the α-form was the major product, whereas at temperatures in excess of 1400°C, the β-form predominated[18].

During the last decade an extensive research effort has been undertaken at the University of Newcastle-upon-Tyne to re-examine the crystal chemistry of silicon nitride. These studies involved a combination of refined X-ray diffraction, direct oxygen analysis by neutron activation, and an attempt to establish the thermochemical conditions under which the α- or β-phases were formed, and in 1972 Wild et al.[19] reported that α-silicon nitride was in fact an "oxynitride". They proposed that the α- and β-forms were not merely low temperature and high temperature structural modifications of the same compound, but were "high oxygen potential" and "low oxygen potential" modifications respectively. They described the α-form as having a defect structure with oxygen replacing nitrogen on some sites, nitrogen vacancies in others, and with the appropriate number of silicon vacancies to maintain electrical neutrality. The α-silicon nitride used was in whisker form and the study might be criticised in that it did not take into consideration the presence of an oxide layer covering the whiskers. That such a layer exists has been subsequently confirmed by Maruyama and Suzuki[20] and Evans and Sharp[21]. More recent observations[22,23,24,25,26] leave no doubt that the α-form can exist without the level of oxygen proposed by Wild et al.

The present concensus of opinion concerning the α- and β-forms is that they are true polymorphs of Si_3N_4[23,26,27,28], with the α-modification being a metastable form, and that either kinetic factors of impurities, or both, very significantly influence the nucleation and growth of either phase.

The α-crystal structure is strained to a greater extent than the β-form and would be expected to have the higher free energy[28]. The observed high temperature conversion[13,29,30] of the α-form to the β-crystal structure supports this viewpoint. Other supporting evidence is that the formation of the α-phase appears to be favoured by reactions in the vapour state; all deposits of silicon nitride formed by chemical-vapour-deposition are found to be amorphous or α-silicon nitride[31], and it is well known that the α-phase can be prepared by reaction between silicon monoxide and nitrogen[32].

Evans and Davidge[33], and many other workers, have shown the preferential formation of the β-form when the reaction between silicon and nitrogen involves silicon in the liquid state, and there is also some evidence to suggest that the presence of aluminium favours the production of the β-phase during the nitridation of silicon powder[34].

With the available evidence to date, there seems no justification to suppose that the α- and β-forms are not true polymorphs of Si_3N_4, and it remains an open question whether or not either structure is stabilised by impurities.

2.2 Reaction-bonded silicon nitride

2.2.1 Formation of the ceramic: technology and background science

Essentially, the manufacture of a reaction-bonded silicon nitride (RBSN) component involves heating a preformed silicon powder compact in a nitrogenous atmosphere. The preform can be fabricated from the silicon powder, the mean particle size of which is typically 10 μm, by any of a variety of standard methods, including die or isostatic pressing, slip-casting, and extrusion. In many cases a compacted blank is formed which, after a short sintering in argon at temperatures in the region of 1200°C, can be machined using standard metal-working equipment. Recently the injection moulding of plasticised silicon powder has been successfully

developed. This fabrication route, however, involves a special firing to burn out the plasticiser.

Having formed the powder compact, it is then nitrided. Special temperature/time, nitriding schedules have been developed and these frequently involve two stages; one during which the nitriding component is held at a temperature below the melting point of silicon (1420°C), and a second during which the temperature is raised above 1420°C. During the first stage of the nitriding process a skeletal structure of silicon nitride is developed, capable of preventing coalescence of the silicon during the second, high temperature, stage.

The nitriding reaction is a slow process with commercial firing schedules typically extending over a few days; the purpose of the high temperature stage of the schedule is to minimise this firing time.

An unusual feature of the reaction-bonding process is that, although the conversion of silicon to silicon nitride involves a volume expansion of approximately 22%, the compact changes its dimensions by only of the order of 0.1% during the reaction bonding. This dimensional stability occurs because the nitride formed by the reaction is accommodated in the voidage of the silicon compact, and it removes the necessity for expensive diamond machining to achieve engineering tolerances.

It is clear from what has been said that the microstructure will be changing considerably as the reaction proceeds and, in particular, the voidage will be continuously reduced to a final level of approximately 20%, which is typical for RBSN.

A more detailed description of the manufacture of RBSN components can be obtained from references (35) and (36).

The nitridation of a silicon powder compact can be thought of as occurring in two stages:

1. transport of nitrogen into the continuously changing pore system of the compact, and
2. reaction between silicon and nitrogen.

The slower of these two processes will control the overall reaction and the possibility of gas access control must be considered. It is evident[37,38] that a critical combination of compact size and "green" density exists beyond which gas permeation becomes reaction rate-restrictive and the only quantitative data available is that by Atkinson et al.[39] who found that gas flow control was unimportant for compacts of less than 5.0 cm diameter (green density 1500 kg m^{-3}).

Published data would support the view that the gas-particle reaction is the overall rate-determining step in the nitridation of small (~ 1 cm dia.) silicon compacts, the rate of gas flow into the compact being of minor importance until critical 'green' densities and compact sizes are approached. Messier and Wong[40] demonstrated a strong dependence of reaction rate on silicon particle size, and Atkinson et al.[39] observed an exponential dependence of compact reaction rate on temperature. Both of these observations are evidence that, in small compacts at least, the overall reaction rate-determining step is the silicon-nitrogen reaction at the particle/gas boundary. The present state of understanding of this reaction is outlined below.

2.2.2 The nitrogen/silicon reaction

Under most conditions, high temperature reactions between gases and metals result in the formation of a uniformly thick film or scale on the metal surface, the most widely studied systems being those associated with the reaction between metals and oxygen. The initial step in the oxidation process is the chemisorption of oxygen on to the metal surface, followed by the nucleation of oxide at favourable sites, for example, impurities and the ends of dislocations. The subsequent kinetics of oxidation depend on the type of film formed and its growth mechanism, and can usually be described by logarithmic, parabolic or linear relationships. The logarithmic law describes the low temperature

(Fe < 200°C) growth of very thin (100 Å) highly protective films; at higher temperatures, thermal energy may cause continued growth by ionic diffusion, usually leading to a parabolic time dependence. It should be stressed, however, that a parabolic dependence may also result when growth is controlled by gaseous diffusion through fine pores in the film[41,42]. The linear law applies to the initial stages of oxidation, before diffusion becomes the rate-controlling process and also whenever the scale is non-protective.

The principles pertaining to metal oxidation are also expected to apply to the nitridation of metals and, although the basic equation for silicon nitride formation is simple, viz:

$$3Si_{(s)} + 2N_{2(g)} \rightleftharpoons Si_3N_{4(s)} \qquad \Delta G^\circ = -206 \text{ kJ/mol. at } 1650^\circ K,$$

the reaction mechanism is not. The free energy change is the overall driving force for the reaction but it, of course, bears no relation to the reaction rate. Various types of kinetics for the nitridation of silicon have been reported in the literature, including parabolic[43,37], logarithmic[44], and sigmoidal[45]. Much of the literature, however, describes studies carried out under unsatisfactory experimental conditions; silicon purity was usually not greater than 99% and the silicon particles were normally covered by a "native" oxide film of approximate thickness 3 nm[46].

In an attempt to rationalise the situation, the mechanism and kinetics of the nitridation of spectrographically pure silicon have been studied at Leeds and the results recently reported[12]. The study was part of an overall programme aimed at improving the mechanical properties and reliability of RBSN and, because it provides much of the background to the present study, it is necessary to describe it in some depth.

Using a thermogravimetric method the nitridation kinetics of de-oxidised compacts of spectrographically pure silicon powder were studied

as a function of temperature (1250-1370°C) and pressure (20-760 torr) and the results are summarized below. The kinetics could be described in the following three stages:

1. a linear region,
2. a region of decreasing rate, and
3. a "zero" rate, although unnitrided silicon remained in the compact.

The microstructure of the growing nitride and the reaction kinetics were correlated using the following model.

(a) First, nitride nuclei form on the silicon surface by a process involving chemisorption and surface diffusion of nitrogen. The areal density of nuclei is increased at high pressure and low temperature. (Fig. 3a.)

(b) During stage (a), the nuclei grow both laterally and vertically and pores develop within the underlying silicon. The rate determining step is probably the combined chemisorption and surface diffusion of nitrogen on both the nitride and silicon surfaces. The migration of silicon to growth sites is either by surface diffusion or via the vapour phase or, probably, by a combination of both. (Fig. 3b.)

(c) During stage (b) the rate at which silicon is supplied to the growth sites decreases as exposed silicon surface also decreases. The nitridation rate therefore decreases and is controlled by the transport of silicon from remaining free silicon surfaces. (Fig. 3c.)

(d) Eventually all the silicon surfaces are covered by nitride and the reaction effectively stops. (Fig. 3d.)

The onset of stage c depends on the texture of the nitride layer; large gaps between developing nitride growths being more difficult to block than small ones. Hence thicker nitride layers are produced when

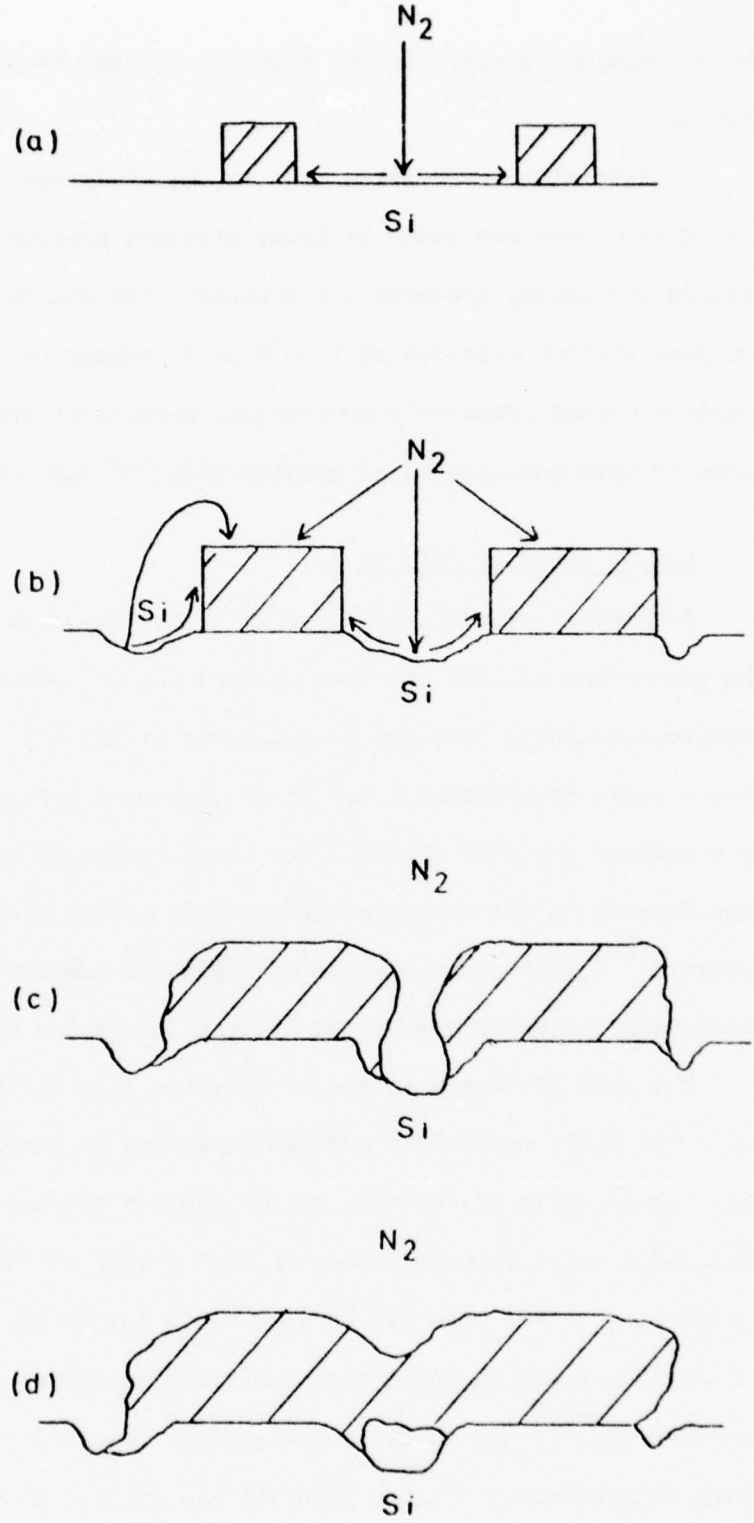


Fig.3. Model for the nitridation of high purity silicon, after Atkinson et al (12).

the nucleation density is low, that is, at high temperatures and low pressures.

A surprising observation made in the study was that, although the nitridation rate was lower at lower nitrogen pressures, the amount of nitride eventually produced was greater. For example, it was found that for pure silicon nitrided at 1370°C in 1 atmosphere of nitrogen, the reaction ceased after ~7% conversion, whereas at pressures of nitrogen below 50 torr conversions of greater than 90% were obtained.

2.2.3 Impurity effects

As already stated, the majority of the research work concerned with the production of RBSN has been carried out on commercial grade silicon powders containing metallic contaminants at the 1 w/o level. These powders also contain approximately 0.3 w/o of oxygen, a proportion of which exists as a surface layer of silica. The exact amount of oxygen present therefore depends on the specific surface area of the powder. It has been reported[47] that other sources of oxygen in commercial powders are iron oxides and silicates present as discrete particles in the silicon powder.

The role of oxygen in the nitridation of a silicon powder compact is still not fully understood and the situation is complicated by the fact that the majority of research on the subject has been carried out in sintered alumina furnace tubes. A high purity and controlled reaction environment is not possible in such tubes due to the loss of oxides of Si, Ca, Mg, Na, K and Al under the conditions necessary for nitridation.[48,49,50] Sin Shon Lin[51] has analysed the gaseous reaction products during nitridation in a sintered alumina tube and his studies showed that the oxygen content, as monitored on a mass spectrometer, of the outgoing gas did not decrease even after long reaction times (24 hours). Therefore the silicon powder compact cannot be the major source of oxygen under such reaction conditions.

The role of oxygen and moisture in the nitriding atmosphere in producing silicon monoxide gas was first suggested by Parr and May[18] in 1967. They proposed that silicon monoxide was 'continuously decomposed and reproduced' but gave no details of the reaction mechanism in which it was involved. More recently, Elias and Lindley[52] found that the amount of α-silicon nitride produced in the reaction between silicon powder and nitrogen was proportional to the oxygen and water vapour content of the nitriding gas and proposed that the α-phase was formed by a reaction involving silicon monoxide and nitrogen. They also proposed that the β-form was the result of a direct silicon-nitrogen reaction, probably involving silicon in the vapour phase. Campos-Loriz and Riley[53] have also suggested that the form in which silicon arrives at the nitride growth site determines the crystal structure of the silicon nitride product, and that the nitridation process consists of two independent reactions, an α-forming and a β-forming one.

Although oxygen in the nitriding atmosphere can affect the silicon-nitrogen reaction, it is also necessary to consider the oxygen present as a layer of SiO_2 on the silicon particles, as it is known that this native oxide film retards, and that a thick oxide film (1 μm) can effectively completely stop, the nitridation reaction[54]. It has long been thought that the presence of certain metallic impurities, particularly iron, in the silicon powder assists in the removal of the oxide film from the silicon surface[37,55]. The results of a recent study by Boyer et al.[56] suggest that during the nitridation of iron-contaminated silicon, disruption of the surface silica occurs, exposing free silicon and allowing the silica layer to be removed as silicon monoxide by active oxidation, as proposed by Wagner[57].

Boyer et al. proposed that the nitridation of oxide-covered silicon in the presence of iron involves two parallel, independent reactions:

1) Surface nucleation and growth of nitride through the oxide layer, a process which has also been suggested by Huttinger[58] and by Messier and Wong[43].

2) Oxide removal followed by further nitride nucleation induced by the presence of iron.

Boyer et al.[56], in a reanalysis of Atkinson and Moulson's data[59], found that maximum nitridation rates and final weight gains were proportional to the concentration of iron in the silicon powder, suggesting therefore that, as well as promoting the removal of silicon, iron plays a major role in the later nitride nucleation and growth processes. Liquid phases are a major factor to be considered in this context as iron forms a low melting point eutectic with silicon, and it has been shown that iron-induced enhanced nitridation ceases below 1200°C[59], the Fe-Si solidus temperature. The presence of $FeSi_2$ during the nitridation of commercial grade silicon has been confirmed by Messior and Wong[43] using electron-probe microanalysis.

Other metals which have been shown to increase reactivity are Cr, Mn and Ni[54], and Boyer et al.[56] suggest that in order to enhance nitridation a metallic contaminant should:

a) devitrify silica under nitriding conditions;

b) form a liquid with silicon at the nitriding temperature;

c) nitride less readily than silicon.

It must be pointed out that the results of Boyer et al. only apply to the nitridation of silicon containing iron up to the 250 ppm level, with no other metallic impurities present. It is, therefore, difficult to relate their results to the commercial situation, where impurity levels are much higher and the variety of impurity much greater. Indeed a general problem in understanding the nitridation of silicon powder compacts is the difficulty associated with investigating the interdependence of all the

significant variables in the system.

The different types of reaction kinetics described in Section 2.2.2 have probably been affected by the presence of different impurity types and levels in either the silicon powder or nitrogenous atmosphere. Impurity phases may also affect the microstructure and properties of RBSN and can cause gross inhomogeneities in the material[47,60], as shown in Fig. 4.

A clearer understanding of the role of impurity phases during nitridation is required if development work towards an improved RBSN is to proceed intelligently.

2.3 RBSN Microstructure and its Growth Mechanisms

As stressed in the previous section, the reaction between silicon and nitrogen can be influenced by very small amounts of impurity associated with either the silicon or nitriding gas. It would be expected therefore that if kinetics are so affected, then growth morphology and microstructure will also be dependent on impurity content. There is, however, very little information available on the effect of impurities on RBSN microstructures and the published work to date has shown a general agreement on the major microstructural features[61,62,33].

The microstructure of RBSN commonly reveals silicon nitride, unreacted silicon, porosity, and some impurity phases; a representative photomicrograph is shown in Fig. 5.

In the commercial production of RBSN, and in the early stages of nitriding at temperatures below the melting point of silicon, the formation of a fibrous mat is a common feature of the developing microstructure. X-ray analysis of the silicon nitride formed during this initial period has shown that it is mostly of the α-form[61,53]. The growth of an interpenetrating mat of silicon nitride whiskers was first described by Parr et al.[63], who suggested that the mat was microporous and permitted

Fig. 4: Isostatically pressed compact of Dunstan and Wragg silicon powder. Large void caused by melting of impurity phase during argon-sintering at 1190°C.

Photomicrograph by courtesy of P. Arundale, Dept. of Ceramics, University of Leeds.

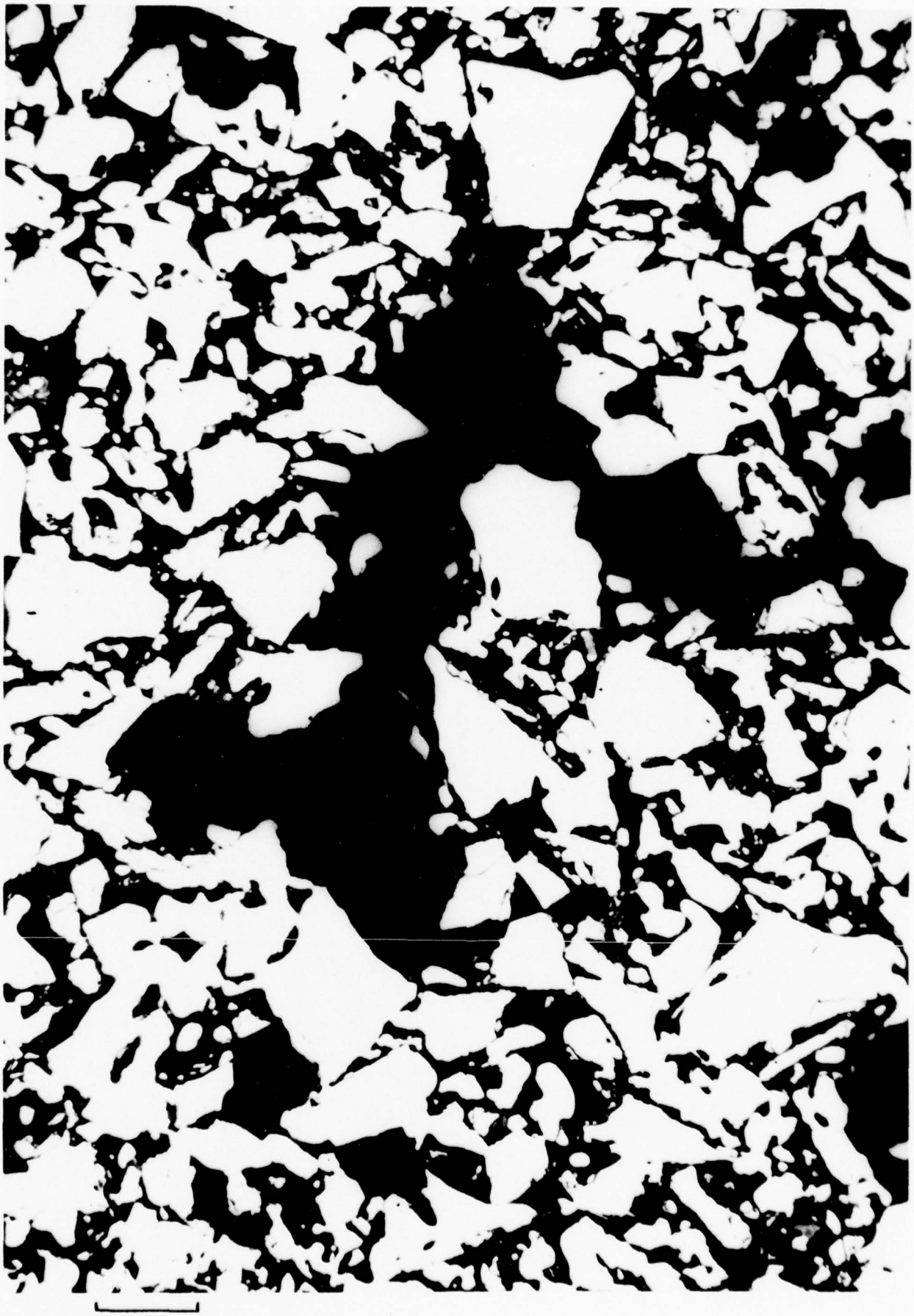
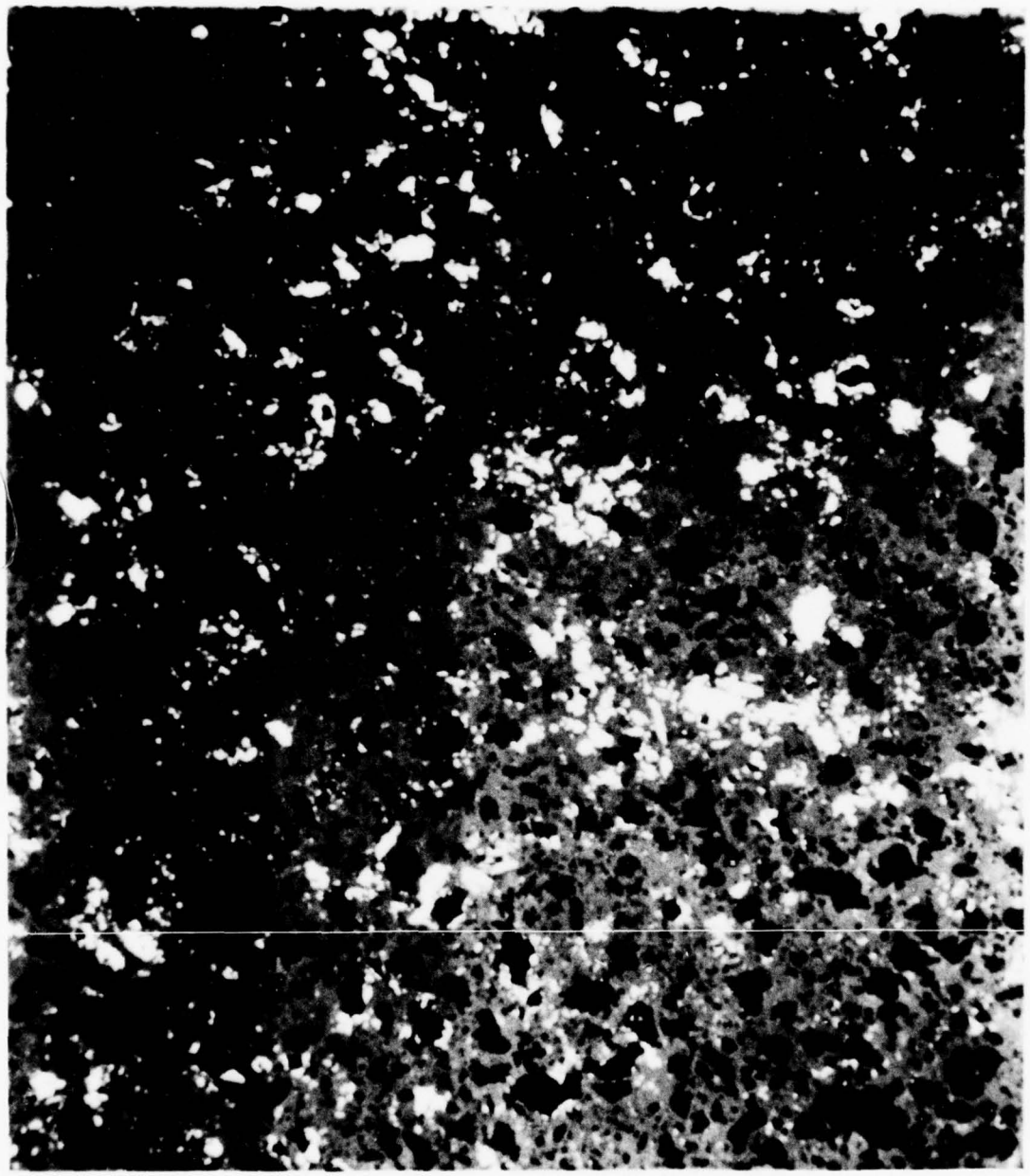

20 μm

Fig. 5: Representative photomicrograph of a polished section of RBSN.

Black - porosity

Grey - silicon nitride

White - silicon.



70μm

continuous access of nitrogen to the interior of the compact as nitridation proceeded. After a skeleton of silicon nitride has formed, the reaction temperature is usually raised to above the silicon melting point in order to increase reaction rate. The residual silicon droplets are converted to silicon nitride and produce polycrystalline islands of dense nitride in the original mat[18]. The use of temperatures above the silicon melting point invariably leads to an increase in the proportion of β-silicon nitride in the final product[61], but the exact reason for this is still not explained.

The pore space in fully nitrided material is mostly on a size scale of less than 1 μm[62,64], although isolated pores as large as 50 μm are so common as to be properly regarded as a principal feature of the microstructure[64]. Evans and Davidge[33] found that on nitriding at temperatures below the silicon melting point the largest pores in the final product were of a similar size to those in the green compact. On nitriding at temperatures above the silicon melting point they detected larger pores, equivalent in size to the maximum silicon particle size, and concluded that certain silicon particles, when molten, had flowed into the surrounding mat resulting in the formation of large voids in the material. Evans and Davidge also showed that molten silicon will wet silicon nitride, and a more recent study[65] has confirmed this phenomenon at elevated nitriding temperatures, viz. 1450°C. Additionally, it was shown[65] that Fe-Si alloys, which are molten during the low temperature nitridation stages, 1250-1350°C, have a very small contact angle with silicon nitride at these temperatures. In impure powders, therefore, it is necessary to consider the possibility of large flaws being produced by the flow of such alloys.

Whiskers of silicon nitride are nearly always formed during the nitridation of impure silicon powder. That the growth of silicon nitride

whiskers may be influenced by impurities in either the silicon powder or nitriding atmosphere was first proposed by Popper and Ruddlesden[37], and Parr and May[18] found that the presence of oxygen and hydrogen in the nitriding atmosphere was essential for the growth of whiskers under their experimental conditions.

There are numerous gas/metal reactions in which whisker formation has been observed[66,67,68], but the amount of reaction product contained in whiskers usually represents a minor part of the total. Although whisker growth greatly increases the total surface area of the system in which it occurs, there is no evidence that the growth of whiskers has a marked effect on the overall gas/metal reaction. Indeed the coverage of the metal surface afforded by whiskers is very small, and Per Kofstad[66] suggests that whisker formation is not a normal oxidation phenomenon, and probably occurs as a result of effects secondary to the major reaction. Whisker formation during the reaction-bonding of silicon powder compacts, however, has been considered to be of major importance, and it has been suggested that the strength of the ceramic is due to the formation of an interlocking mat of whiskers[69], and many studies of whisker growth and morphology in the silicon/nitrogen system have been undertaken.

Evans and Sharp[62], from transmission electron microscopy examination, described two major types of whiskers:

1) Long, narrow whiskers having a diameter of 0.05 μm, and
2) relatively coarse fibres of 0.2 μm diameter.

The coarse fibres exhibited a dark core region along their axis, thought to be the original whisker onto which further silicon nitride had grown during the later stages of the nitriding process. Cored fibres have also been reported by Danforth and Richman[70], who described the inner core as crystalline and the outer sheath as amorphous, as determined by the lack of tilt contrast of the outer sheath when examined by transmission

electron microscopy. Danforth and Richman found that some fibres had a helical banded structure and they proposed that this was due to the segregation of impurity bands as a vapour/solid interface progressed helically along the axis of the fibre. The cored fibres were not observed to exhibit impurity bands.

The presence of beads on the tips of some whiskers has been widely reported[70,43] and is in accordance with the vapour/liquid/solid growth mechanism proposed by Carr and Bartlett[71], who found that whiskers comprised a mixture of alpha-silicon nitride and Fe_2SiO_4. Iron is a common silicon powder contaminant and the presence of the low melting point (1220°C) iron disilicide, $FeSi_2$, in RBSN has been reported by Godfrey and Lindley[64], and Messier and Wong[43]. Not all whiskers, however, exhibit the characteristic feature of the VLS mechanism, and therefore it is likely that more than one growth mechanism is involved in whisker formation.

One other possibility is that whisker growth may be controlled by surface transport in a "quasi-liquid" impurity phase layer, along the surface of the whisker, as suggested by Pfefferkorn and Vahl[68].

The formation of granular silicon nitride during the reaction-bonding process has not received the attention afforded to the whisker phase formation. The granular form, usually considered to be β-silicon nitride, is found as discrete grains surrounded by the whisker mat[61], and Evans and Sharp[62] suggested that the β-grains were formed by a liquid/vapour reaction but they did not suggest any possible growth mechanism. In contrast, Danforth and Richman[70] proposed that the β-phase was nucleated at the solid silicon surface and grew into the silicon particle, with the rate controlling process being the solid state diffusion of nitrogen through the β-lattice to the nitride/silicon interface. The 22% volume increase on conversion was accommodated, according to Danforth and Richman, by the

transformation of the silicon structure from diamond cubic to the denser hexagonal form.

The well-formed prismatic crystal habit exhibited by the majority of β-grains[72], and the increase in the amount of β-type product formed when the temperature is raised above the silicon melting point, suggests that much of the β-silicon nitride present in RBSN is formed via crystallisation from a liquid phase. Liquid phase reactions are also possible below the silicon melting point, in impure powders, both iron and aluminium form low melting point eutectics with silicon, at 1220°C and 577°C respectively. The phase diagrams of Fe-Si and Al-Si are shown in Fig. 6.

The review so far has been concerned with the microstructural characteristics of the nitride developed during the nitridation of impure commercial silicon powders. The microstructure of RBSN produced from spectrographically pure silicon powder under carefully controlled atmospheric conditions, however, has been studied by Atkinson et al.[12] and one major feature of the work was that no whisker or fibre morphologies were observed in the range of nitrogen pressure and temperature investigated. It seems therefore that whisker formation is associated with impurities, possibly including the silica layer covering the silicon, in the nitridation system.

For a silicon powder compact of green density 1500 $kg.m^{-3}$, the original porosity can only accommodate 50% of the nitride formed and therefore at least 50% must be formed within the original boundaries of the silicon particles. This fact would seem to have been ignored in many of the microstructural studies of RBSN; but Atkinson et al.[12] have provided microstructural evidence of the formation of porosity and silicon nitride within the silicon particles.

In a previous paper by Atkinson et al.[73] it was suggested that the porosity in the silicon was generated by vacancy condensation following

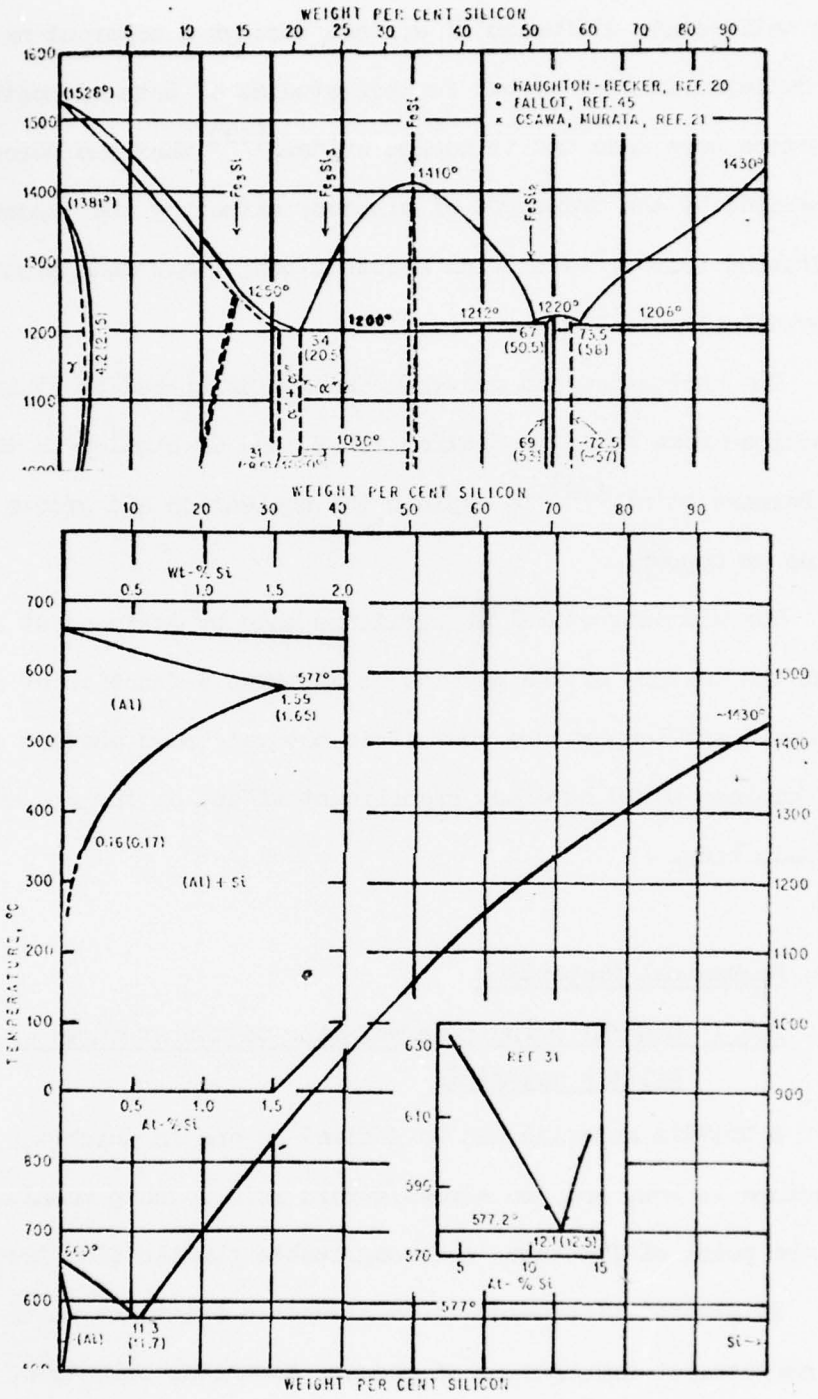


Fig.6. Phase diagrams for the systems Fe-Si and Al-Si.

From: Silicon Semiconductor Technology,

W.R.Runyon, McGraw-Hill, London.

the solid-state diffusion of silicon through a coherent nitride layer, as depicted in Fig. 7, but further studies of both microstructure and kinetics were made and it became evident[12] that the porosity was generated by the transport of silicon, either by the vapour or surface diffusion routes, to nitride growth sites; this mechanism is shown schematically in Fig. 3.

The nucleation and growth mechanism described by Atkinson et al. is described more fully in Section 2.2.2, and is similar to that proposed by Bernard et al.[74] to explain the nucleation and growth of cuprous oxide on copper.

The microstructural observations made by Atkinson et al. showed that the texture of the nitride product was a function of nitrogen pressure and temperature, but it is not yet known whether such textural differences would have any significant effect on the properties of the ceramic body.

2.4 Mechanical Properties

2.4.1 General principles relating to the strength of brittle materials

A brittle material can be defined as one in which the work of fracture is low, and the stress/strain relationship remains linear up to the point of fracture, no recognizable plastic flow preceding fracture.

In general with ceramics, a situation exists in which texture, that is macroscopic arrangement of phases, dominates structure, i.e. lattice arrangement of atoms, in determining mechanical properties, and currently attainable strengths are considerably below estimates predicted from theoretical considerations. The practical strengths of ceramics are limited by the presence of cracks and flaws, and ceramic materials have a characteristic value of critical strain (the ratio of fracture strength to Young's modulus) of 10^{-3}. The elimination of flaws has been attempted

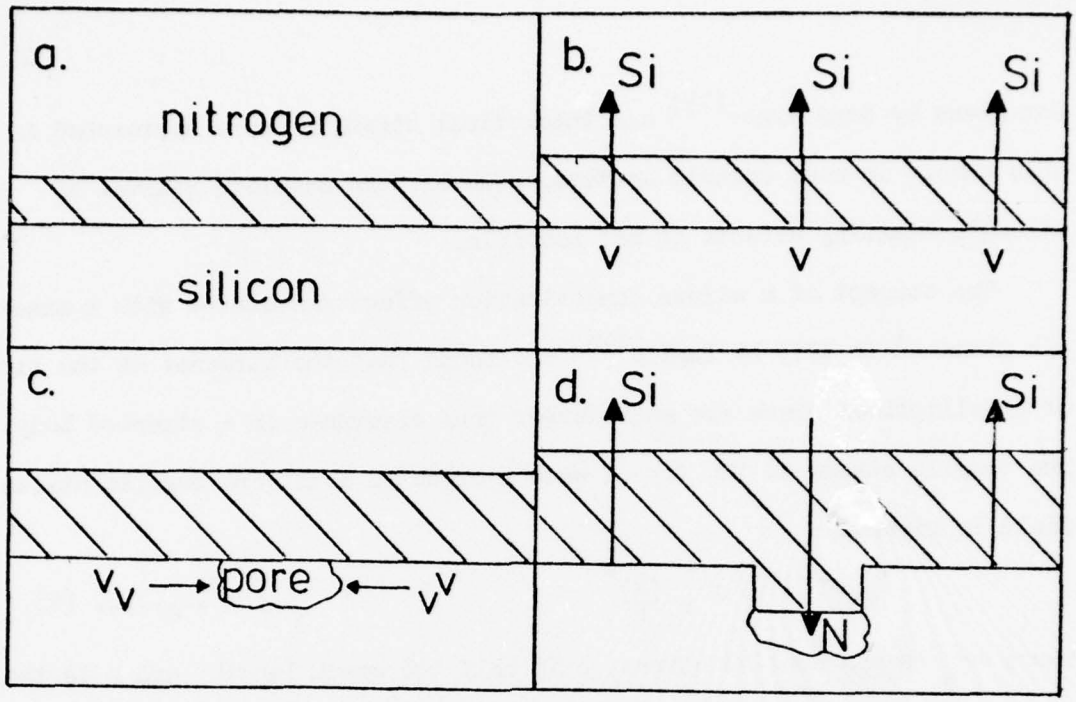


Fig.7. Solid-state diffusion model for the nitridation of silicon.

(a) Silicon is covered with a layer of nitride.

(b) Outward migration of silicon leaves vacancies in the silicon lattice.

(c) The vacancies condense to form a pore at the nitride/silicon interface.

(d) The nitride grows into the pore and the pore migrates into the silicon particle.

for glass by Ernsberger[75] and theoretical strengths were approached in this case. In most ceramic systems, however, the complete removal of strength-limiting defects is not possible.

The concept of a stress concentration effect associated with a crack was examined in 1913 by Inglis[76] who found that the stresses at the tip of an elliptical crack are much larger than elsewhere in a stressed body. The tensile stress at the tip of such a crack in a uniform tensile stress field is given by:

$$\sigma = 2\sigma_a \left(\frac{c}{p}\right)^{\frac{1}{2}} \qquad \ldots\ldots\ldots (1)$$

where σ_a is the applied stress, c is half the crack length, and p is the radius of curvature at the crack tip.

In the above equation it is possible to set the concentrated stress (σ) equal to the theoretical stress for fracture, and solve the equation for the applied stress required for fracture. In practice, however, a lack of knowledge concerning the theoretical fracture stress and p makes determination of σ_a extremely difficult.

Griffith[77] derived the same square root dependence of strength on crack length by assuming that the change in strain energy as a crack grows is equal to the energy necessary to produce the new surface. This leads to the well-known criterion for fracture:

$$\sigma_f = \frac{1}{Y}\left(\frac{2E\gamma_i}{c}\right)^{\frac{1}{2}} \qquad \ldots\ldots\ldots (2)$$

where σ_f is the critical applied stress for failure, E is Young's modulus, γ_i is the thermodynamic surface energy, and Y is a constant dependent on crack geometry.

In contrast to equation (1), the Griffith criterion can be used to establish fracture conditions provided it is recognised that the surface energy term must take account of all chemical and mechanical processes occurring at the crack tip during fracture.

One commonly used strength index is the "critical stress intensity" factor denoted by K_c. This factor arises from the work of Irwin[78] who calculated the work required to close up a small portion of a crack by superpositioning appropriate forces along the crack surface.

Irwin calculated the work required to close up a crack, per unit of its length, as:

$$G = \frac{K^2}{E} \qquad \ldots\ldots\ldots (3)$$

Conversely, Irwin reasoned that the same amount of stored energy must be released when a crack is allowed to extend by unit length, and thus named G the "strain energy release rate".

Unlike Griffith, Irwin did not specify that cracking involved only the appearance of thermodynamic surface energy but that energy dissipation could involve other processes occurring at the crack tip, for example, plastic deformation. Irwin simply stated that crack extension would occur when G is equal to a critical value G_c. For materials which, on fracture, lack any mechanism of energy dissipation other than the appearance of thermodynamic surface energy, then $G_c = 2\gamma_i$. (In cases where dissipation by other processes is involved, then γ_F, the fracture energy, is the appropriate parameter.) From equation (3) then: $K = (2E\gamma_F)^{\frac{1}{2}}$, and for a crack of length 2a in a body subjected to a stress σ_a: $K = \sigma_a Y(2a)^{\frac{1}{2}}$.

The "critical stress intensity factor" K_c, which is the value of K corresponding to the critical value of σ_a, provides a useful means of characterizing the strength of a material and of calculating the critical defect size, and is a material constant dependent on physical processes occurring at the crack tip during fracture.

K_c is extensively used for material specification in engineering applications, but there are problems associated with its measurement in brittle inhomogeneous ceramic materials, particularly when the introduction

of artificial cracks are involved in the measuring technique. The immediate surrounding of the artificially introduced crack may be very different from that in the vicinity of the critical flaw.

For the above reasons, K_c is not extensively applied to brittle materials development work, but it can be used to give useful semi-quantitative guidance to the designer concerned with ceramic material specification.

2.4.2 Mechanical properties of RBSN

The strength of RBSN has naturally attracted very considerable research and development interest and, although much data are contained in the literature, they represent a wide range of sample preparation and measuring techniques. This review will, therefore, not give close consideration to any particular published values of mechanical properties, but rather will be concerned with the more general effects which fabrication and processing variables can have on the achieved strength values.

The fabrication of the green body can have a pronounced effect on the resulting properties of the fired ceramic, and the choice of shaping process and powder particle size and size distribution are all important considerations in this context.

Because of die-wall friction, die-pressing of silicon powder, whether uniaxial or biaxial, produces laminations in the green structure and relics of these will be present after nitriding; therefore this fabrication process cannot be considered if optimum strength is sought. Isostatic pressing eliminates many of the problems associated with die-pressing, but careful tailoring and control of the process is still very necessary if laminations and internal flaws are to be avoided. High strength RBSN can, at the present time, be produced from powder compacts prepared by the flame spraying[64] and slip-casting routes, both of which are potentially capable of producing homogeneous particle packing and

high green densities; however gross inhomogeneities can be encountered in the slip-casting route[60].

All the mechanical properties of RBSN are dependent on the density of the nitrided silicon powder compact. Rupture modulus values for densities of 2200 and 2600 $kg.m^{-3}$ are approximately 100 and 200 MNm^{-2} respectively and, according to Barnby and Taylor[79], the dependence of Young's modulus on porosity for fully nitrided material obeys the empirical expression:

$$E = E_o (1 - 2.2 P_v)$$

where E_o is the modulus value of fully dense silicon nitride, i.e. ~ 310 GNm^{-2}[80], and P_v is the volume fraction of pores. Fracture surface energy data cover a wide range of values, but for material of density 2600 $kg.m^{-3}$ a typical value would be 10 Jm^{-2}. A summary of the properties is given in Table 2.

The effect of the initial silicon particle size on the strength of the ceramic has been the subject of study[87,83] and the concensus of opinion is that the smaller the silicon particle size the greater the potential for producing a high strength reaction-bonded material. This is particularly so if a reaction temperature above 1420°C is employed during the process, since Evans and Davidge[33] have shown that the melting and subsequent flow of residual silicon particles into the surrounding structure can be the source of large strength-controlling defects.

Starting with a small silicon particle size (typically < 5 μm) and good compaction procedure are obvious necessary precursors to the development of a uniformly fine scale texture to the green microstructure. A further advantage of very small silicon particles is that because the surface area of a given powder compact is inversely proportional to particle size and under conditions when the reaction rate is controlled

Young's Modulus/GN.m^{-2}	Density/Kg.m^{-3}	Reference
98	2000	Parr and May (18)
170	2400	" " "
218	2650	" " "
126*	2370	Fate (81)
140*	2500	"
175*	2700	"
123	2460	Barnby and Taylor (79)
134	2780	" " "
140*	2400	Jones et al. (69)
153*	2610	Dalgleish & Pratt (61)
137*	2350	" " "
Rupture Modulus/MN.m^{-2}		
110	2200	Parr and May (18)
210	2650	" " "
204	2600	Thompson & Pratt (82)
200	2300	Jones & Lindley (83)
146	2330	Barnby & Taylor (79)
Compressive Strength/MN.m^{-2}		
705	2650	Parr and May (18)
Fracture Surface Energy/J.m^{-2}		
23.5	2330	Barnby & Taylor (79)
23.5+	2330	" " "
6.0	2550	Evans and Davidge (33)
30.0+	2610	Dalgleish & Pratt (61)
10.0	2610	" " "

*determined by a dynamic technique.

+value obtained using blunt notches.

Table 2: Mechanical Properties of RBSN

by the gas/particle reaction, nitriding times can be kept short. Although the use of small particles can offer benefits it does present problems also. Particle agglomeration and poor powder flow characteristics can lead to low density, inhomogeneous 'green compacts'.

The reaction-bonding temperature and its relationship to achieved strength values has received much attention in the commercial production of the ceramic, not only because of the possibility of the particle melt-out phenomena mentioned above, but also because of local melting caused by reaction exotherms and low melting point impurity phases. Many production processes now employ a long firing schedule during which the temperature is not raised above 1300°C. This however is not below the solidus temperature for the Al-Si and Fe-Si eutectics which are the most common low melting point materials likely to be encountered. The use of these low temperature schedules has resulted in much improved rupture modulus values, and the removal of impurity phases may enable the strength to be improved still further.

The significance of impurity phases in any consideration of the strength of RBSN has recently been illustrated in studies of the high temperature creep characteristics of the material. It has been suggested that impurity phase segregation at grain boundaries can cause viscous flow and grain boundary sliding in some reaction-bonded silicon nitrides at elevated temperatures, i.e. 1200°C.

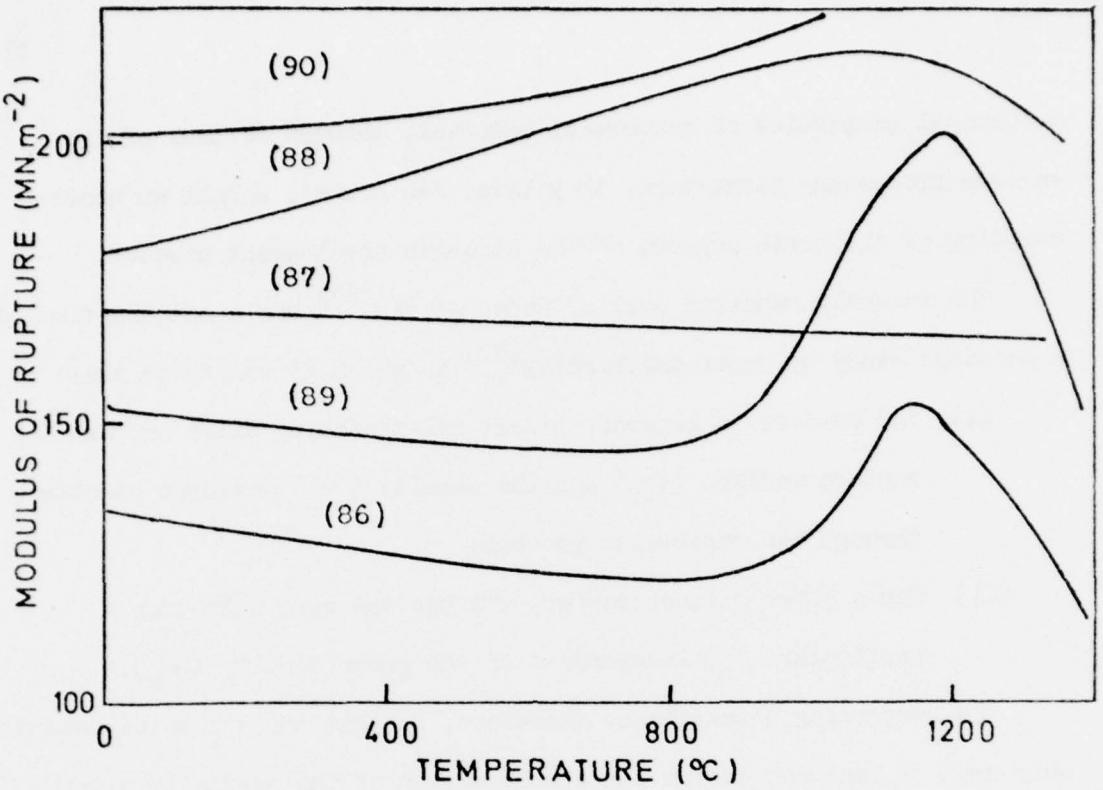
Salah ud Din and Nicholson[84] found that the development of triangular grain boundary voids was a characteristic feature observed during the high-temperature creep of RBSN, and they reported that the steady-state creep-rate could be halved by reducing the calcium level in the silicon nitride from 0.1 to 0.04 W/o. Spectrographic examination revealed that the grain boundary impurity phase was probably $CaO-2Al_2O_3-2SiO_2$, the refractoriness of which increases as the CaO content is lowered. Marcus et al.[85] provided supporting evidence for such grain

boundary segregation; by Auger analysis they found segregation of Ca, Al and O_2 on the surfaces exposed by room temperature fracture of RBSN. The interpretation does rely on the correctness of the assumption of a predominantly intergramular fracture. The occurrence of Ca, Al and O_2 in a fracture surface (assumed grain boundary region) has also been reported by Mangels[86], and he found that after nitriding similar silicon powder in an atmosphere containing 1.8% H_2, no trace of Ca or Al could be detected. Mangels was able to correlate the loss of Ca and Al with improved strength and creep resistance of the RBSN at temperatures up to 1400°C.

The high-temperature strength behaviour of RBSN is shown in Fig. 8. The data are not entirely consistent for the rupture modulus (σ_f) but this is probably due to different impurity types and levels in the starting powder. Those materials exhibiting a decrease in σ_f at temperatures $>$ 1200°C also show an increase in σ_f up to this point. Concurrent with the increase in σ_f there is a decrease in Young's modulus (E) and an increase in the fracture surface energy (γ_F); the effects are probably associated with the onset of plasticity in the material.

Returning to the room-temperature mechanical properties of RBSN, most studies have been concerned with the fracture mechanics approach, and have reported values of K_c and γ_F for a variety of silicon powders and nitriding procedures. Whilst providing useful general data relating to the engineering application of the ceramic, this type of approach has done very little towards gaining an understanding of the actual development of strength during reaction-bonding. There is, in fact, still no answer to the question: 'how is a weak particulate compact transformed into a strong silicon nitride ceramic?'

The only long term systematic effort to understand the way in which the mechanical strength of RBSN develops during the reaction-bonding process has been made by the group at the Admiralty Marine Technology Establishment. Although their prime objective is to optimise the



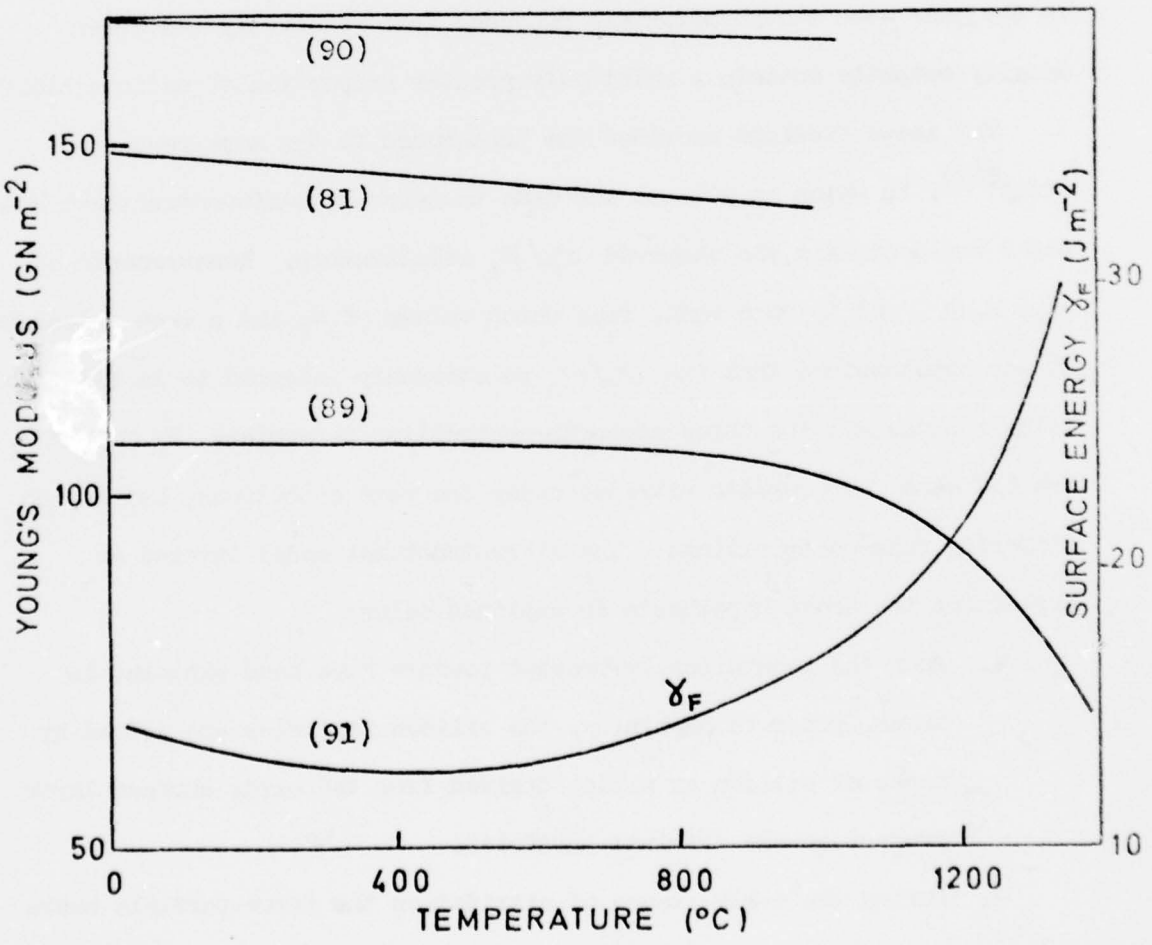


Fig.8. High-temperature mechanical properties of RBSN.

mechanical properties of commercial material, through control of the various processing parameters, they have, 'en route', sought an understanding of the basic science of the strength development process.

The recently reported work of Jones et al.[69] was a continuation of a previous study by Jones and Lindley[92] in which it was found that:

(i) for powders in general, linear relationships exist between the rupture modulus (σ_f) and the density (ρ_n) measured at stages through the conversion process;

(ii) for a given silicon powder, σ_f has the same value for a particular ρ_n, independent of the green density (ρ_g).

The surprising observation, therefore, is that the σ_f value depends only upon ρ_n and not on the phase composition of the partially nitrided compact (Si, Si_3N_4 and porosity). That is, for a given ρ_n, the strength is the same even though materials produced from relatively low green density compacts contain a relatively greater proportion of silicon nitride.

The above findings provided the background to the more recent study[69], in which an attempt was made to describe a microstructural model which would explain the observed σ_f/ρ_n relationship. Measurements of σ_f, E, ν, and K_c were made, from which values of γ_F and c were calculated. It was hypothesized that the σ_f/ρ_n relationship referred to in (ii) above holds because all the three strength-controlling parameters, E, γ_F and c, are the same for compacts nitrided under the same conditions, but having differing phase compositions. The microstructural model invoked as explaining the above hypothesis is outlined below:

1. When the isostatically pressed powders have been sintered in argon, prior to machining, the silicon particles are joined by necks of silicon or silica derived from the oxide surface layer present on the original particles.
2. During the early stages of nitridation the inter-particle necks are removed.

3. Silicon nitride begins to form in the void space between silicon particles, resulting in the development of a continuous skeletal network of whisker-like silicon nitride. The densification of this network on further nitridation gives rise to the linear portions of the σ_f/ρ_n and E/ρ_n relationships.

A low green density (lgd) material will have a larger average pore size than a high green density (hgd) material, and Jones et al.[69] suggest that at a particular value of ρ_n, then the compensating greater amount of conversion in the lgd compact will lead to the same values for c in the two materials.

The fact that the Young's modulus values of the two materials are equal is explained by the fact that a proportion of the silicon nitride formed does not contribute to the stiffness of the developing structure. The larger void space in the lgd material would result in a greater proportion of "redundant" silicon nitride in this material. Therefore, at a particular ρ_n, even though the starting ρ_g values differ, the amount of silicon nitride contributing to the stiffness of the material is the same. It is also suggested that a higher degree of conversion from silicon to silicon nitride will be required to form a continuous network in the more porous, lgd structure.

Jones et al.[69] offered no suggestions to explain the equivalence of fracture surface energy values.

The above model is open to criticism and particularly so is the aspect concerning strength development in the nitriding silicon compact. Furthermore, it must be emphasized that the green density range covered by the study was only 1330-1550 $kg.m^{-3}$.

Jones et al.[69] consider the strength of the material to reside in a skeletal whisker network. However, as Thompson and Pratt[82] have already pointed out, if the strength was primarily due to a whisker network, it is difficult to see why it should be so dependent on porosity,

and they concluded, therefore, that it is largely dependent on the amount of intergranular contact and the properties of the bulk material. The fracture path in RBSN is predominantly intergranular[91], and if a whisker mat were responsible for the strength, a greater proportion of transgranular fracture might be expected.

The linear relationship between Young's modulus and nitrided density observed by Jones et al.[69] was found to extrapolate to the modulus value for fully dense hot-pressed silicon nitride, and it is not easy to reconcile this linear extrapolation with the proposed model. If a proportion of the silicon nitride formed during the early stages of the reaction does not contribute to the Young's modulus of the structure until the later stages of conversion, then during these later stages Young's modulus should show a stronger dependence on density than the early stage linear dependence. Put another way: if the initial E/ρ_n relationship was only dependent on densification of a whisker mat, the same relationship cannot describe the concurrent effects of continuing network densification and the involvement of previously "redundant" silicon nitride.

An important observation made in the study described above, and in several others by the same group, is the influence of nitrogen flow rate, during conversion, on the strength of the resulting RBSN. Materials produced under 'static' nitrogen conditions have shown 30% higher rupture modulus values compared with RBSN produced in flowing nitrogen, and similar increases have been observed for Young's modulus. Jones et al.[69] argue that the critical defect size (60 μm) is appreciably smaller in RBSN produced under static conditions than that (100 μm) produced under nitrogen flow conditions.

It should be borne in mind that in order to calculate the critical defect size, the fracture surface energy must be known. At the present time, values of γ_F show such a large spread that it would seem unwise to

place too much confidence in the estimate of a critical defect size. Values of γ_F measured by several techniques are: 6 Jm^{-2}[33], 11.4 Jm^{-2}[69] and 23.5 Jm^{-2}[79] for RBSN of similar density. It is not surprising, therefore, that estimates of critical defect size can range from 20 μm[33] to as large as 400 μm[79].

Although the factors affecting the strength of RBSN are not very well understood, the strength of the material available for engineering applications continues to be improved. However this improvement in properties has mainly been due to improved processing leading to a steady increase in density of the ceramic. Very little improvement has been due to the microstructural engineering approach, and this is a subject requiring further study.

3. AIMS OF THE STUDY

Throughout the history of the development of reaction-bonded silicon nitride, emphasis has been placed on the identification of strength-controlling defects in the ceramic body. The understanding of why the material is weak is a perfectly valid route to improving the mechanical performance of an engineering material but only against the background knowledge of why the material possesses mechanical strength. This is particularly important in the case of RBSN where the starting material is a loosely-bound powder compact. In the author's opinion the strength developing processes occurring in the silicon powder compact during nitridation have not been sufficiently investigated and where studies have been attempted unsatisfactory experimental conditions, particularly silicon purity, have masked the important features of silicon nitride growth and compact microstructure.

As early as 1966 Thompson and Pratt[82] asked why the strength should be so dependent on porosity if the material was predominantly bonded by a mat of silicon nitride whiskers. The uncertainty surrounding strength development in RBSN still exists today and is typified by the appearance in the literature of unsubstantiated, complex nitride growth and microstructural development mechanisms.

The aim of the present study was to attempt to identify the basic mechanism of reaction-bonding and to relate this to the development of strength in the powder compact during nitridation. In order to achieve this, two essentials are necessary:

1. The ability to resolve RBSN microstructures in order to recognise important features of strength development in the compact.
2. An accurate index of strength development that will reflect the features of strength development and be sensitive to changes in the strengthening mechanism.

In view of the two essentials outlined above the study was based on the nitridation of high purity silicon powder (99.99%), and strength development was monitored by the measurement of Young's modulus by an accurate dynamic method. The normal index of mechanical strength used in studies of RBSN is the rupture modulus, σ_f, but in view of the large number of samples required for an accurate assessment of σ_f, this method was not suitable for the present study.

In addition to the high purity silicon powder, a commercial powder of similar particle size distribution was utilized in the study to provide a comparison between the pure and commercial systems.

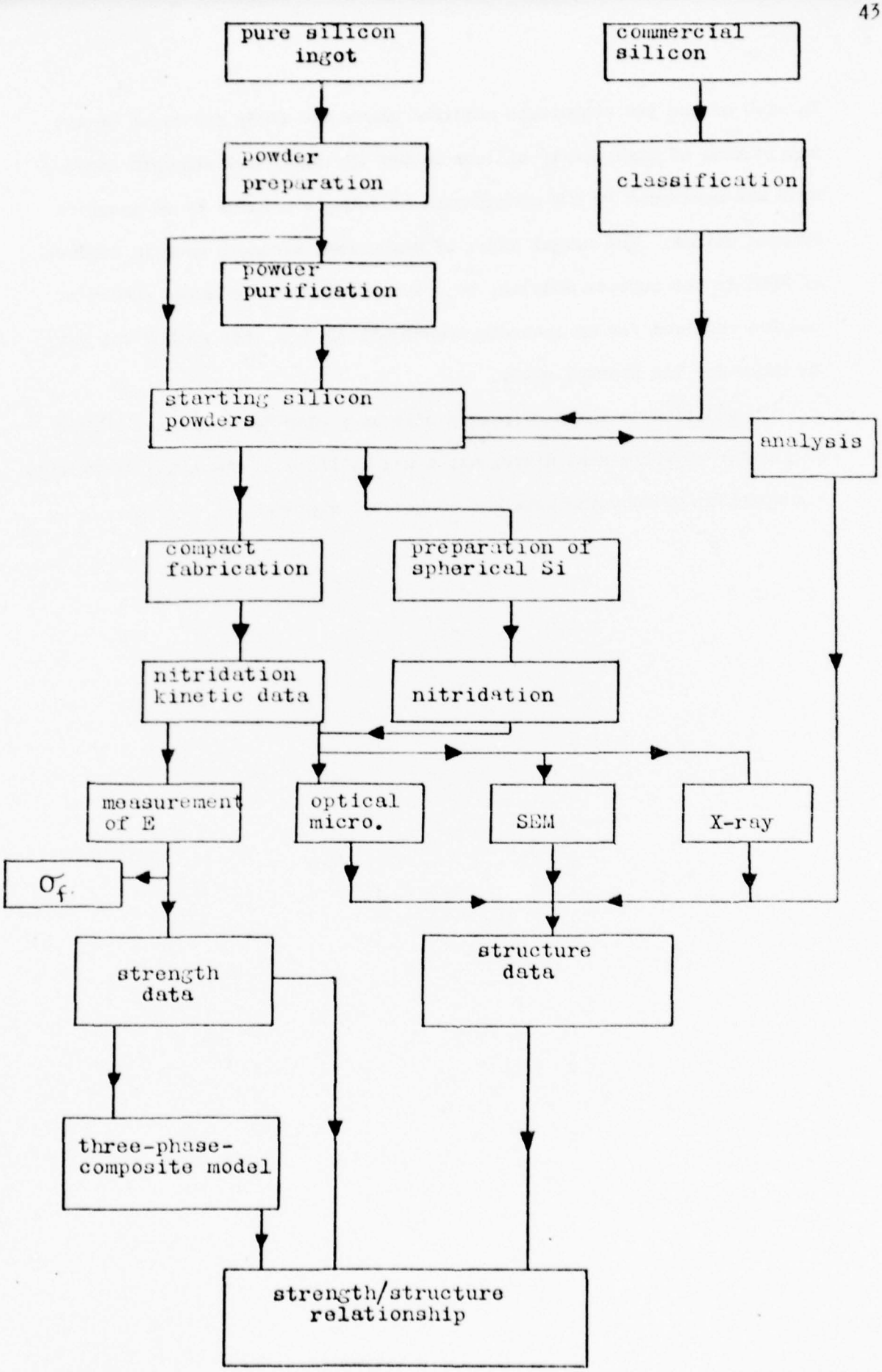


Fig.9. Flow diagram of aspects of the study.

4. APPARATUS AND EXPERIMENTAL PROCEDURE

4.1 Materials

4.1.1 Preparation of silicon powders

Silicon, in the form of undoped semiconductor grade ingots, was obtained from Monsanto Ltd. of Ghent, Belgium.

The ingots were impacted against each other in polythene bags to produce pieces of size approximately $\frac{1}{2}$" which were then milled for three minutes in a stainless steel-lined "Shatterbox"*.

The resulting powder was classified in a series of bronze mesh sieves, the fraction between 53-65μ m being retained for the production of spherical silicon powder, and the fraction below 45 μm for making powder compacts.

Because the metallic impurities introduced during the comminution and classification procedures described above were all soluble in hydrochloric acid, pure powder fractions could be obtained by washing in 1M hydrochloric acid for 72 hours followed by distilled water. After this washing procedure, the powders were dried in air at 40°C for 48 hours.

A commercial silicon powder marketed by Koch-Light Laboratories was also used in the study. This powder was classified in order to remove particles larger than 45 μm, but it was not acid-washed.

4.1.2 Production of spheroidized silicon powder

The process adopted for the production of spherical silicon powder was based on the free fall of irregularly shaped powder particles through a hot-zone of sufficient temperature and length to cause each particle to melt and be reshaped into a sphere by surface tension forces. The molten spheres continued their free fall through a cooler zone for sufficient time to permit solidification. This general principle is discussed in U.S. Patent No. 2,038,251 (1936), and also by Wahll et al.[93].

*Planetary mill, supplied by Glen Creston Ltd., Stanmore, England.

The spheroidizing apparatus is shown diagrammatically in Figure 10. The furnace comprised a 39 mm internal diameter alumina* furnace tube wound with 1 mm diameter molybdenum wire, operating up to 1800°C. The molybdenum winding was protected by a flowing 95% N_2/5% H_2 gas mixture. The heating zone was 300 mm in length with a hot-zone of ± 5% of the peak temperature over the central 50 mm. The temperature of the hot-zone was measured using a Pt-5% Rh/Pt-20% Rh thermocouple situated inside the furnace tube.

In order to ensure maximum heat transfer between the furnacetube wall and the silicon particles, and also to prevent silicon oxidation, a hydrogen atmosphere was used inside the spheroidizing apparatus. Prior to the introduction of the hydrogen atmosphere, the apparatus was flushed with high-purity argon.

The rate of feed of the silicon powder was controlled by a ground-glass ball-valve operated through an 'O'-ring seal. A uniform powder feed was achieved by using an electric vibrator attached to the side of the vessel containing the silicon powder. The glass powder-feed vessel was attached to the spheroidizing furnace tube via a water-cooled 'O'-ring vacuum union.

The spheroidized powder was collected in a copper tube of internal diameter 25 mm and length 650 mm; the upper 120 mm of the collecting tube was water-cooled in order to aid solidification of powder particles.

A series of preliminary experiments was carried out to optimise the conditions for the spheroidization of the acid-washed Monsanto silicon particles (53-65 μm). As a result of these, the operating conditions were subsequently fixed as follows:

(a) a downward flow of hydrogen of 250 cc/min.

(b) a powder-feed rate of < 10 g/hour, and

(c) a hot-zone temperature of 1720°C.

*All alumina used in the study was "Purox" grade sintered alumina, supplied by Morgan Refractories Ltd., Neston, Wirral, Cheshire, U.K.

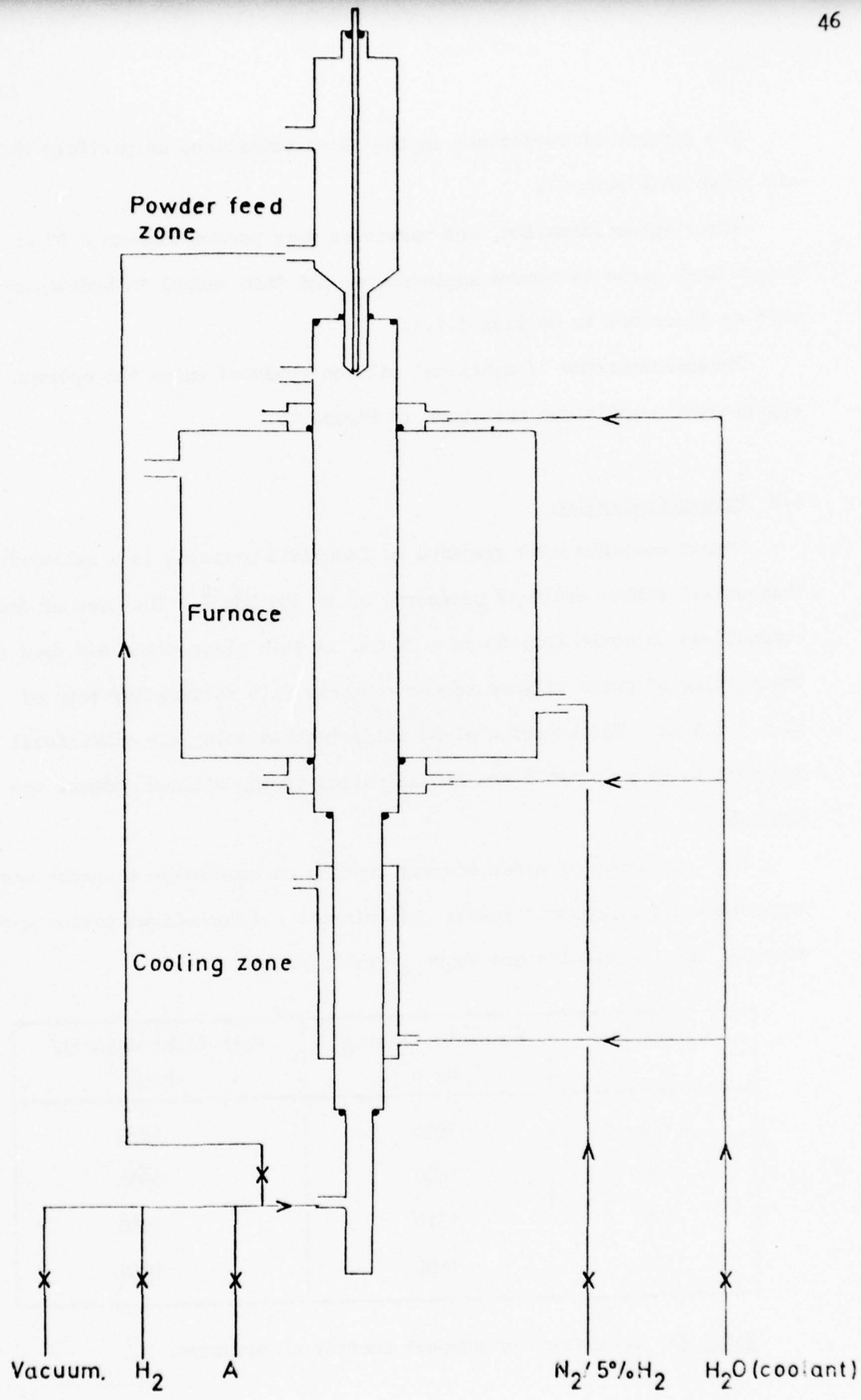


Fig.10. Apparatus for spheroidization of silicon powder.

The effects of variations in the above conditions on particle shape are shown in Figure 11.

After spheroidization, the particles were passed through a 65 μm bronze mesh sieve to remove agglomerates and then washed in hydrochloric acid as described in Section 4.1.1.

Photomicrographs of spherical silicon produced under the optimum experimental conditions are shown in Figure 12.

4.2 Powder Compaction

Powder compacts were prepared by isostatic pressing in a cylindrical thin-walled rubber mould at pressures up to 350 MNm^{-2}. The size of each compact was approximately 60 mm x 20 mm. A thin glass slide was used for the cutting of green silicon powder compacts into rectangular bars of 30 x 5 x 5 mm. The use of a glass slide enabled tolerable dimensional accuracy to be maintained and contamination of the silicon compact was avoided.

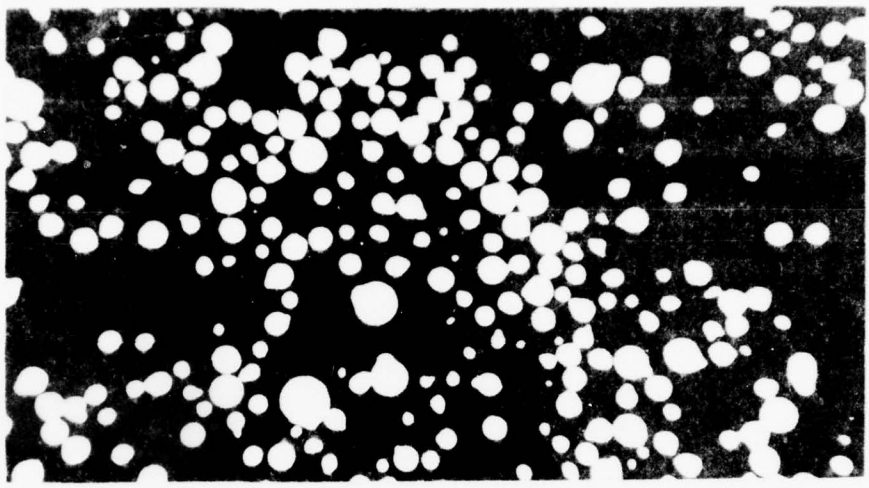
The dependence of green compact density on compaction pressure was investigated for Monsanto powder < 45 microns and Koch-Light powder < 45 microns, and the results are shown in Table 3.

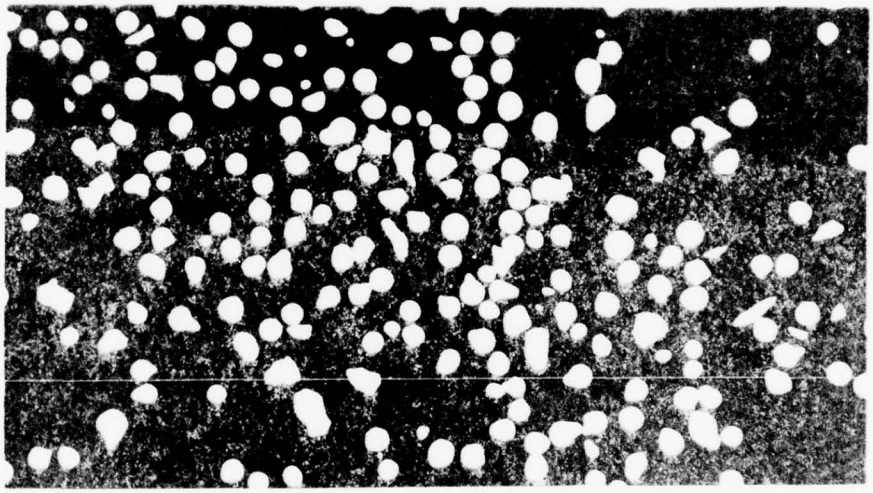
Pressure/MNm^{-2}	Monsanto density/ $kg\ m^{-3}$	Koch-Light density/ $kg\ m^{-3}$
105	1450	1470
140	1490	1500
175	1510	1510
350	1580	1560

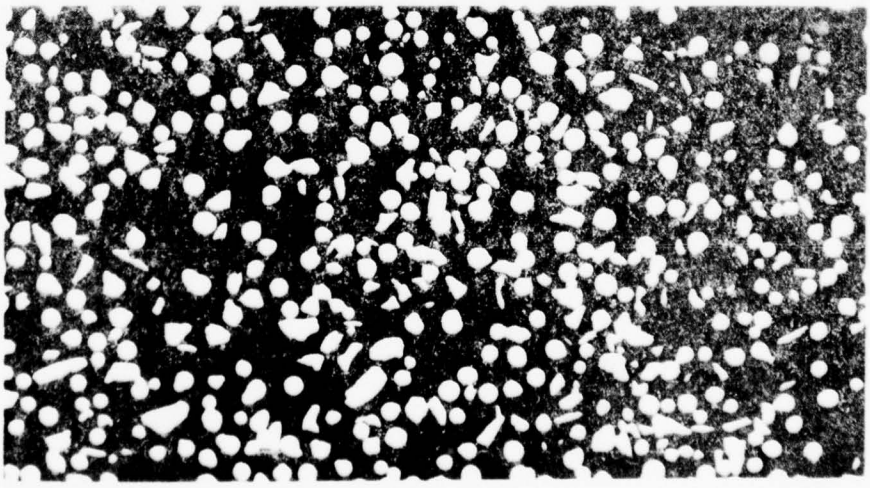
Table 3: Dependence of compact density on pressure.

Fig. 11: Spherical silicon produced under different experimental conditions.

	Powder feed/g/hr.	Temp/C	H_2 flow/cc/min.
a	9	1720	250
b	9	1680	250
c	15	1680	250







all particles 53 - 65μm

Fig. 12: Spherical silicon produced under optimum experimental conditions. SEM.



For pressures above 140 MNm^{-2} problems were encountered with the compact cracking on removal from the mould. The use of a powder binding agent was not attempted as it would have introduced an unwanted impurity variable during subsequent nitridation and therefore all powder compacts were isostatically pressed at 140 MNm^{-2}.

Polished sections of green compacts of Monsanto and Koch-Light powders are shown in Fig. 13.

4.3 Nitriding Furnace

The essentials of the nitriding apparatus were a nitrogen purification and supply line, a furnace operating at temperatures of 1200-1500°C, a suspension system enabling the sample to be moved in and out of the furnace hot-zone, a vacuum and gas pressure control system and provision for monitoring the experimental conditions. A diagram is shown in Figure 14.

The nitriding gas, 'White Spot' nitrogen (< 5 ppm O_2), was passed through a flow-meter, an oxygen trap*, and a vertical column of phosphorous pentoxide, and entered the furnace through a needle-valve. The water vapour level of the outgoing nitrogen could be measured by an electrolytic hygrometer**, typical values being < 5 ppm. A fixed pressure of nitrogen, in the range 0-760 torr, could be maintained in the apparatus by the use of the "manostat", which is described in detail in Figure 14.

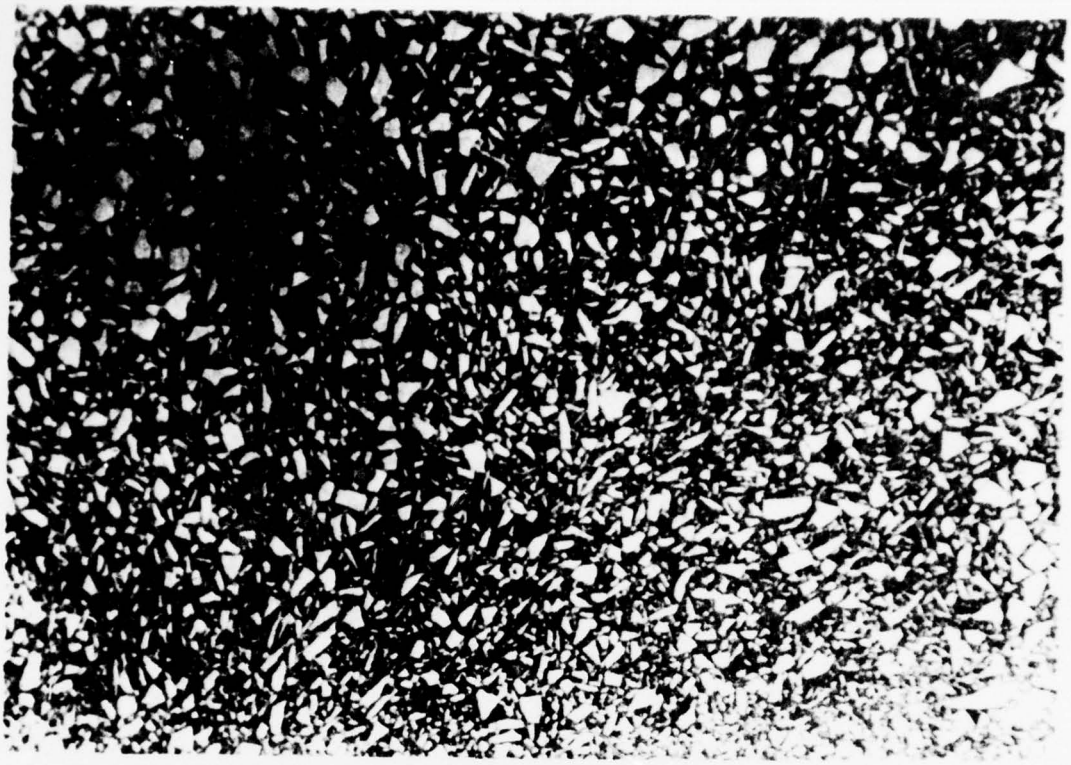
The furnace comprised an alumina tube (32 mm i.d.) carrying a 1 mm diameter molybdenum winding, and an alumina "work" tube (28.5 mm i.d.) which passed through the winding tube. The furnace case was continuously flushed with a $N_2/5\%\ H_2$ gas mixture to protect the winding from oxidation. Vacuum-tight connections to the alumina work-tube were made via water-cooled 'O'-ring sealed brass end-fittings. Temperature control was

*Alltech Associates "Oxy-Trap", Illinois, U.S.A.

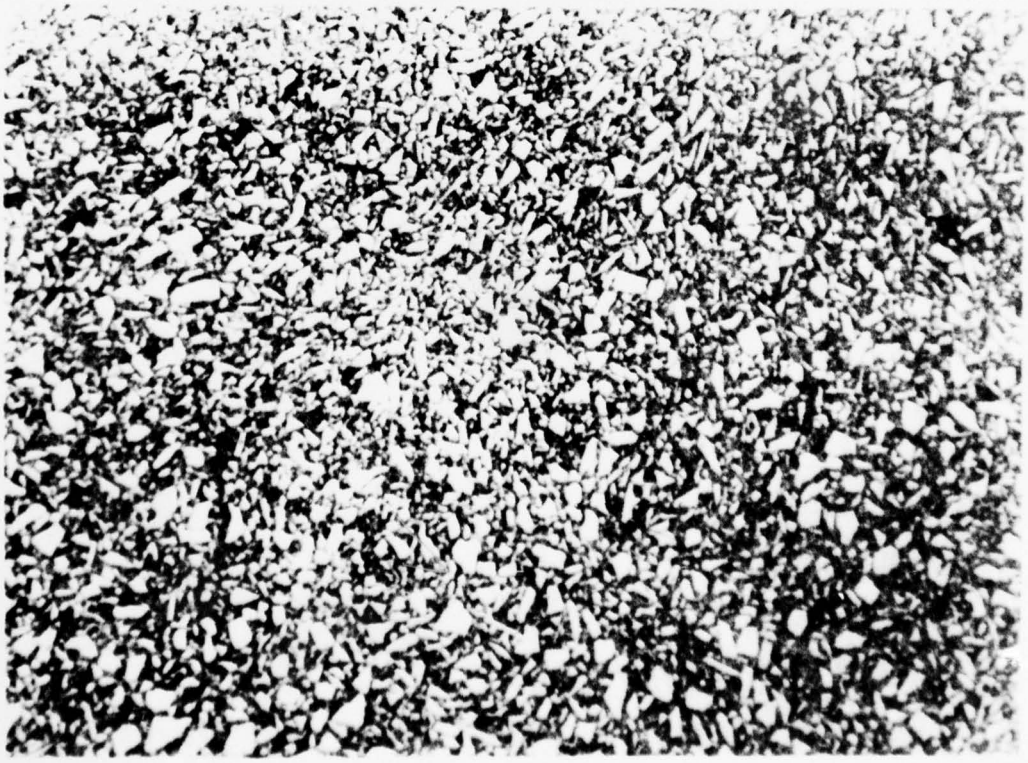
**Salford Electrical Instruments Ltd., Salford, U.K.

Fig. 13: Green compact structure of isostatically pressed (a) Monsanto and (b) Koch-Light 99.9% silicon powders.

Polished sections, reflected light.



100μm



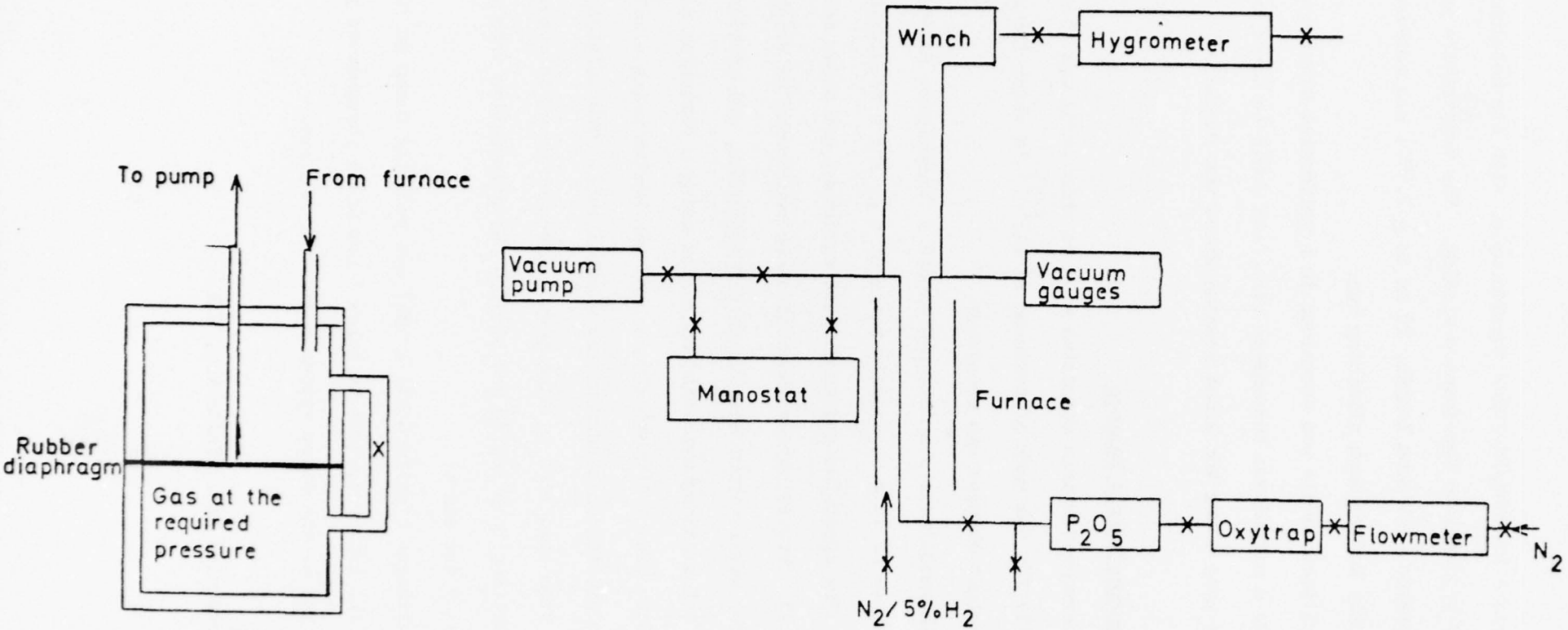


Fig.14. Schematic diagram of the nitriding apparatus.

achieved via a Pt-5%Rh/Pt-20%Rh thermocouple, with its hot-junction positioned adjacent to the furnace winding. The temperature at the sample position (hot-zone length, 20 mm to $\pm$ 2.5°C) was measured independently before each nitriding run.

The silicon sample was contained in a perforated alumina crucible attached to a molybdenum suspension wire, and could be moved in and out of the hot-zone using the winch mounted above the furnace.

4.4 Thermogravimetric balance

The thermogravimetric apparatus used in this study was that designed specifically for the work of Atkinson et al.[12] in which the recording of small weight changes was necessary.

The thermobalance was designed around a "Microforce Balance"*. It had a capacity of 19 g, a dynamic-range of 3 g, and a resolution of $\pm$ 100 μg. The apparatus and associated equipment are shown schematically in Figure 15. Provision for the continuous monitoring of weight, temperature, water vapour and oxygen was available, and nitridation at pressures below atmospheric was controlled using a Cartesian manostat. The work-tube was of 'Purox' alumina and was heated using a molybdenum resistance winding on a surrounding alumina tube. The molybdenum was protected from oxidation by high purity nitrogen so as to ensure that gas compositions both inside and outside the nitridation tube were substantially the same.

The nitrogen ('White Spot' grade) was purified using an 'Oxy-trap' to reduce the oxygen content to below 1 ppm and a phosphorous pentoxide column to reduce the water vapour content to $\sim$ 3 ppm.

*C.I. Electronics Ltd., Salisbury, U.K.

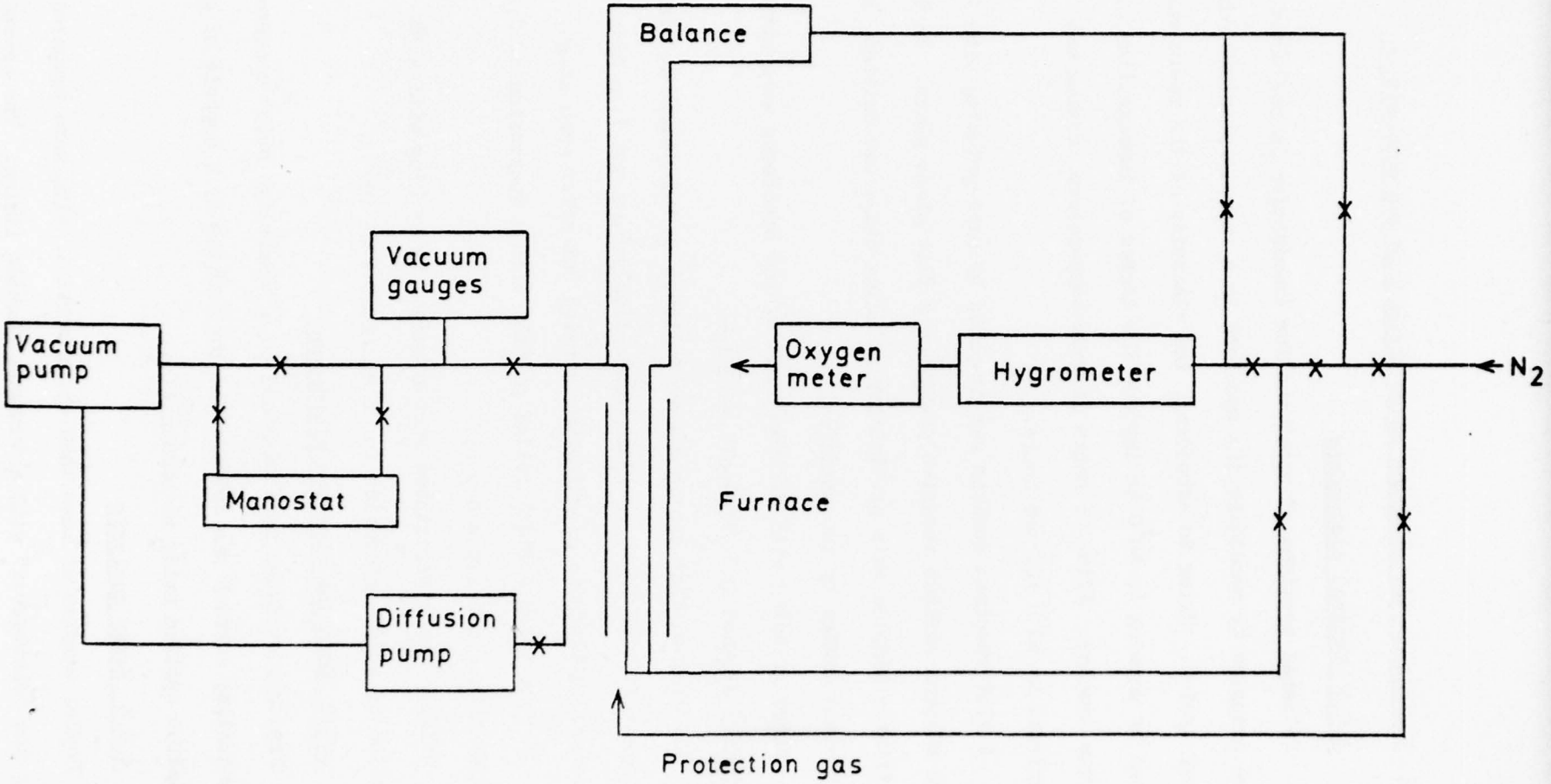


Fig.15. Schematic diagram of the thermogravimetric balance.

4.5 Techniques for studying phase morphology and composition

4.5.1 Optical microscopy

Polished sections of specimens for examination in reflected light were prepared by embedding the specimen in a room-temperature curing epoxy system. Prior to embedding, the viscosity of the resin was reduced by warming to 60°C to improve the degree of impregnation of the porous samples. After 16 hours at room-temperature, curing was completed at 60°C for two hours.

A flat specimen surface was prepared by hand-grinding with 1200 mesh silicon carbide abrasive powder on a flat glass plate. In the case of friable samples this preliminary grinding stage was omitted, in order to prevent damage by the abrasive.

After grinding with silicon carbide, the specimens were ultrasonically cleaned in a "Teepol" solution.

The cleaned flat sections were polished in two stages on diamond impregnated cloth laps, carrying respectively 6 μm and 1 μm diamond abrasive. Ultrasonic cleaning was carried out after each stage.

In some cases a final relief polish, with a suspension of 0.25 μm alumina on a cloth lap was used.

Silicon grain structures were examined by etching with a 5% solution of sodium hydroxide for five minutes at 100°C.

4.5.2 Scanning electron microscopy

Fracture surfaces were examined on a "Cambridge S600" microscope. A conducting surface was obtained on the samples by a deposit of gold/palladium applied prior to examination.

4.5.3 X-ray analysis

Powder samples of less than 45 μm particle size were prepared using the "shatterbox" with a tungsten carbide lining. The crystalline phases present in the material were identified by X-ray diffraction.

A line scan of a typical sample of RBSN, using CuKα radiation is shown in Figure 16.

The relative proportions of α- and β-silicon nitride in each sample were determined from the peak heights of the $\beta(210)$ and $\alpha(102)$ reflections using the calibration chart shown in Figure 17.

4.6. Measurement of Young's Modulus

4.6.1 Dynamic Young's Modulus determined by an electrostatic drive and detection method.

Dynamic methods for the determination of the elastic moduli of materials have been in use since 1930, and the original work was reviewed by Ide[94] in 1935. The basic requirements of such methods are an arrangement for vibrating the specimen and a means of detecting the resonance condition. Both the "drive" and "pick-up" may be magnetic, piezoelectric or electrostatic. In the present study the electrostatic method was employed. An early description of this method is given by Bancroft and Jacobs[95] and more recent reviews are given by Davis[96] and by Booker and Saga[97].

The mathematical description of the dynamic mechanical behaviour of materials is given in Appendix 1.

To determine the fundamental resonant frequency of a specimen it is convenient to make dynamic measurements on a rectangular bar, clamped at its mid-section, and to drive and detect by methods which do not impart any mechanical loading on the ends of the specimen. The electrostatic drive and detection method fulfills these requirements.

The electrostatic method, in which the drive is obtained by the application of an alternating voltage to a capacitor formed by the end of the specimen and a small fixed plate parallel to it, is applicable to longitudanal vibrations in metal bars. Non-conducting materials can be used if they are coated with a suitable conducting layer. Since the

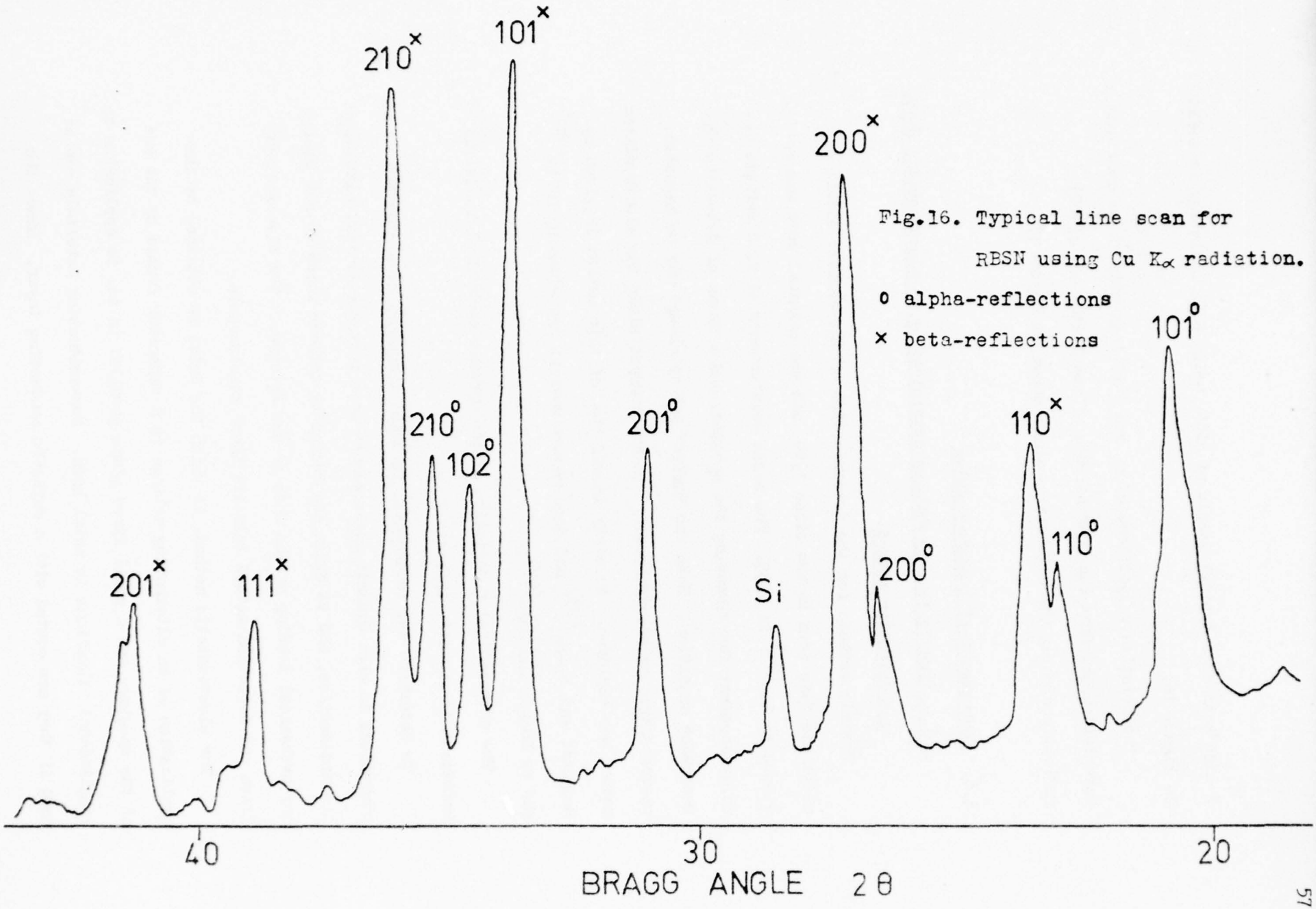


Fig.16. Typical line scan for RBSN using Cu K_α radiation.

o alpha-reflections

× beta-reflections

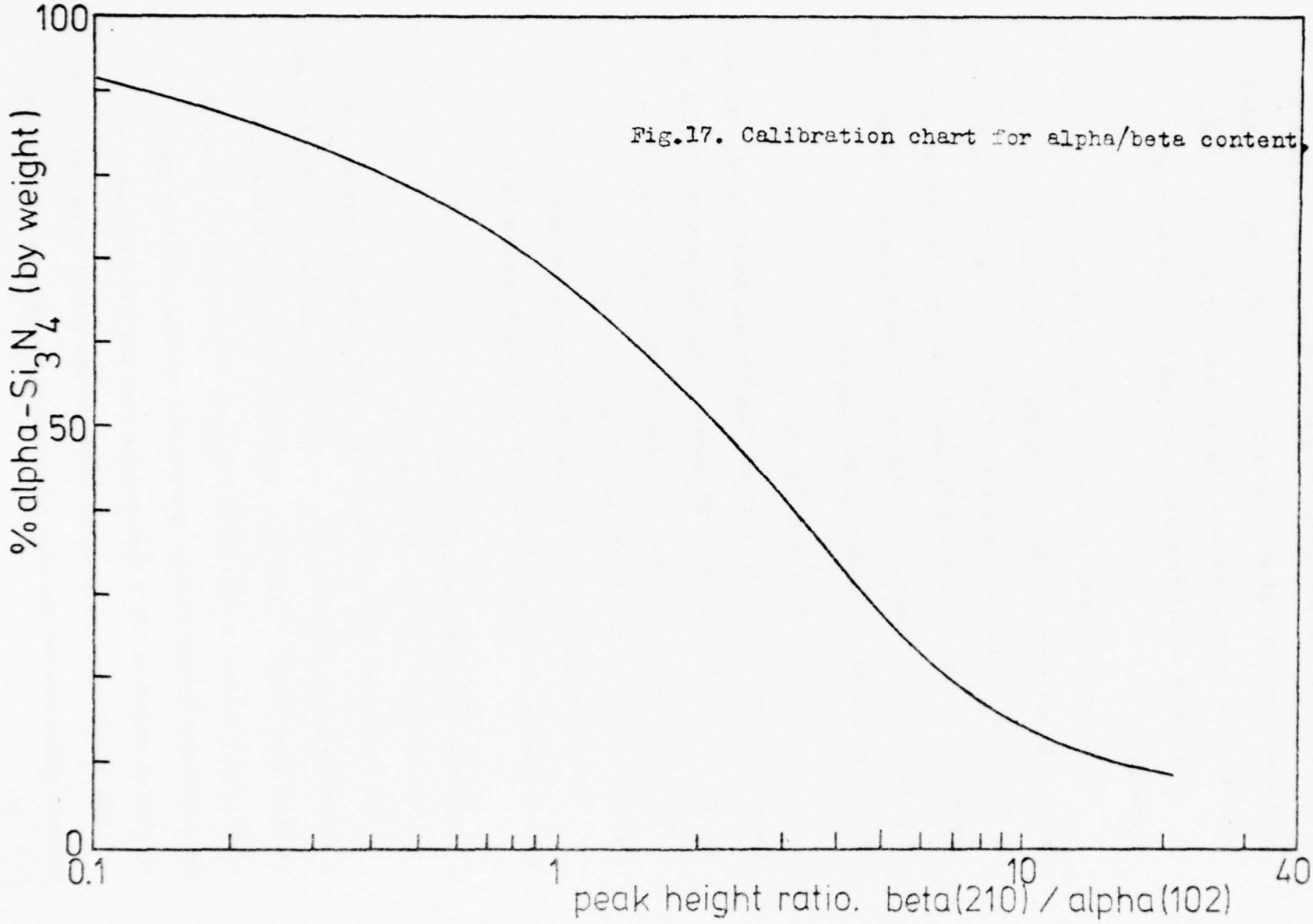


Fig.17. Calibration chart for alpha/beta content

means of excitation and detection make no physical contact with the specimen, there is negligible loading on the sample and its resonant frequency can be measured to a high accuracy, typically 1 in 10^4.

The theory of electrostatic drive and detection is given in Appendix 2.

In the present study it was necessary to determine values of Young's modulus in the range 20 GNm^{-2} to 200 GNm^{-2} at RBSN densities of 1900 kg m^{-3} to 2400 kg m^{-3}. The maximum length of the samples was limited to 5 cm due to the dimensions of the nitriding furnace and the problems associated with the isostatic pressing of samples of large length to diameter ratio. The above factors are related by the expression:

$$E = 4 \times 10^{-3} \times n^2 l^2 \rho \ Nm^{-2}$$

where E is Young's modulus, n is the fundamental, longitudinal, resonant frequency, l is the length of the sample in mm, and ρ is the density in g cm^{-3}. From this expression the range of frequency expected to be encountered can be calculated, i.e. 30 kHz - 100 kHz.

The electrostatic method covered the required frequency range and also enabled an accurate determination of Young's modulus to be made.

4.6.2 "Electrostatic" apparatus

The apparatus is shown in Figure 18.

The oscillator was a Wayne-Kerr A.F. S121 Signal Generator, covering a frequency range 1Hz to 120 kHz, in 44 overlapping bands. Stability was within 1 part in 10^4. The output signal was sinusoidal with a r.m.s. value of 2.5 volts. A Dawe 3001A Frequency Meter was used to monitor

all particles 53 - 65μm

means of excitation and detection make no physical contact with the specimen, there is negligible loading on the sample and its resonant frequency can be measured to a high accuracy, typically 1 in 10^4.

The theory of electrostatic drive and detection is given in Appendix 2.

In the present study it was necessary to determine values of Young's modulus in the range 20 GNm^{-2} to 200 GNm^{-2} at RBSN densities of 1900 kg m^{-3} to 2400 kg m^{-3}. The maximum length of the samples was limited to 5 cm due to the dimensions of the nitriding furnace and the problems associated with the isostatic pressing of samples of large length to diameter ratio. The above factors are related by the expression:

$$E = 4 \times 10^{-3} \times n^2 l^2 \rho \ Nm^{-2}$$

where E is Young's modulus, n is the fundamental, longitudinal, resonant frequency, l is the length of the sample in mm, and ρ is the density in g cm^{-3}. From this expression the range of frequency expected to be encountered can be calculated, i.e. 30 kHz - 100 kHz.

The electrostatic method covered the required frequency range and also enabled an accurate determination of Young's modulus to be made.

4.6.2 "Electrostatic" apparatus

The apparatus is shown in Figure 18.

The oscillator was a Wayne-Kerr A.F. S121 Signal Generator, covering a frequency range 1Hz to 120 kHz, in 44 overlapping bands. Stability was within 1 part in 10^4. The output signal was sinusoidal with a r.m.s. value of 2.5 volts. A Dawe 3001A Frequency Meter was used to monitor the oscillator output signal. The 'drive' voltage amplifier gave a sinusoidal output of 100 V peak-to-peak over the whole frequency range.

The signal from the detector electrode was picked up by the cathode follower which matched the high impedance of the detector electrode to

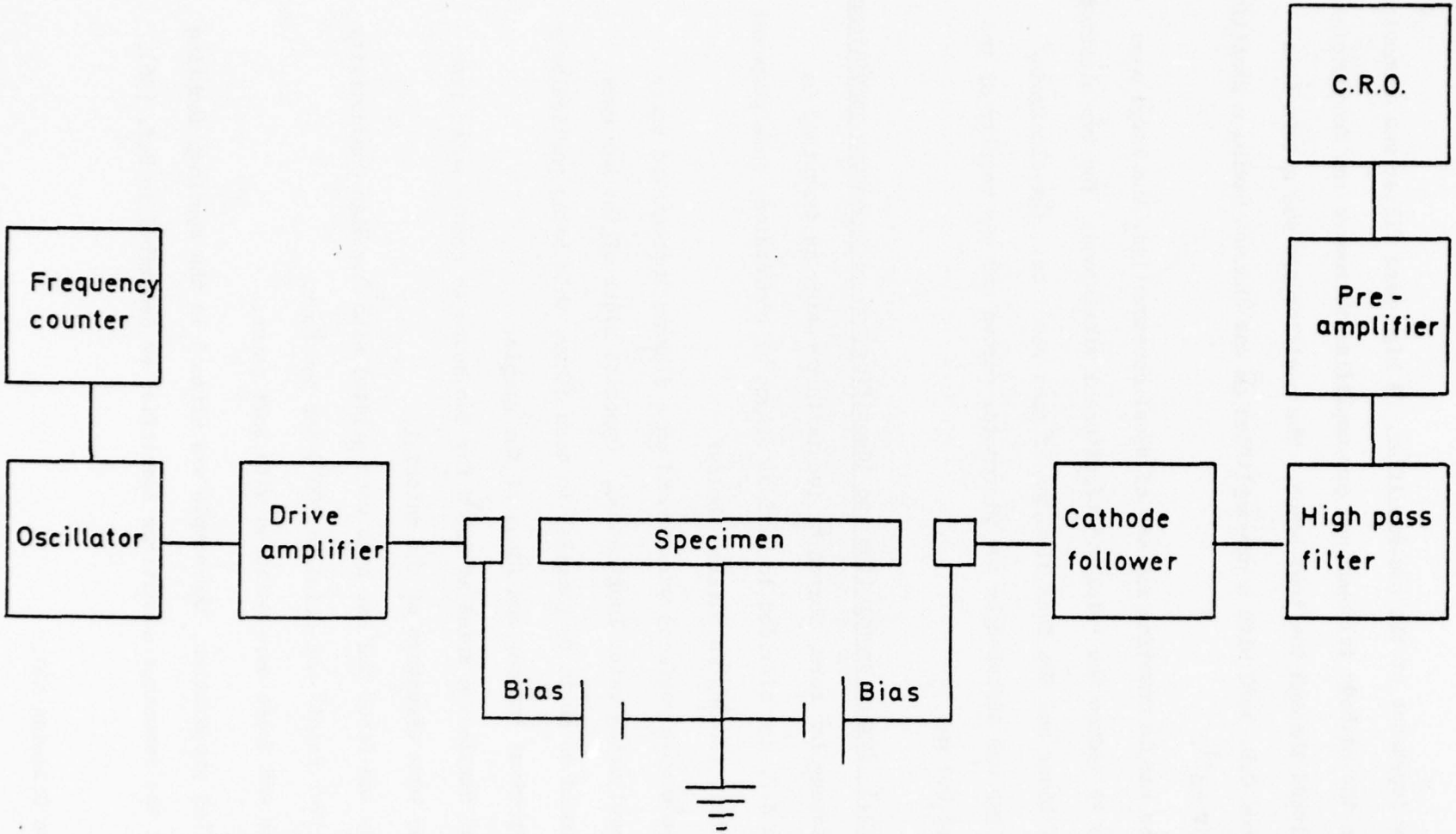


Fig.18. Electrostatic apparatus for the determination of Young's Modulus.

the low impedance of the pre-amplifier. A high-pass filter was connected between the cathode follower and pre-amplifier to remove low frequencies transmitted through the test-bench. The oscilloscope was a twin beam Solartron C.D. 1400 with a pre-amplifier on one channel having a sensitivity of 100μV cm^{-1}.

The sample mounting rig was of steel construction, the large mass helping to reduce the 'pick-up' of external vibrations. The two electrodes were of brass and the face diameter of each was 1 cm; the electrode/sample gap was adjusted by two micrometer screws and was usually of the order of 0.1 mm.

4.6.3 Sample preparation and identification of resonance conditions

Rectangular bars, formed by isostatic pressing as described in Section 4.2, and nitrided to various stages of conversion, were prepared for dynamic testing as outlined below:

1. The sample surfaces were ground on a diamond impregnated brass wheel using water lubrication. Opposite sides of the bar were ground so as to be parallel to each other, this being particularly important for the end faces of the sample.
2. The sample was dried at 100°C for two hours to remove water from the pore structure of the material.
3. The end faces and one side were painted with Dag High Conductivity Silver Paint* and dried at 100°C for one hour.
4. The end faces were polished with soft paper.

After preparation, the sample was aligned in the specimen mounting rig and the resonance conditions identified as described in Ref. (96).

*Acheson Colloids Ltd.

4.7 Determination of Modulus of Rupture

Although not a major aspect of the present study, rupture modulus was measured for all samples after Young's modulus had been determined. The same rectangular bar was used for both measurements. An Instron was used with a three-point bend jig and a crosshead speed of 0.8 mm/min.

4.8 Determination of Bulk Density

The bulk density of RBSN samples and silicon compacts was determined using a Doulton SC/3 bulk densitometer.

4.9 Microhardness Testing

A Vickers microhardness attachment with a diamond pyramid indentor was used with a Vickers M55 microscope for the determination of microhardness.

Samples were prepared by polishing on 6 μm diamond abrasive for two hours followed by 1 μm abrasive for $\frac{1}{2}$ hr., using the procedure described in Section 4.5.1.

5. RESULTS AND DISCUSSION

5.1 Characterisation of Silicon Powders

5.1.1 Silicon powder purity

The metallic impurity concentration in the three silicon powders used in the study was determined by X-ray fluorescence analysis*. The elements determined were those expected to have been introduced during the comminution and classification procedures, i.e. iron, chromium and nickel from the stainless steel shatterbox, and copper and zinc from the sieves. The concentration of aluminium was also determined as it is a common contaminant in commercial silicon powders, and such a powder, Koch-Light 99.9%, was used in the present study. The other powder samples analysed were acid-washed Monsanto silicon ($< 45\ \mu m$) and unwashed Monsanto silicon ($< 45\ \mu m$); these powders were prepared as described in Section 4.1.

The results of the XRF analysis are shown in Table 4.

Element	Powder		
	Acid-washed Monsanto concentration/ppmw	Unwashed Monsanto concentration/ppmw	Koch-Light 99.9 concentration/ ppmw
Copper	< 100	200	< 100
Nickel	< 100	< 100	< 100
Zinc	< 100	< 100	100
Aluminium	< 100	200	14,500
Chromium	< 100	< 100	< 100
Iron	30	40	3,000

Table 4: Analysis of Silicon Powders

During the microscopical examination of polished sections of the spheroidized silicon powder, large impurity concentrations were observed in some of the particles. An example of such impurity is shown in

*Carried out at the laboratories of the British Ceramic Research Association.

Figure 19, the metallic contaminant was identified as aluminium using electron-probe microanalysis.

5.1.2 Powder particle size and structure

The particle size (diameter) details of the silicon powders, as determined by a line counting, microscopical method are given in Table 5.

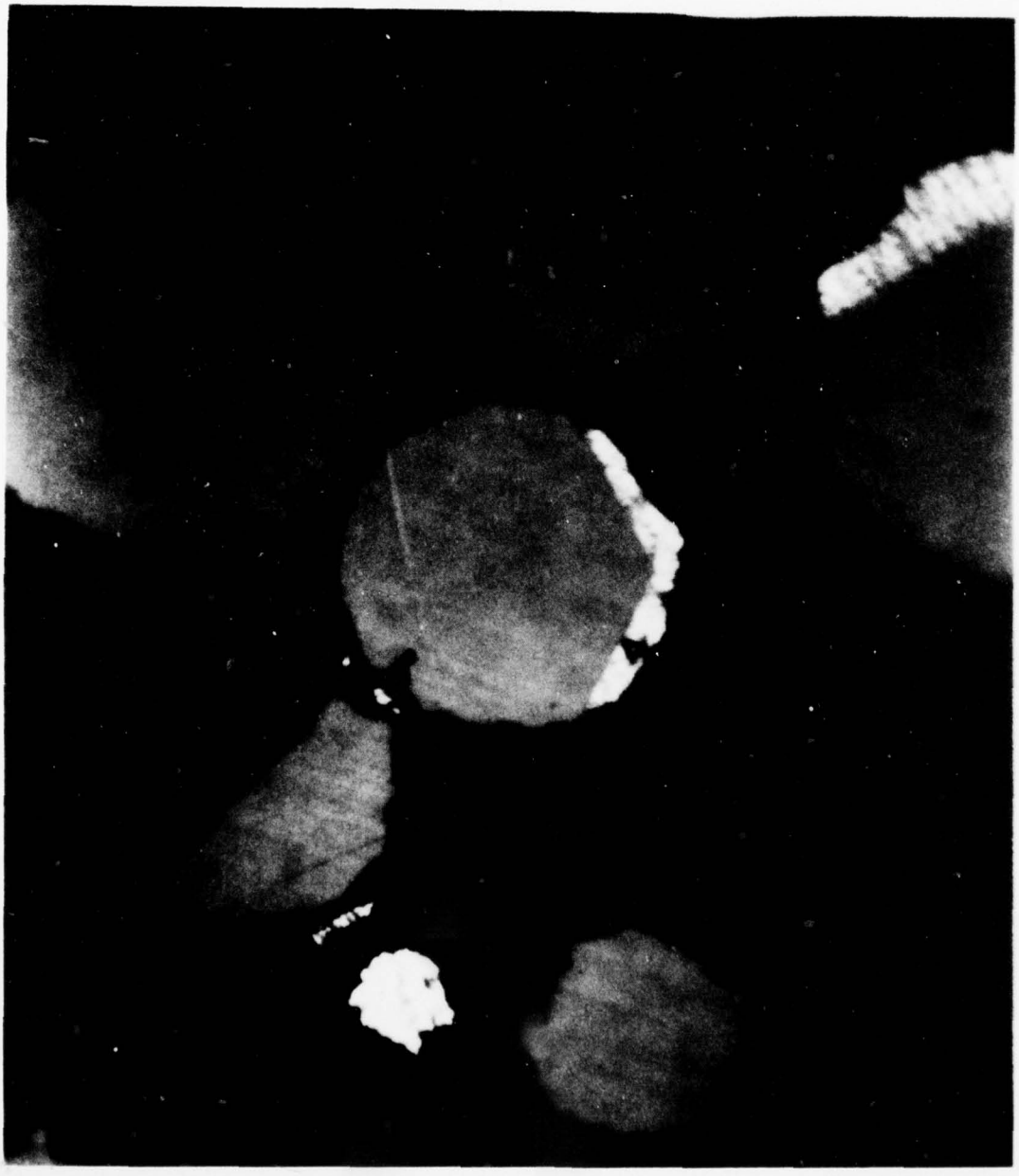
Powder	Minimum size/ μm	Mean size/ μm	Maximum size/ μm
Monsanto (Shatterbox)	-	20	45
Monsanto (Spherical)	53	-	65
Koch-Light 99.9%	-	17	45

Table 5: Particle Size of Silicon Powders

Etched polished sections of silicon particles showed that all the powders, with the exception of the spherical Monsanto, consisted of single crystal particles. The spherical particles were polycrystalline and some particles exhibited dendritic type features. Typical etched structures of the spherical particles are shown in Figure 20.

Fig. 19: Aluminium-rich impurity in spherical Monsanto silicon.

Polished section, reflected light.



60μm

Fig. 20: Grain structure of spherical Monsanto silicon. Etched in 5% NaOH solution for 3 minutes at 100°C.

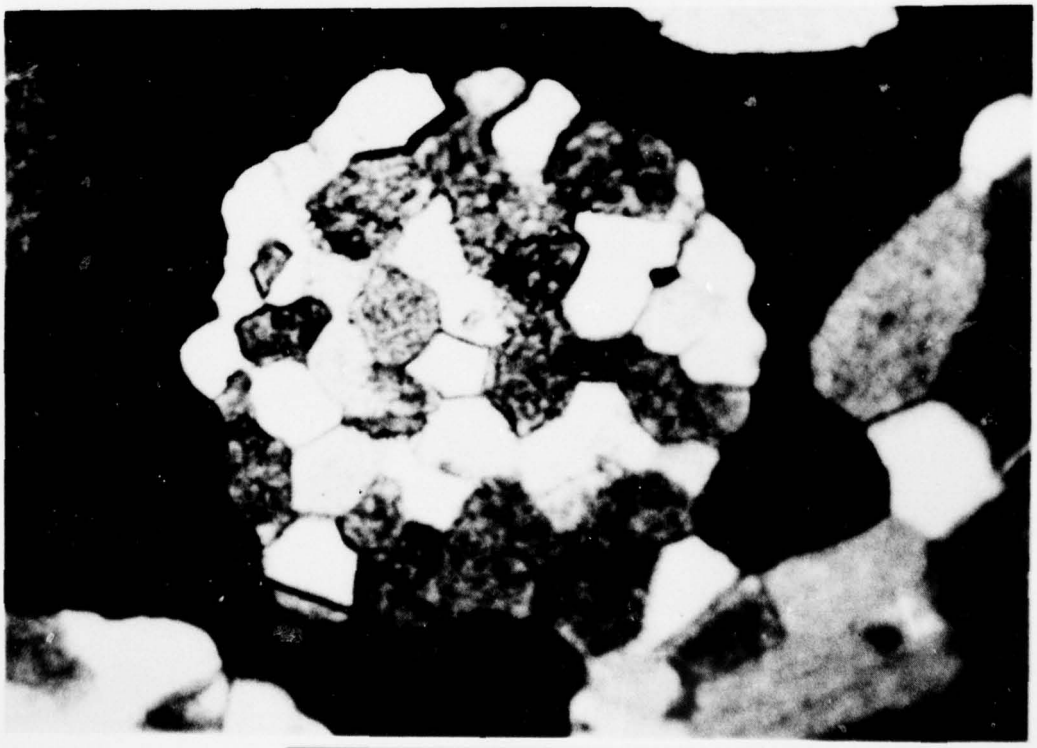
Polished sections, reflected light.

a) As spheroidized powder.

b) Nitrided in 50 torr of N_2, at 1370°C for 15 minutes.



60μm



50μm

5.1.3 Discussion

The analysis of the three silicon powders illustrates the high impurity concentration in the commercial material, i.e. 2^{w}/o metallic impurity in a powder of stated purity 99.9%. As expected, aluminium 1.45^{w}/o, and iron 0.30^{w}/o were the main impurity elements present.

The laboratory-prepared Monsanto powder has a much lower impurity concentration than the Koch-Light silicon, with the acid washed powder having a purity of >99.99%. The iron contamination from the steel shatterbox was much lower than expected in the Monsanto powder, but there is a clear indication of pick-up of copper from the sieving operation. The 200 ppm of aluminium in the unwashed powder can only be explained by aluminium being present in the original silicon ingot.

The particle size analysis of the silicon powders shows the Monsanto <45 μm powder to have a similar size distribution to the Koch-Light powder. Thus a meaningful comparison of RBSN produced from the two powders could be made.

The narrow particle size range of the spheroidized powder facilitated the interpretation of the observed microstructure of the nitrided powder; the aluminium impurity in the spherical particles, however, led to uncertainty in the interpretation of microstructure and growth morphology. The polycrystalline nature of the spherical particles might also have affected the silicon nitride formation mechanism and the resulting microstructure.

The aluminium present in the spherical powder can be attributed to the instability of the alumina tube, used in the production of the powder, under conditions of high temperature (1720°C) and a reducing atmosphere (H_2). The instability of alumina under these conditions has been demonstrated by Steele and Williams[48].

5.2 Nitridation of Silicon Powder Compacts

5.2.1 Washed Monsanto silicon powder

The reaction between silicon powder and nitrogen to form RBSN is normally carried out at a nitrogen pressure of 1 atmosphere. A previous study, however[12], has shown that for pure silicon powder complete conversion is not possible at this pressure of nitrogen. The dependence of nitridation kinetics on nitrogen pressure was therefore determined using the thermogravimetric balance.

Powder compacts of < 45 μm particle size, isostatically pressed at 140 MNm^{-2}, and having a green density of 1500 Kgm^{-3}, were reacted with pure nitrogen at 1370°C. Prior to the sample being lowered into the furnace hot-zone the system was evacuated to 5×10^{-4} torr and nitrogen then admitted until the required pressure was reached. Pressure control was achieved using the manostat in conjunction with a small nitrogen leak via a needle valve.

The results for powder compacts of mean weight 1.5 gm are shown graphically in Fig. 21. The kinetics were in agreement with the results of Atkinson et al.[12] and at any particular nitrogen pressure three kinetic regimes could be distinguished, viz. a linear regime, a regime of decreasing rate and a regime of zero rate. The time span of the linear regime was inversely proportional to nitrogen pressure with the highest conversion of silicon to silicon nitride being obtained at lower pressures of nitrogen. Conversion at 760 torr N_2 was limited to 7% and for conversions of $> 90\%$ nitrogen pressures of $\lesssim 100$ torr were found to be necessary.

In order to investigate the effect on the nitridation kinetics of the removal of the oxide layer on the silicon, the powder compacts were held in the furnace hot-zone at 1370°C in a vacuum of 5×10^{-4} torr for 20 minutes prior to nitridation. The oxygen pressure in the vicinity of

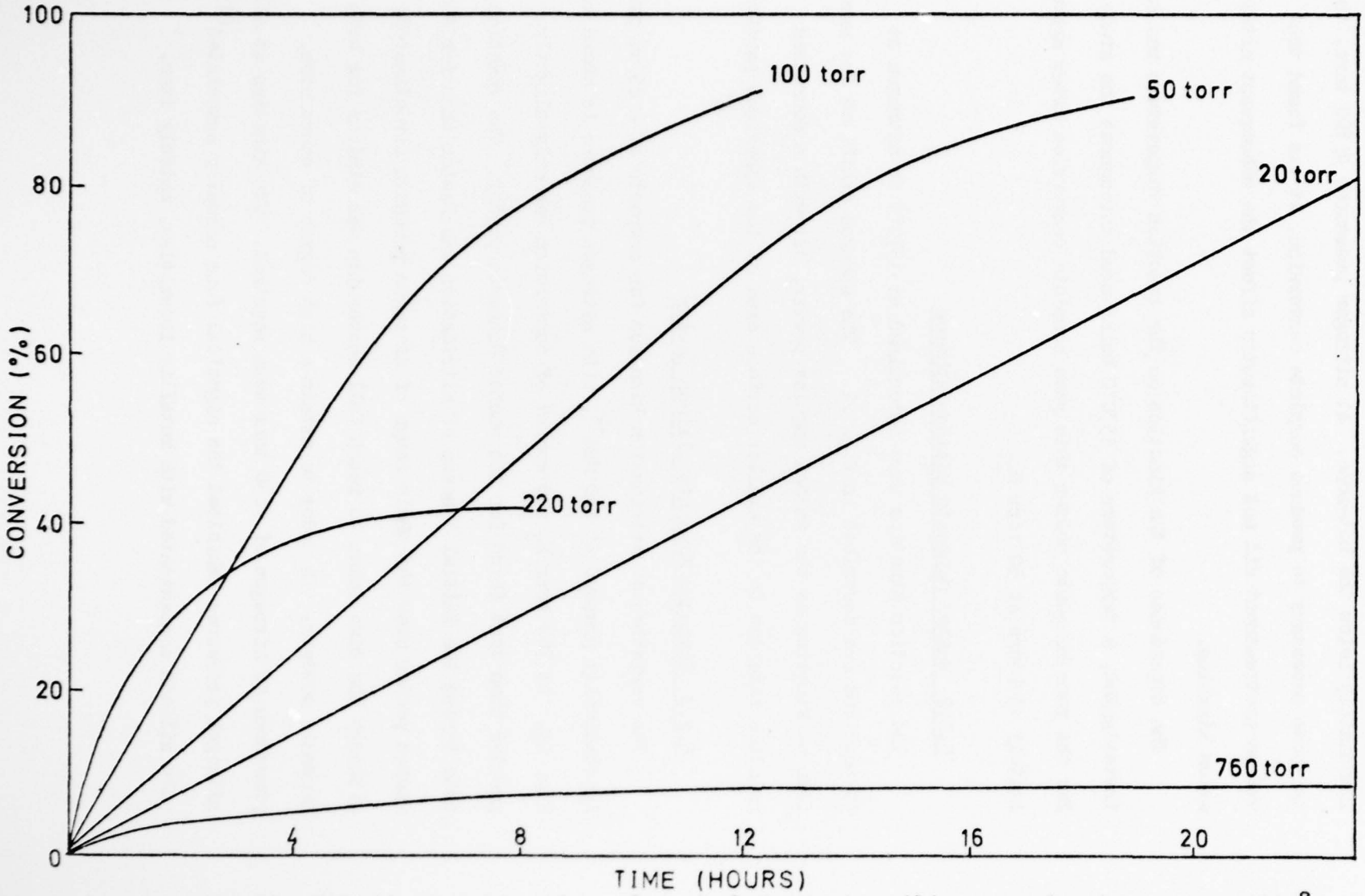


Fig.21. Nitridation kinetics of washed Monsanto silicon powder compacts, 1370°C.

the sample was lowered by the positioning of a zirconium getter immediately below the hot-zone. At nitrogen pressures $\lesssim 100$ torr, that is those necessary to produce complete conversion, it was found that vacuum pretreatment did not significantly affect the subsequent nitridation kinetics.

The dependence of the kinetics on the reaction temperature was not investigated, a temperature of 1370°C being used throughout the study. For the pure Monsanto powder this gave complete conversion after approximately 15 hours at 50 torr N_2.

5.2.2 Washed Monsanto silicon spheres

The reaction kinetics were determined at 1370°C in nitrogen at 50 torr and are described in Fig. 22. The spheres exhibited the same form of kinetics as the washed angular powder, but with a decreased reaction rate due to the smaller surface area of the spherical particles.

5.2.3 Unwashed Monsanto silicon powder

The variation of nitridation kinetics for compacts of < 45 μm powder, isostatically pressed at 140 MNm^{-2}, with nitrogen pressure is shown in Fig. 23. At 760 torr N_2 the amount of conversion was only slightly greater than that found for the washed Monsanto powder. The reaction rate during the initial 5 hours of nitridation was faster than for the washed powder over the whole range of nitrogen pressure investigated, although the time taken to reach full conversion was similar for both Monsanto powders. In order to attain a high degree of conversion, pressures of nitrogen of < 50 torr were required. The kinetics at all nitrogen pressures exhibited the sigmoidal form normally associated[45] with silicon contaminated with metallic impurities, notably iron.

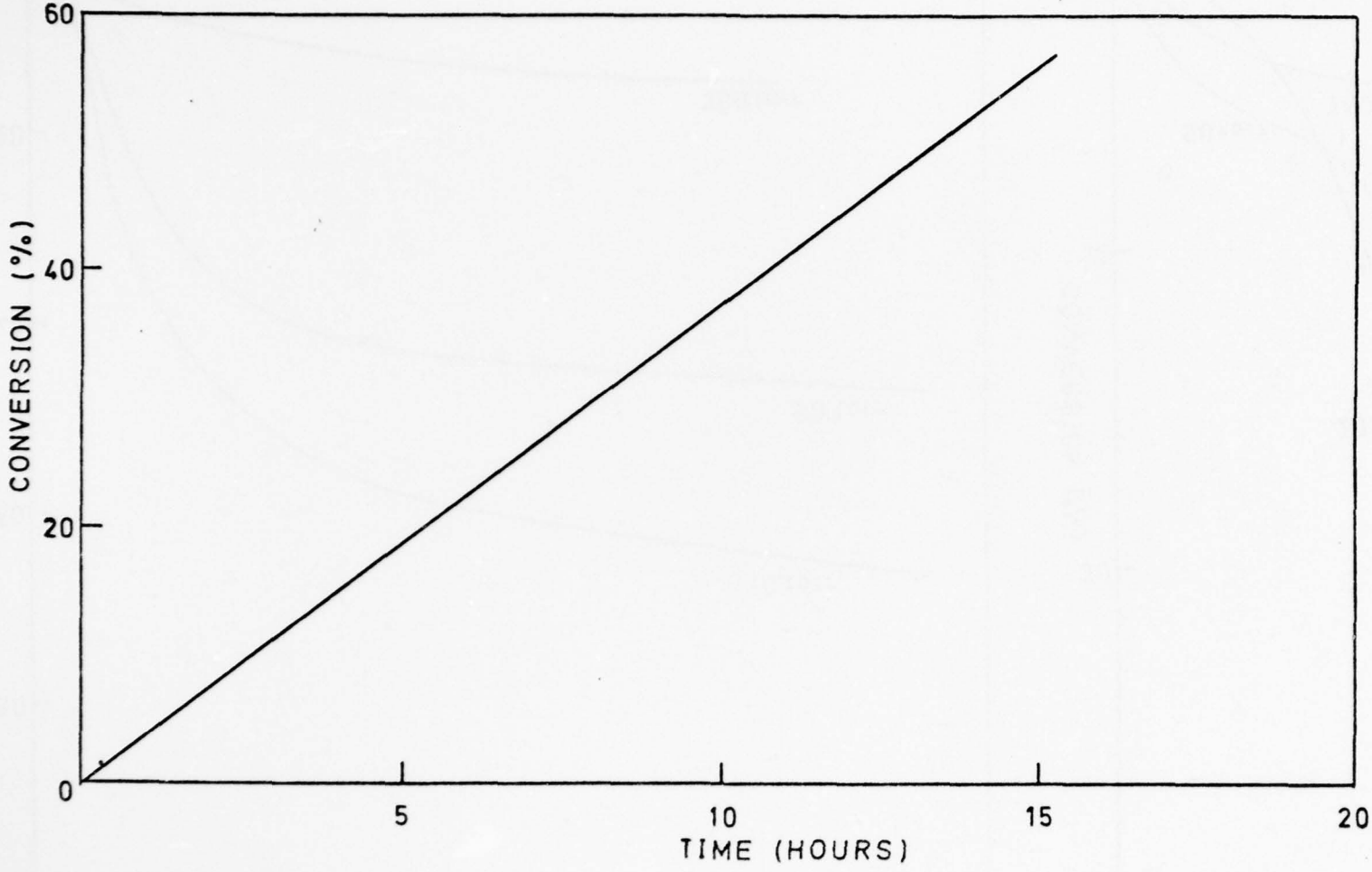


Fig.22. Nitridation kinetics of washed Monsanto silicon spheres, 1370°C, 50 torr N_2.

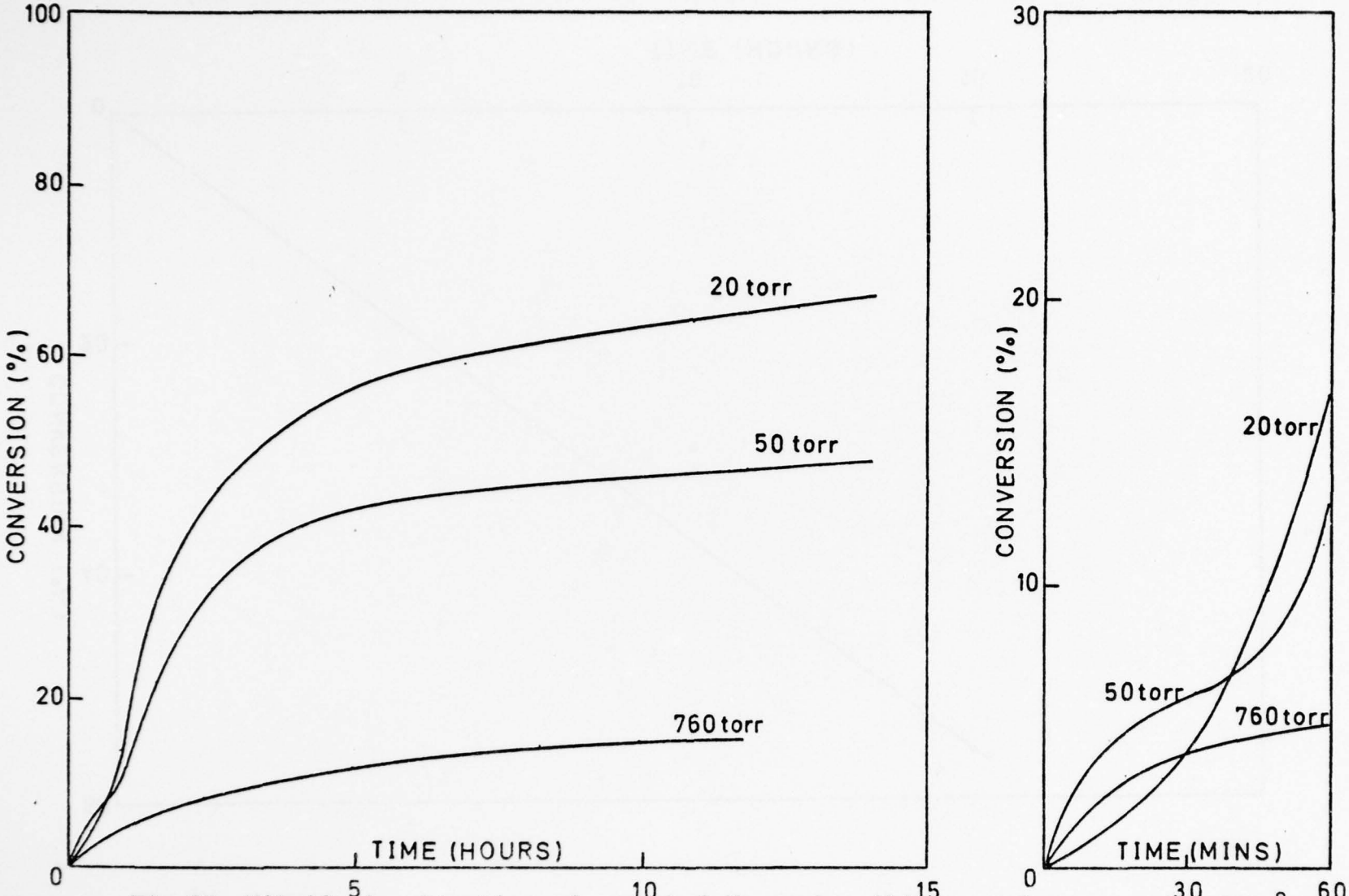


Fig.23. Nitridation kinetics of unwashed Monsanto silicon powder compacts, 1370° C.

5.2.4 Koch-Light 99.9% powder

Isostatically pressed powder compacts of particle size < 45 μm and green density 1490 Kgm^{-3} were nitrided at 1370°C in 760 torr of nitrogen. The kinetics are described in Fig. 24; they were found to obey a parabolic relationship with complete conversion being attained after approximately 50 hours.

5.2.5 Discussion

Considering the kinetics exhibited by the different types of silicon powder at 760 torr of nitrogen, the overall rate of conversion is proportional to the impurity content of the silicon, and for the two Monsanto powders, nitridation at 760 torr and 1370°C would not be suitable for the production of RBSN as only low degrees of conversion are obtained.

For the washed Monsanto powder the pressure dependence of the kinetics can be explained by the model of Atkinson et al.[12] which is described in Section 2.2.2.

In the case of unwashed Monsanto powder sigmoidal nitridation kinetics were observed and hence the situation is more complex. The duration of the induction part of the sigmoid, however, is proportional to the nitrogen pressure and probably corresponds to the removal of the surface layer of silica from the silicon particles. This has been demonstrated, for pure silicon doped with iron, by Atkinson and Moulson[59].

The parabolic kinetics exhibited by the Koch-Light powder cannot be satisfactorily explained but the high aluminium content of the powder is probably significant.

5.3 Development of Young's modulus during the nitridation of silicon powder compacts

The technique used for the measurement of the Young's modulus (E) of RBSN is that described in Section 4.6. E was measured as a function of

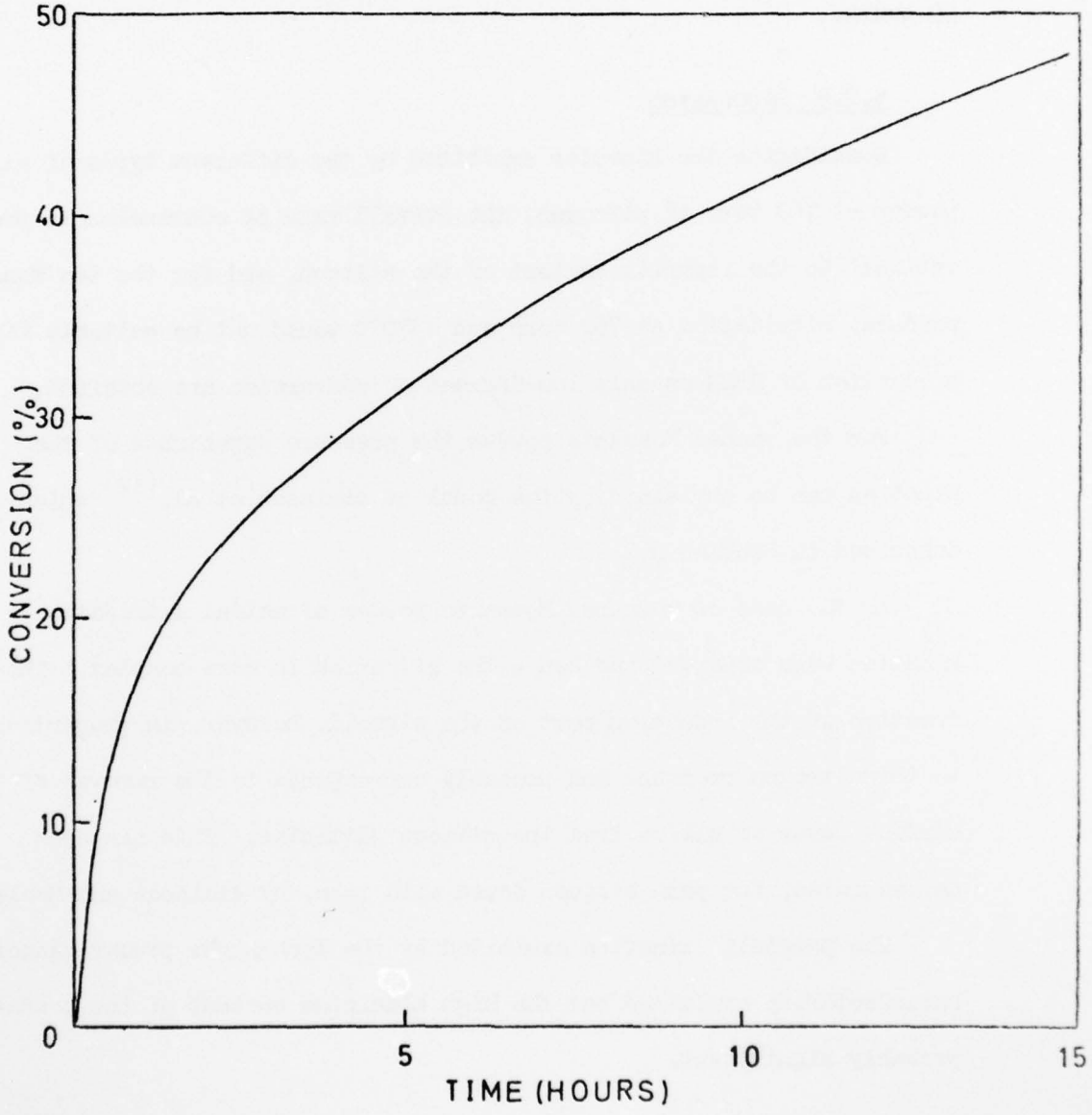


Fig.24. Nitridation kinetics of Koch-Light 99.9% silicon powder compacts, 1370°C, 760 torr N_2.

nitrided density (ρ_n) of the RBSN samples, ρ_n being a function of the amount of conversion of silicon to silicon nitride which has taken place in the powder compact.

5.3.1 Washed Monsanto silicon powder

The relationship between E and ρ_n for compacts of acid-washed Monsanto powder, <45 μm, ($\rho_g = 1500$ Kgm^{-3}), nitrided at 1370°C in nitrogen at 50 torr is shown in Fig. 25. Three different stages in the development of E can be distinguished, viz:

(1) an initial stage during which E increases very rapidly;

(2) a second stage during which E develops at a decreasing rate w.r.t. ρ_n;

and (3) a third and linear stage.

In order to determine the effect of a vacuum pre-treatment on E, compacted powder bars were heated at 1370°C in vacuo (10^{-4} torr) for times of 5–120 minutes. The modulus of the bars was then measured; the data obtained are shown in Table 6.

"Green" density/ Kgm^{-3}	Time in vacuo/ mins.	E/GNm^{-2}	Fired Density
1490	5	28	1490
1490	30	34	1490
1500	60	35	1500
1500	120	34	1500

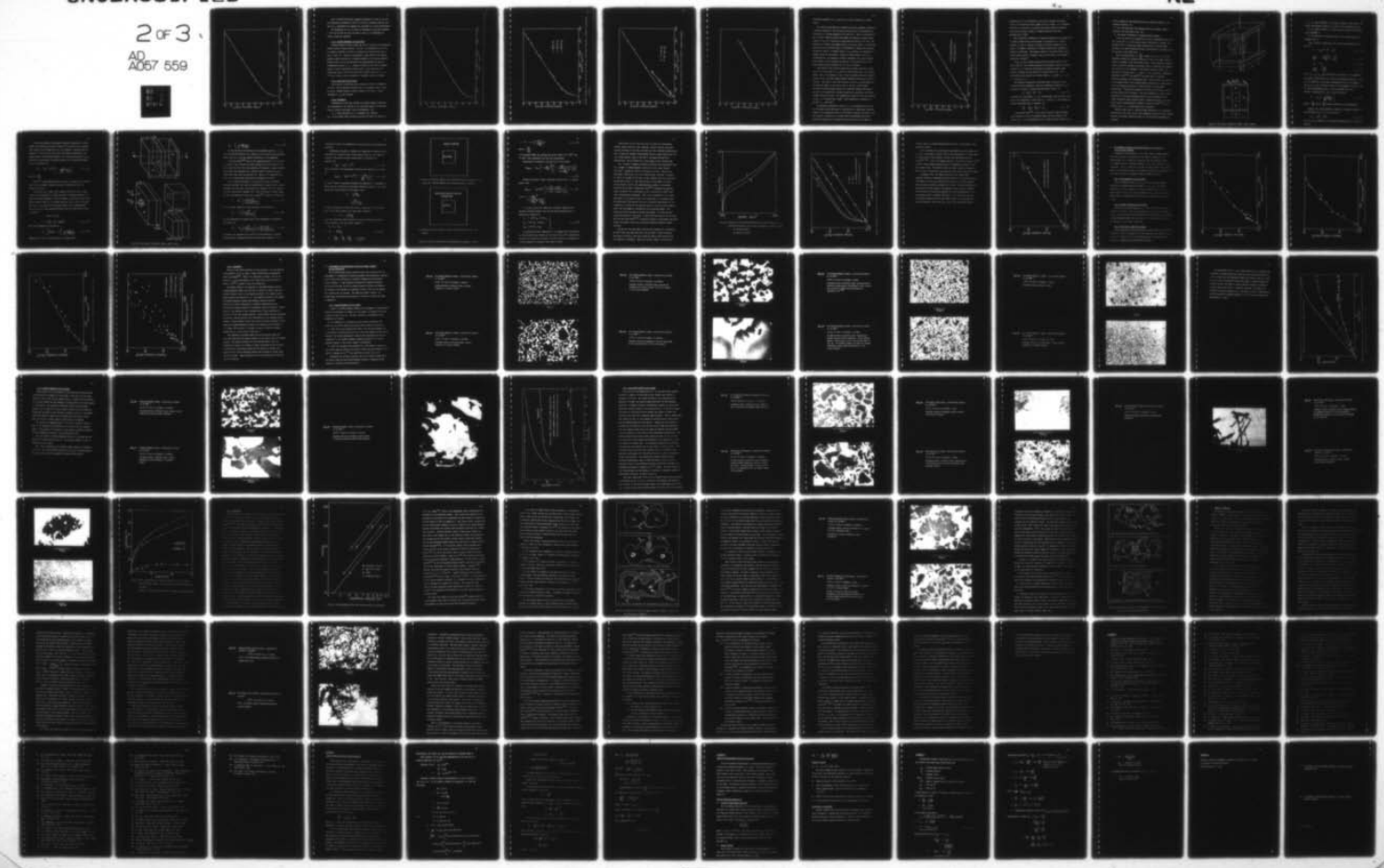
Table 6: Effect of vacuum pretreatment on Young's Modulus of Silicon Compacts

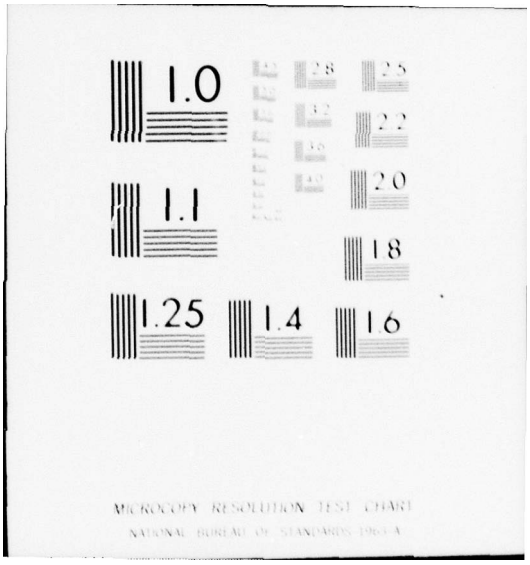
It is known that the Young's modulus of the 'green' bars was less than 6 GNm^{-2}, and therefore a significant increase in modulus occurred within 5 minutes of the introduction of the sample into the furnace. No increase in modulus was observed after the vacuum-pretreatment time exceeded 30 minutes and no densification of the samples was detected.

AD-A057 559 HOULDSWORTH SCHOOL OF APPLIED SCIENCE LEEDS (ENGLAND)--ETC F/G 11/2
THE DEVELOPMENT OF THE MECHANICAL STRENGTH OF REACTION-BONDED S--ETC(U)
APR 78 A J MOULSON, P LONGLAND DA-ERO-75-G-078

UNCLASSIFIED NL

2 OF 3
AD
A057 559




1.0
1.1
1.25
1.4
1.6
2.8
2.5
3.2
2.2
3.6
2.0
4.0
1.8
MICROCOPY RESOLUTION TEST CHART
NATIONAL BUREAU OF STANDARDS 1963-A

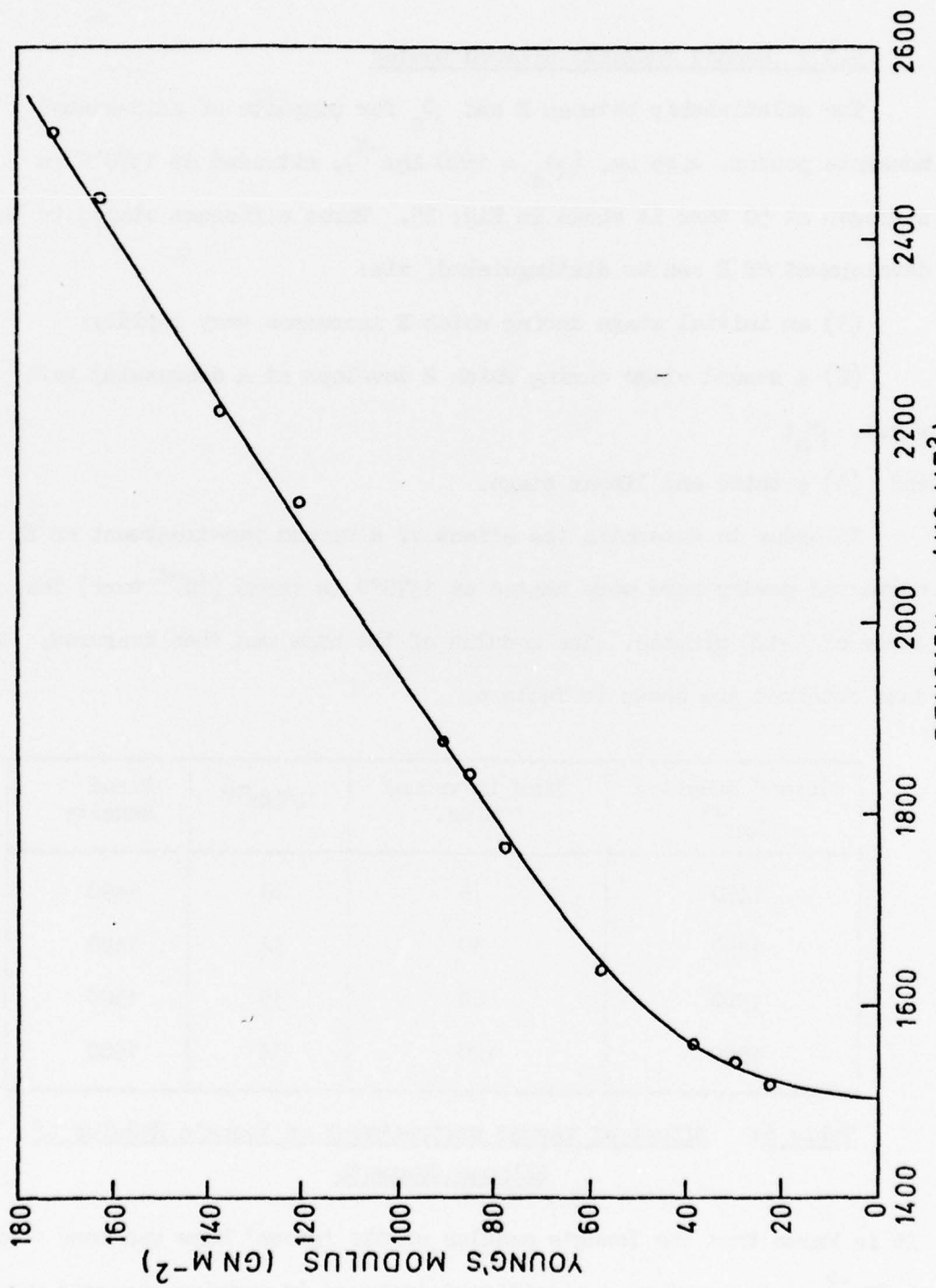


Fig.25. Young's Modulus vs nitrided density, acid washed Monsanto.

Fig. 26 shows that silicon compacts pretreated in vacuo for 30 mins. and subsequently nitrided at 1370°C in 50 torr of nitrogen exhibited the same E/ρ_n relationship as compacts not subjected to a vacuum pretreatment.

The dependence of E on ρ_n was also determined at nitrogen pressures of 100 torr and 200 torr and, as shown in Fig. 27, no difference in modulus values was detected.

5.3.2 Unwashed Monsanto silicon powder

Unwashed Monsanto silicon powder was used in the form of isostatically pressed compacts (powder fraction <45 μm). The dependence of E on ρ_n for compacts nitrided at 1370°C in nitrogen at 50 torr and 760 torr is shown in Fig. 28. A similar relationship to that found for the washed Monsanto powder nitrided at a nitrogen pressure of 50 torr was observed. Modulus values for the two materials were approximately the same at corresponding values of ρ_n. Compacts nitrided in 760 torr of nitrogen showed a linear relationship between E and ρ_n with the value of E approaching that of the 50 torr material at higher values of ρ_n. At 760 torr, however, only low degrees of conversion could be attained.

5.3.3 Koch-Light 99.9% powder

Isostatically pressed bars were nitrided at 1370°C in nitrogen at 760 torr. The relationship between E and ρ_n is shown in Fig. 29 and, as for the unwashed Monsanto powder nitrided at 760 torr, a linear dependence on ρ_n was observed.

5.3.4 Discussion

Considering all the data obtained for Young's modulus values and their dependence on the density of the nitriding compact, two distinct forms of modulus development can be distinguished, viz:

(1) a linear dependence on ρ_n throughout the reaction,

and (2) an initial large increase in modulus followed by a region of

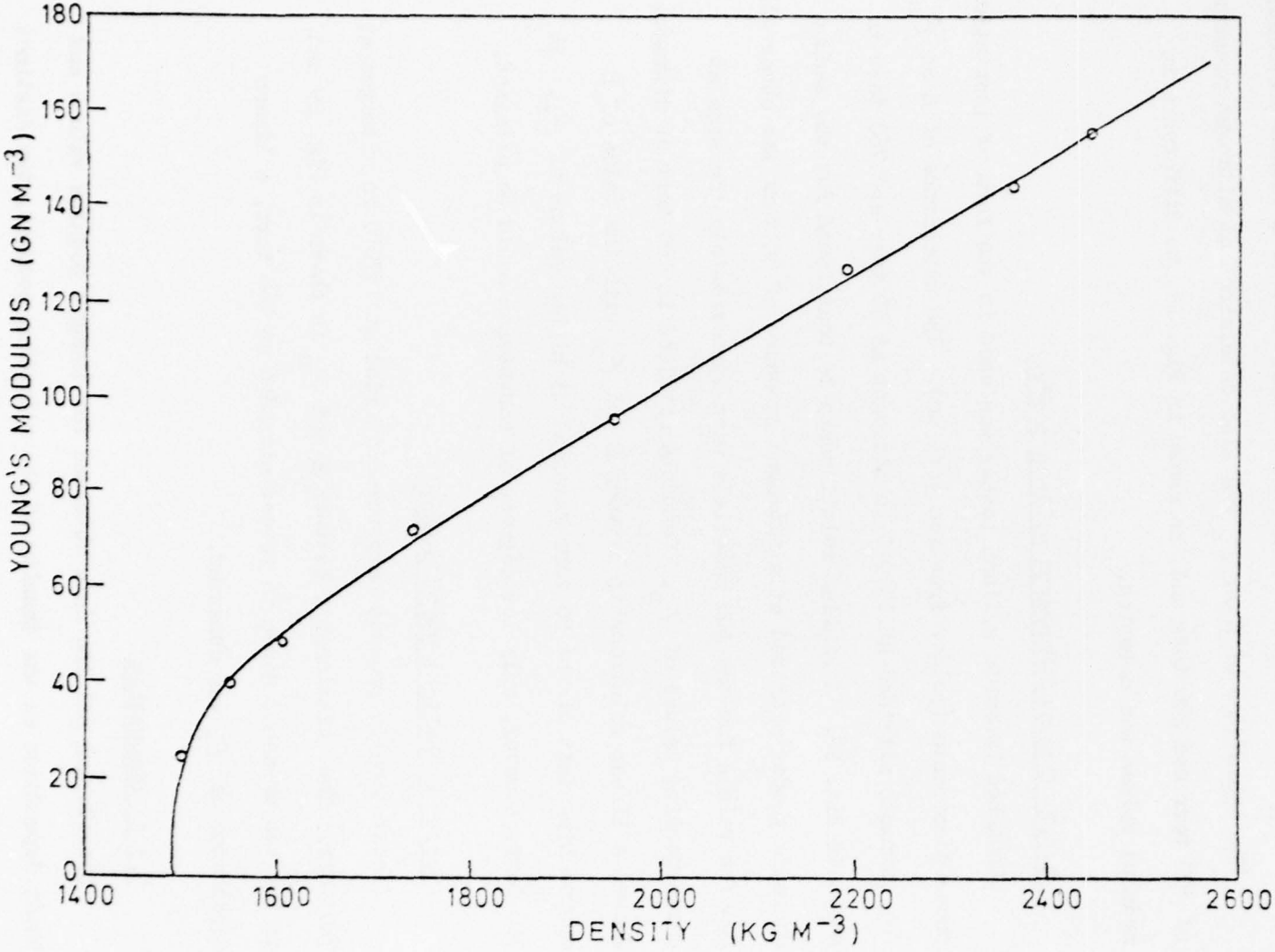


Fig.26. Young's Modulus vs nitrided density, acid-washed Monsanto with vacuum pre-treatment.

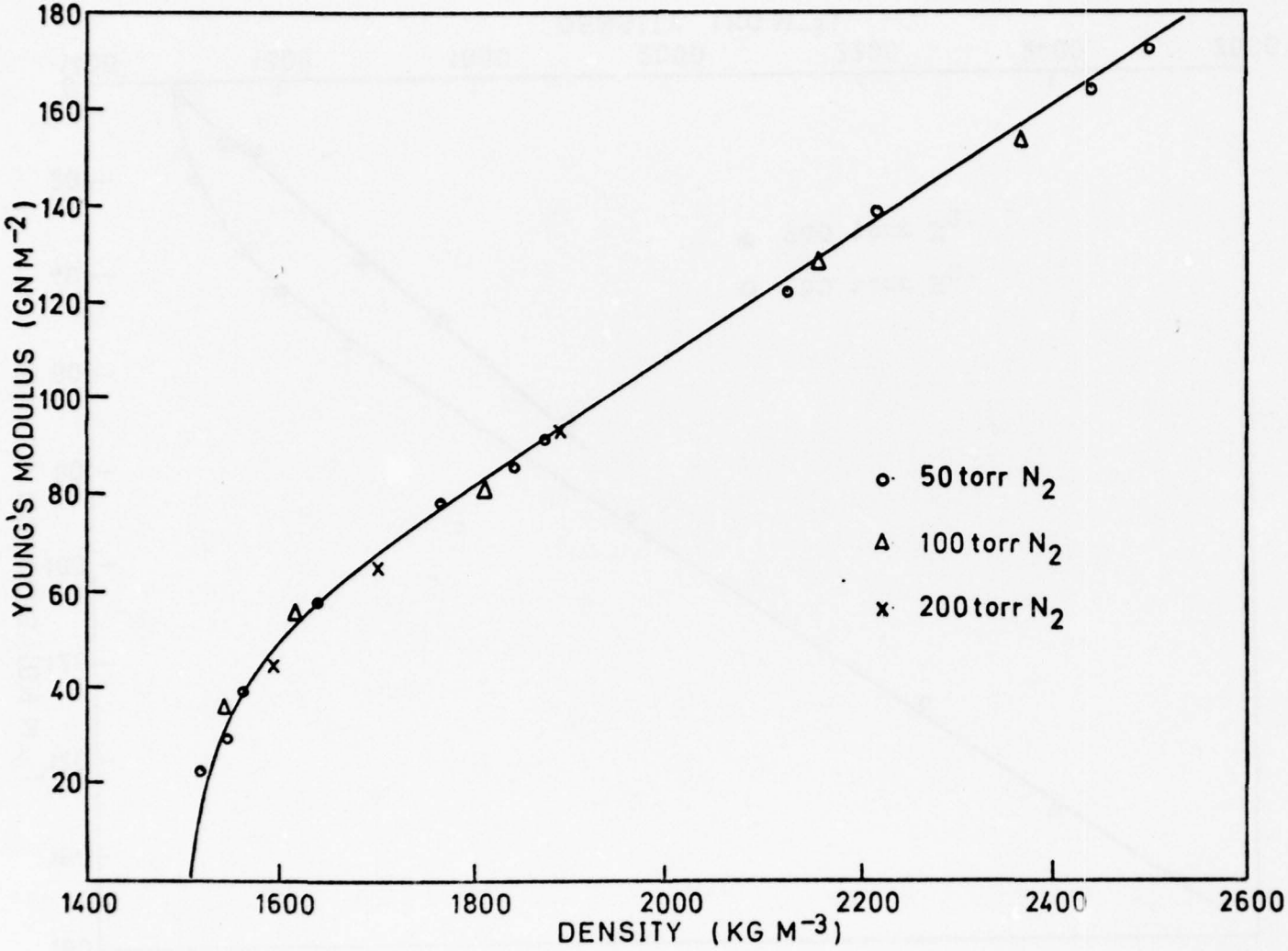


Fig.27. Young's Modulus vs nitrided density, acid-washed Monsanto, effect of nitrogen pressure.

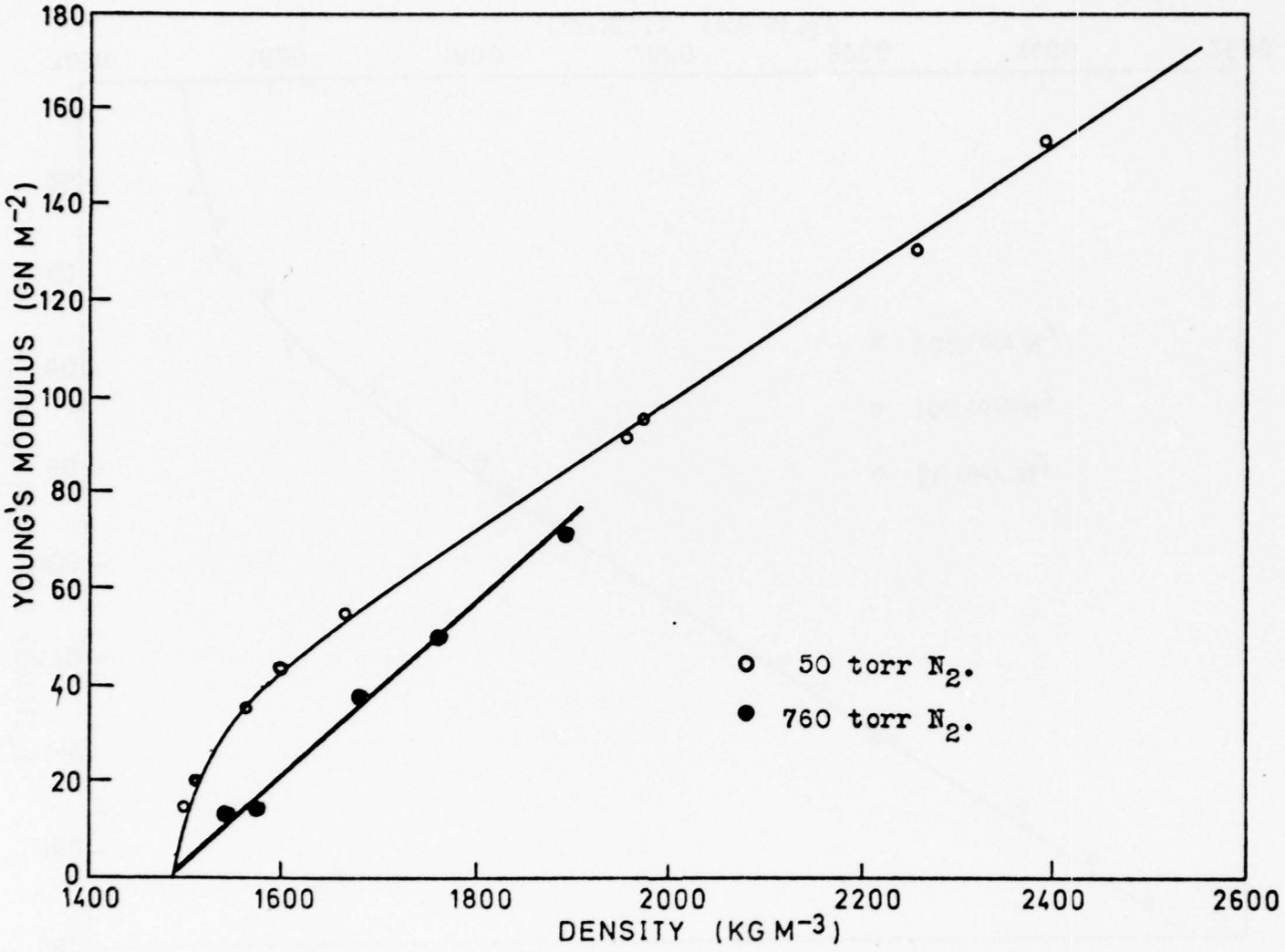


Fig.28. Young's Modulus vs nitrided density, unwashed Monsanto.

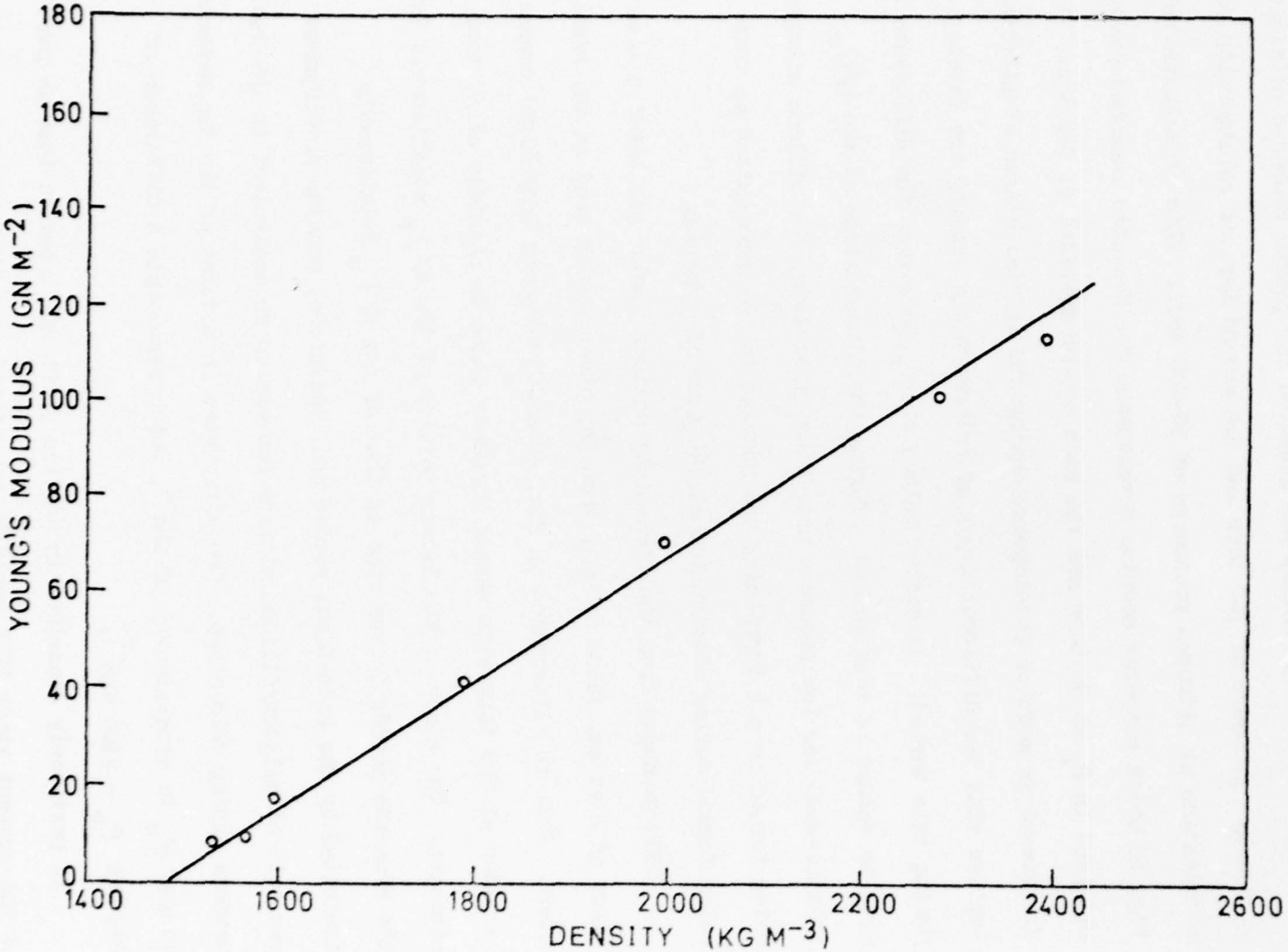


Fig.29. Young's Modulus vs nitrided density, Koch-Light 99.9%.

decreasing dependence on ρ_n which is, in turn, followed by a linear region.

The linear relationship was observed for powder compacts nitrided at a nitrogen pressure of 760 torr and the second type of relationship for nitridation at nitrogen pressures of 50-200 torr. This is illustrated in Fig. 28 which compares modulus development for Monsanto unwashed powder nitrided in N_2 at 50 torr and the same powder nitrided at 760 torr. The difference in modulus development during the initial stages of nitridation implies that two different types of interparticle bonding are developing during this period. At higher values of ρ_n, however, the difference in modulus values is less marked. During the linear stage of the E/ρ_n relationship for low pressure nitriding, therefore, the silicon nitride being formed is not increasing the modulus to the same extent as that being formed during nitridation at 760 torr of nitrogen.

RBSN produced from the Koch-Light silicon powder exhibited a lower value of E at any value of ρ_n, than any other powder used in the present study. This is illustrated in Fig. 30 which compares Koch-Light compacts nitrided at 760 torr with washed Monsanto compacts nitrided at 50 torr of nitrogen. The slope of the linear portion of the E/ρ_n relationship for the Monsanto powder is the same as that of the E/ρ_n relationship exhibited by the Koch-Light powder and, therefore, modulus development per unit of silicon/silicon nitride conversion is equivalent in the two powders during this stage. The difference in modulus of the two materials at any ρ_n is consistently 30 GNm^{-2}, which represents a difference of 20% for ρ_n = 2400 Kgm^{-3}.

As previously described in Section 3, it was intended that as part of the present study RBSN would be considered as a three-phase composite material, the components being silicon nitride, porosity and silicon, and that through a combination of Young's modulus measurement and microstructural examination at stages during the reaction to form RBSN, an

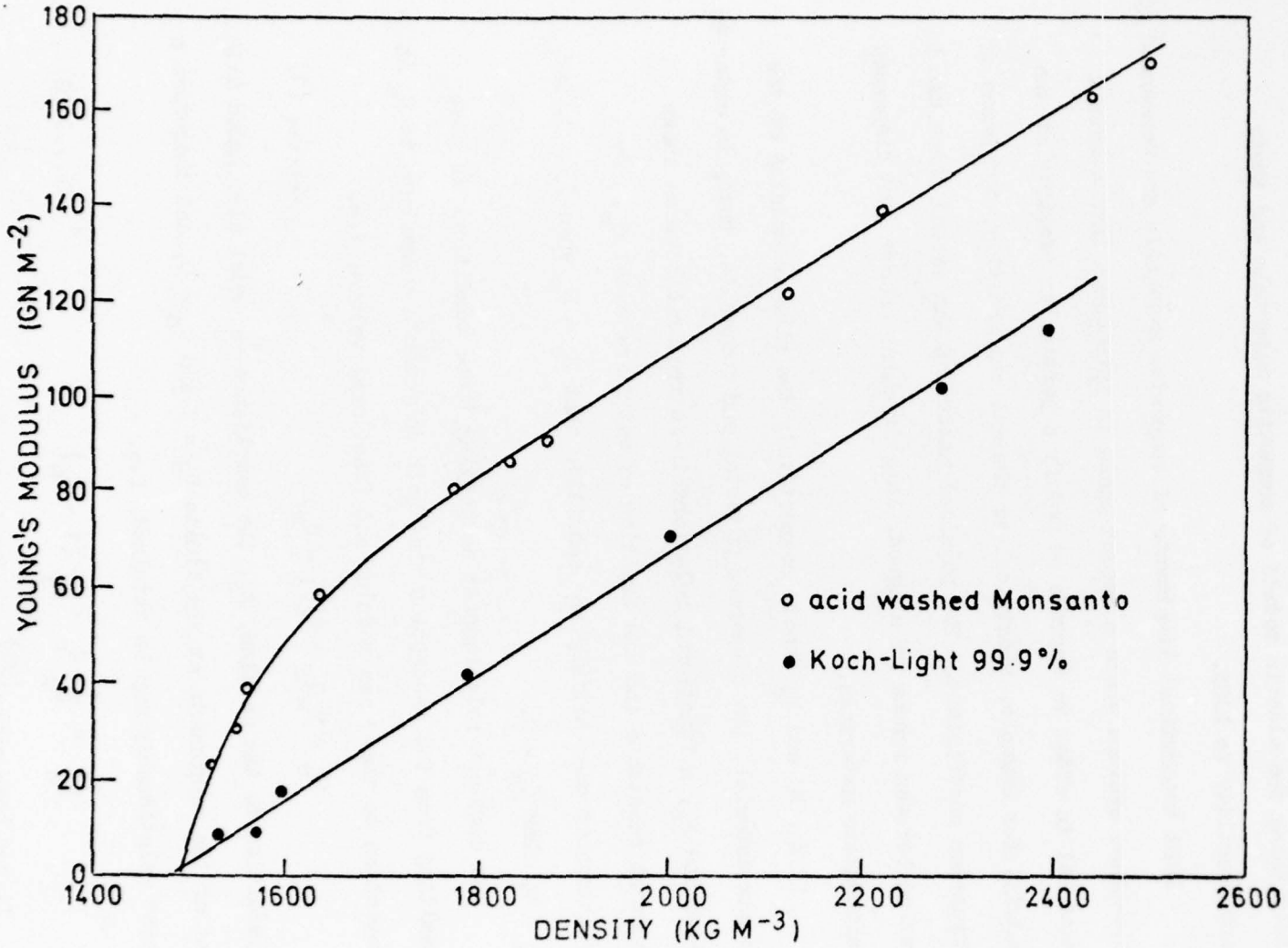


Fig.30. Young's Modulus vs nitrided density, comparison of Koch-Light 99.9% and acid-washed Monsanto.

understanding of how interparticle bonding and strength development occurs in the reacting silicon compact would be sought. It is therefore convenient at this point to consider the various theoretical models describing the elastic moduli of composite materials and their applicability to RBSN.

Most theoretical treatments of composite materials are concerned with two-phase systems where a second phase is introduced into a matrix material in order to improve or modify a particular property of the matrix, for example, electrical or thermal conductivity, toughness or expansion coefficient. The physical nature of the second phase can be varied between random or aligned, long or shirt fibres, and dispersed particulate materials.

If E_m, E_f and E_c denote respectively the elastic modulus of the matrix material, the dispersed material and composite, then, in order to determine E_c, a functional relationship is required between these material constants and the fraction of matrix material C_m. The relationship must satisfy the condition that $E_c = E_m$ when $C_m = 1$, and $E_c = E_f$ when $C_m = 0$.

The simplest relationship satisfying these conditions is that resulting from the assumption that both components contribute to E_c in proportion to their own modulus and fractional volume, i.e.

$$E_c = E_m C_m + E_f(1 - C_m) \qquad \ldots\ldots\ldots (1)$$

In addition to the modulus, E_c, the compliance $\frac{1}{E_c}$ must also agree with that of the components at the limits $C_m = 1$ and $C_m = 0$, and therefore a second relationship may be obtained, i.e.

$$\frac{1}{E_c} = \frac{1}{E_m} C_m + \frac{1}{E_f} (1 - C_m) \qquad \ldots\ldots\ldots (2)$$

It has been shown[98], on the basis of elastic energy theorems, that equations (1) and (2) represent upper and lower bounds on the value of E_c. In the determination of the upper and lower bounds on E_c,

certain assumptions are necessary which are generally applied to all composite theories, viz:

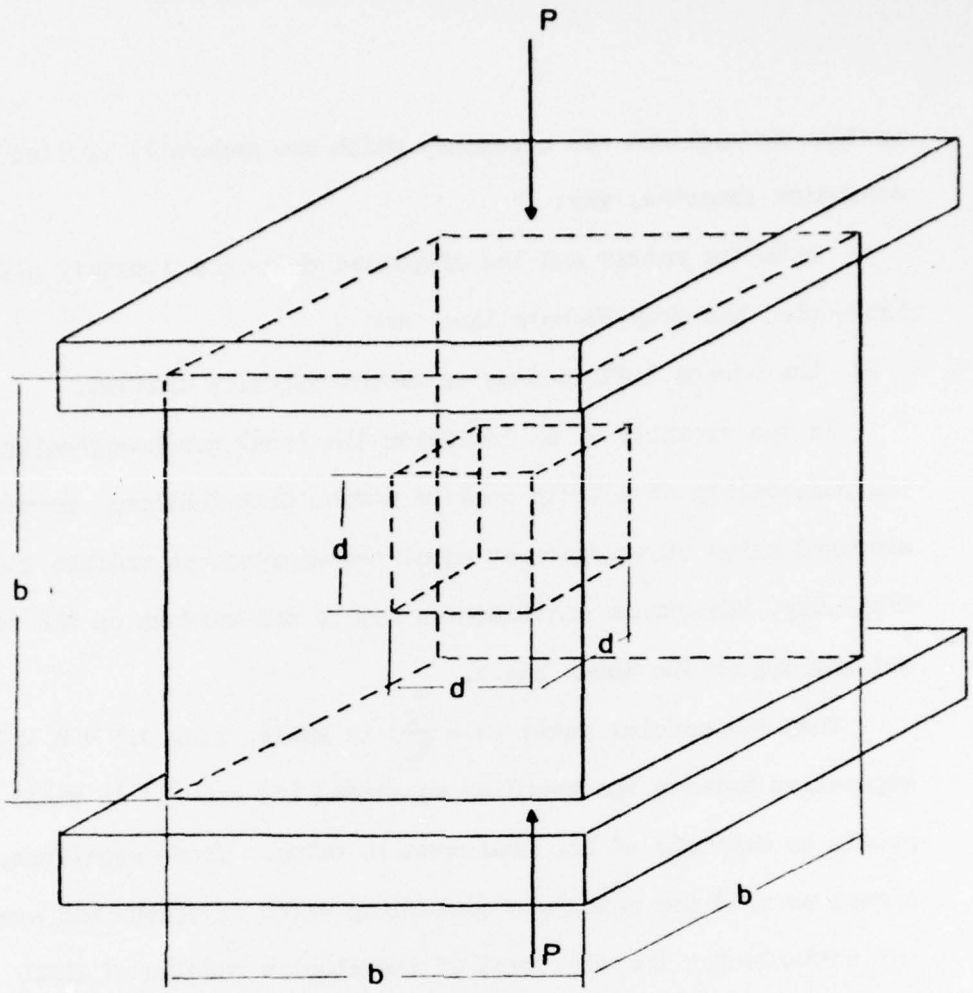
1) both the matrix and the dispersed phase are linearly elastic, isotropic, and obey Hooke's law; and

2) the stress distribution is macroscopically uniform.

In the vicinity of an inclusion the local non-homogeneity rules out the possibility of a truly uniform stress distribution; however, the averaged value of stress must equal the macroscopic uniform stress. Similarly, the strain distribution may be non-uniform on the small scale, but uniform on the large scale.

When the modular ratio ($m = \frac{E_f}{E_m}$) is small, i.e. $0.5 < m < 3$, the separation between the bounding equations (1) and (2) is small enough to obtain an estimate of the true modulus value. These equations, however, cannot be used for materials containing voids or cracks and are therefore not suitable for the treatment of the elastic modulus of RBSN. For composites of modular ratio $m < 1$ and $m = 0$ (i.e. porosity), approximate solutions by Paul[98] and Ishai[99] have been used in comparing predicted behaviour with experimental data. Paul and Ishai both resorted to a two-phase model of an isolated particle embedded in a cubic matrix with the boundaries subjected to uniform stress or displacement respectively. The specific geometry of the model has nothing to do with the real shape of the inclusion. The basic assumption is that a system consisting of discrete dispersed particles can be represented by a single continuous phase confined within a homogeneous matrix. The cubic model has been experimentally verified by Ishai and Cohen[100] for the modular limit, $m = 0$, using porous epoxy composites.

Ishai's model, Fig. 31, assumed normal deformation of the specimen surface (as is the case with any cube compressed between two rigid planes). Dividing the element vertically (Fig. 31) the following conditions are apparent:



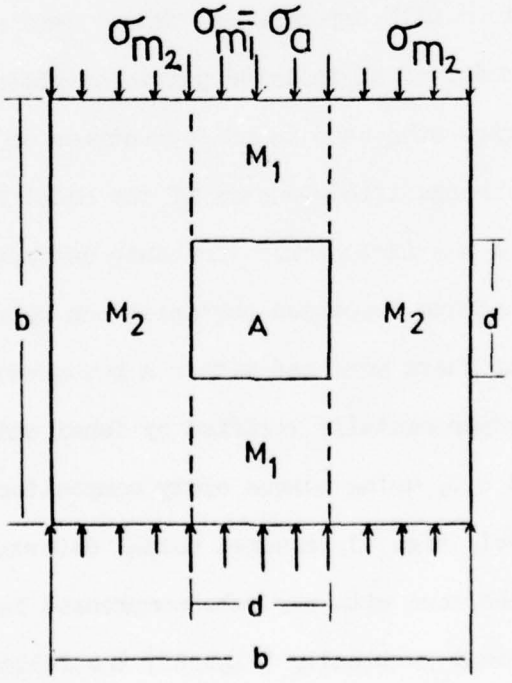


Fig.31. Two-phase composite model, after Ishai.

(a) The axial deformation of the whole element is also that of the central heterogeneous column (A, m_1) and of the encompassing box m_2.

(b) The stress on matrix m_1 in the column is equal to that acting on the aggregate A.

(c) The resultant of stresses acting on both columns equals the external force P.

Under the above assumptions, the following relationships can be derived:

$$P = \sigma_{m_2} (b^2 - d^2) + \sigma_a d^2 \qquad \ldots\ldots (3)$$

$$\frac{\sigma_{m_2} b}{E_m} = \frac{\sigma_{m_1} (b-d)}{E_m} + \frac{\sigma_a d}{E_a} \qquad \ldots\ldots (4)$$

$$\sigma_{m_1} = \sigma_a \qquad \ldots\ldots (5)$$

$$\frac{Pb}{b^2 E_c} = \frac{\sigma_{m_2} b}{E_m} \qquad \ldots\ldots (6)$$

where σ_a, σ_{m_1}, σ_{m_2} are respectively the stresses on the aggregate, the material above and below it, and the encompassing material; b and d are the dimensions of the large heterogeneous cube and the aggregate, and E_a, E_m, E_c are the Young's moduli of the aggregate, the matrix, and the whole heterogeneous cube; P is the external axial force.

Solution of equations (3), (4), (5) and (6) yields:

$$E_c = E_m \left[1 + \frac{C_f}{\frac{m}{m-1} - \sqrt[3]{C_f}} \right] \qquad \ldots\ldots (7)$$

where $m = \frac{E_a}{E_m}$ and $C_f = \frac{d^3}{b^3}$ (volume concentration of the aggregate).

Equation (7) can be modified to describe a two-phase composite of void and matrix ($E_a = 0$, $m = 0$) as follows:

$$E_{cv} = E_m (1 - C_p^{*\frac{2}{3}}) \qquad \ldots\ldots (8)$$

where E_{cv} is the modulus of the matrix-void system and C_p^* is its void content.

We can now consider a three-phase composite consisting of a cubic matrix with modulus E_{cv} and void content Cp^* in which a cubic inclusion with modulus E_a and volume fraction C_a is embedded. Assuming that the presence of the filler does not affect the elastic properties of the porous matrix, the resultant modulus of the three-phase system, E_{c3}, is obtained by substituting the reduced modulus of the matrix-void system for E_m in equation (7):

$$E_{c3} = E_m(1 - Cp^{*\frac{2}{3}}) \left[1 + \frac{C_a}{\frac{m^*}{m^*-1} - \sqrt[3]{C_a}} \right] \qquad \ldots\ldots\ldots (9)$$

where $m^* = \frac{E_a}{E_{cv}}$.

Paul's[98] approximate solution is based on the same cubic configuration but the boundary condition is that of uniform stress and is derived as follows:

The typical unit volume of the composite as used by Paul is shown in Fig. 32 and consists of a single particle of dispersed material in a cube of the matrix material. Since the strain is uniform over the cross-section shown in Fig. 32, the normal stress on area A_1 will be εE_m and that on A_2, εE_a, where ε is the normal strain at the cross-section. The total force on the cross-section must equal the total applied force, F, therefore

$$F = E_m \varepsilon A_1 + E_a \varepsilon A_2$$

$$\therefore \qquad F = \varepsilon \left[E_m + (E_a - E_m)A_2 \right] \qquad \ldots\ldots\ldots (10)$$

The total elongation of the cube is:

$$\delta = \int_0^1 \varepsilon(x)dx = F \int_0^1 \frac{dx}{E_m + (E_a - E_m)A_2} \qquad \ldots\ldots\ldots (11)$$

Defining E_c as F/δ for the unit cube, it follows that:

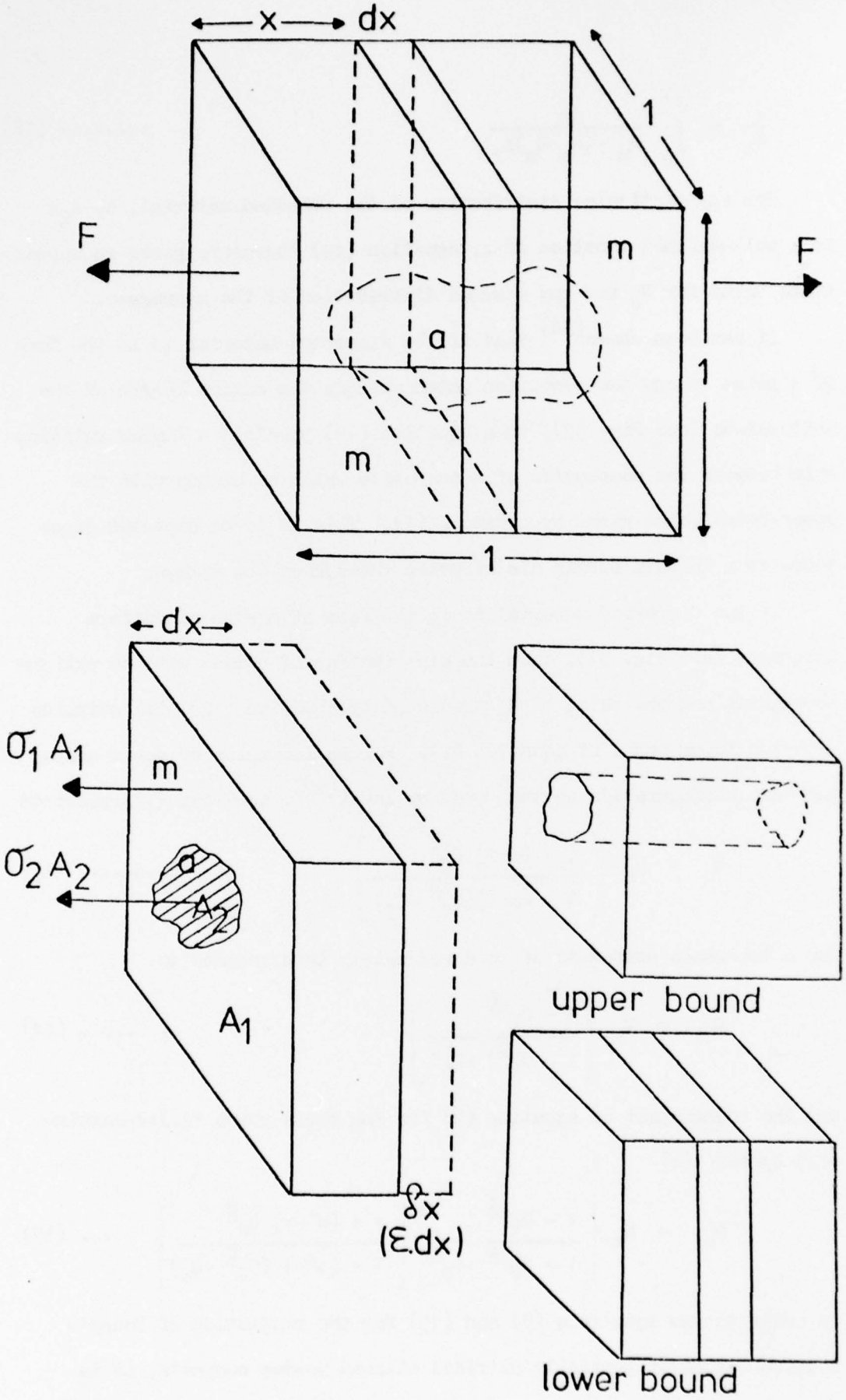


Fig.32. Two-phase composite model, after Paul.

$$\frac{1}{E_c} = \int_0^1 \frac{dx}{E_m + (E_a - E_m)A_2} \qquad \text{..... (12)}$$

For any particular distribution of the embedded material, a, A_2x is a well-defined function of x, equation (12) therefore gives an approximate value for E_c for any assumed distribution of the aggregate.

It has been shown[98] that if the dispersed material is in the form of a prism of any cross-section which extends the entire length of the unit volume (see Fig. 32), then equation (12) predicts a linear relationship between the components of a composite which coincides with the upper-bound value given by equation (1). This is to be expected since there is a uniform strain distribution throughout the volume.

If the dispersed material is in the form of a slab of uniform thickness (see Fig. 32), then the distribution of stress will be uniform throughout and the value of E_c predicted by equation (12) will coincide with the lower-bound of equation (2). For an inclusion of cubic shape, the same configuration as that used by Ishai[99], equation (12) predicts

$$E_c = E_m \left[\frac{1 + (m-1)\, C_f^{\frac{2}{3}}}{1 + (m-1)(C_f^{\frac{2}{3}} - C_f)} \right] \qquad \text{..... (13)}$$

For a two-phase composite of void and matrix this reduces to:

$$E_{cv} = E_m \left[\frac{1 - C_p^{*\frac{2}{3}}}{1 - C_p^{*\frac{2}{3}} + C_p^*} \right] \qquad \text{..... (14)}$$

and the counterpart of equation (9) for the three-phase filler-matrix-void system is:

$$E_{c3} = E_m \left[\frac{1 - C_p^{*\frac{2}{3}}}{1 - C_p^{*\frac{2}{3}} + C_p^*} \right] \left[\frac{1 + (m^*-1)\, C_a^{\frac{2}{3}}}{1 + (m^*-1)(C_a^{\frac{2}{3}} - C_a)} \right] \qquad \text{... (15)}$$

In order to use equations (9) and (15) for the prediction of Young's modulus values of partially nitrided silicon powder compacts, it is

necessary to adjust the equations for a silicon-silicon nitride-porosity composite.

Considering the model to consist of an aggregate of residual silicon surrounded by a porous silicon nitride matrix (see Fig. 33), then the modulus of the porous silicon nitride matrix is obtained from equation (8):

$$E_{PSN} = E_{SN}(1 - C_p^{*\frac{2}{3}}) \qquad \ldots\ldots\ldots (16)$$

and the modulus of the three-phase composite from equation (9) is given by:

$$E_{PSN-Si} = E_{SN}(1 - C_p^{*\frac{2}{3}}) \left[1 + \frac{C_{Si}}{\frac{m^*}{m^*-1} - C_{Si}^{\frac{1}{3}}} \right] \qquad \ldots\ldots\ldots (17)$$

C_p^* and m^* cannot be determined directly and therefore it is necessary to define them as a function of more easily determined factors. C_p^* is the fractional volume porosity of the matrix, hence

$$C_p^* = \frac{V_p}{V_p + V_{SN}}$$

$$= \frac{V_p/V}{V_p/V + V_{SN}/V}$$

in which V_x denotes the fractional volume of component x in the matrix and V is the total volume of the three-phase composite.

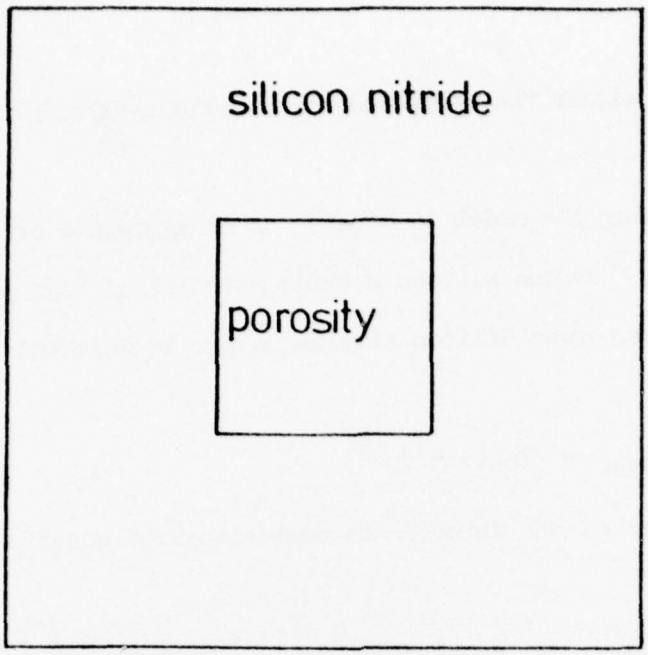
$$\therefore \quad C_p^* = \frac{C_p}{C_p + C_{SN}}$$

C_p is the fractional volume porosity and C_{SN} the fractional volume of silicon nitride in the three-phase composite.

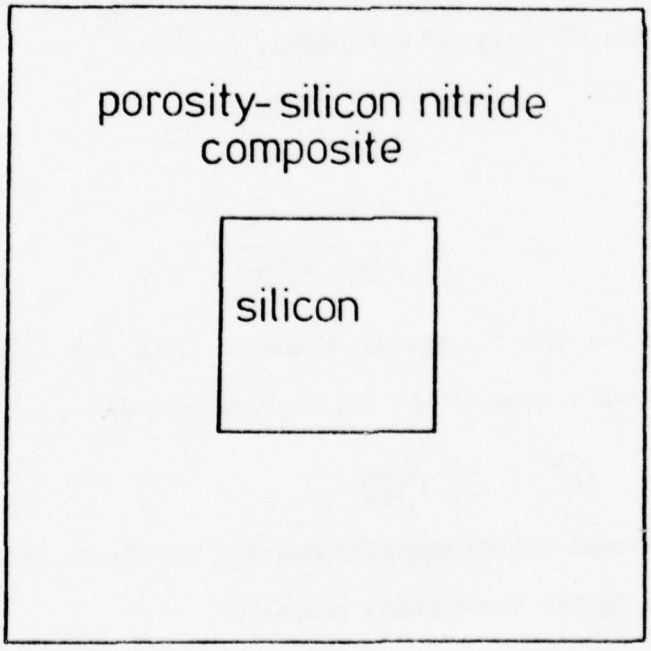
$$C_p + C_{Si} + C_{SN} = 1.$$

$$\therefore \quad C_p^* = \frac{C_p}{1 - C_{Si}} \qquad \ldots\ldots (18)$$

$$m^* = \frac{E_{Si}}{E_{PSN}} = \frac{E_{Si}}{E_{SN}} \times \frac{E_{SN}}{E_{PSN}} = m \left(\frac{1}{1-C_p^{*\frac{2}{3}}} \right)$$



a) Silicon nitride matrix with porosity as the 2nd-phase to give the Young's Modulus of porous silicon nitride.



b) Porous silicon nitride matrix with silicon as the 2nd phase.

Fig.33. Silicon nitride-silicon-porosity composite model.

$$\therefore \quad m^* = m\left(\frac{1}{1 - \left(\frac{C_p}{1-C_{Si}}\right)^{\frac{2}{3}}}\right) \qquad \ldots\ldots (19)$$

where $m = \frac{E_{Si}}{E_{SN}}$.

In the present study, E_{Si} and E_{SN} were given values of 110 GNm^{-2} and 310 GNm^{-2} from references (101) and (80) respectively.

Substitution of equations (18) and (19) in (17) yields:

$$E_{PSN-Si} = E_{SN}\left[1 - \left(\frac{C_p}{1-C_{Si}}\right)^{\frac{2}{3}}\right]\left[1 + \frac{C_{Si}}{\frac{m}{m-1+\left(\frac{C_p}{1-C_{Si}}\right)^{\frac{2}{3}}} - C_{Si}^{\frac{1}{3}}}\right] \qquad \ldots\ldots (20)$$

Treating the model of Paul, equations (14) and (15), in a similar manner, then:

$$E_{PSN-Si} = E_{SN}\lceil x \rceil\left[\frac{1 + (m/x - 1)C_{Si}^{\frac{2}{3}}}{1 + (m/x - 1)(C_{Si}^{\frac{2}{3}} - C_{Si})}\right] \qquad \ldots\ldots (21)$$

where $x = \dfrac{1 - \left(\frac{C_p}{1-C_{Si}}\right)^{\frac{2}{3}}}{1 - \left(\frac{C_p}{1-C_{Si}}\right)^{\frac{2}{3}} + \left(\frac{C_p}{1-C_{Si}}\right)}$

If ρ_g and ρ_n are the 'green' and 'nitrided' densities of a partially nitrided compact, then the following expressions can be derived (see Appendix 3).

$$\left.\begin{aligned} C_p &= 1 - 0.281\,\rho_g - 0.148\,\rho_n \\ C_{Si} &= 1.072\,\rho_g - 0.643\,\rho_n \\ C_{SN} &= 0.791(\rho_n - \rho_g) \end{aligned}\right\} \qquad \ldots\ldots (22)$$

In deriving the above expressions it is assumed that the densities of silicon and silicon nitride are 2.330 and 3.200 $g.cm^{-3}$ respectively, and that the conversion of silicon to silicon nitride is accompanied by a volume expansion of 23% and a mass gain of 66.7%.

Substitution of (22) into (20) and (21) gives the relationship between Young's modulus of the composite, nitrided density, and green density according to the Ishai and Cohen and Paul treatments respectively. Fig. 34 shows the computed relationships between Young's modulus and ρ_n for a green density (ρ_g) of 1900 kgm^{-3}, the green density which, theoretically, can be nitrided to a fully dense silicon nitride body.

Fig. 35 shows a comparison between theoretical and experimental data for a compact of washed Monsanto silicon (< 45 μm), green density 1500 kgm^{-3}, nitrided at 1370°C in nitrogen at 50 torr. The data for Koch-Light 99.9% silicon (< 45 μm), green density 1490 kgm^{-3}, nitrided at 1370°C in nitrogen at 760 torr, is also compared with the theoretical predictions in Fig. 35. The observed rate of development of E with nitride growth (ρ_n) for the washed Monsanto compacts is accurately described by the model of Ishai and Cohen[100], although the predicted values of modulus for a particular ρ_n are consistently 25 GNm^{-2} above those experimentally determined. This is not considered to be of major importance at the present stage of the study since it is intended that microstructural observations will give an improved understanding of how interparticle bonding and the general nature of silicon nitride formation affect the development of stiffness in the nitriding compact. The theoretical model can then be refined accordingly. The data are more accurately predicted by the model of Ishai and Cohen than by that of Paul; this has also been found[100] in previous studies of three-phase composites having low modular ratios and containing substantial porosity concentrations.

The data for the Koch-Light 99.9% silicon compacts are consistently 55 GNm^{-2} lower than that predicted from the model of Ishai and Cohen, the slope of the E/ρ_n line again being the same as that obtained from the theoretical treatment. During the initial stages of nitridation,

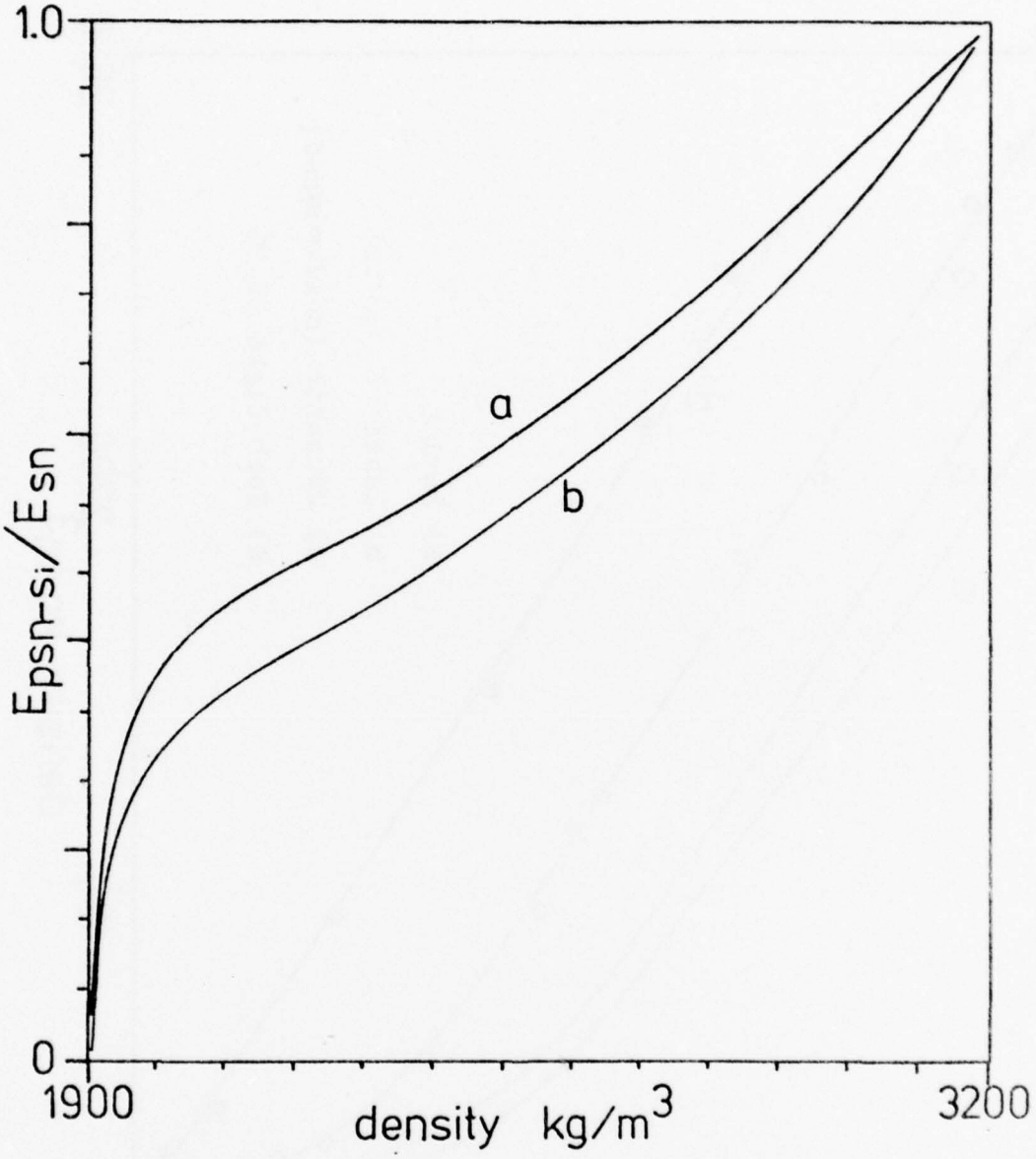


Fig.34. Computed relationships between Young's Modulus and nitrided density, for a green density of 1900 kg./m^3.

a) Paul's model.

b) Ishai's model.

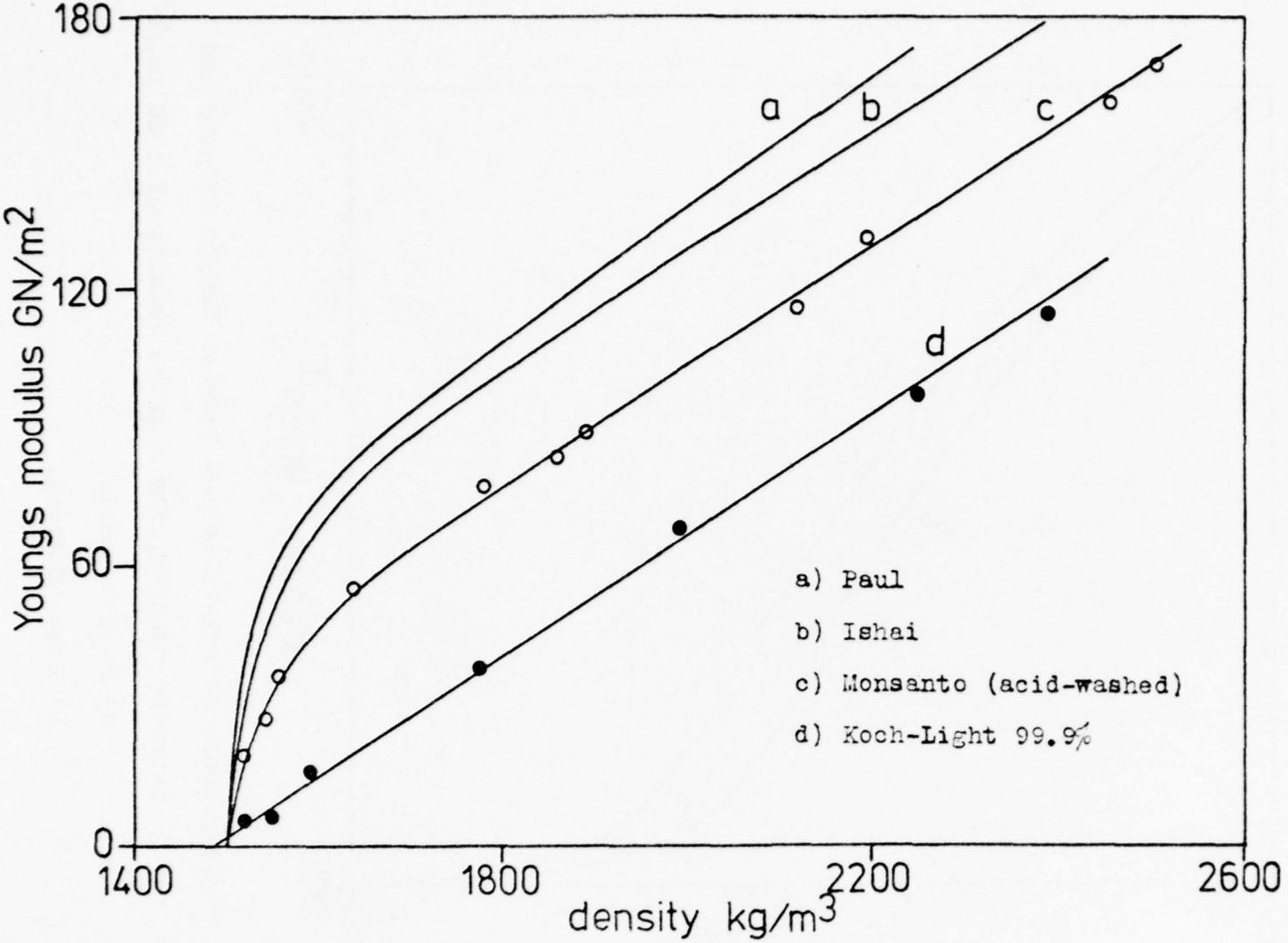


Fig.35. Theoretical and experimental data (E vs p_n), Monsanto and Koch-Light powder compacts.

however, there is a marked departure from the E/ρ_n relationship of the theoretical model.

It is noteworthy that although the experimental data are linear with ρ_n over a wide range of values, they do not extrapolate to a value close to those quoted for the modulus of fully dense hot-pressed silicon nitride[90,101]. This is in marked contrast to the data of Jones et al.[69] in which Young's modulus data was found to extrapolate linearly to the fully dense value. The model of Ishai and Cohen, however, as shown in Fig. 34, does not predict a linear extrapolation to the fully dense value.

In summary, then, the simple modelling of the complex RBSN composite provides a remarkably good description of the observed rate of development of E with ρ_n, particularly in the case of washed Monsanto silicon powder nitrided in nitrogen at 50 torr. The large difference in modulus between RBSN produced from Monsanto silicon and that produced from Koch-Light 99.9% silicon suggests that the microstructures of the two materials must be markedly different. It is interesting to note that Young's modulus data for other RBSN's (Fig. 36), as measured by a similar technique, fall on the E/ρ_n line of the Koch-Light material.

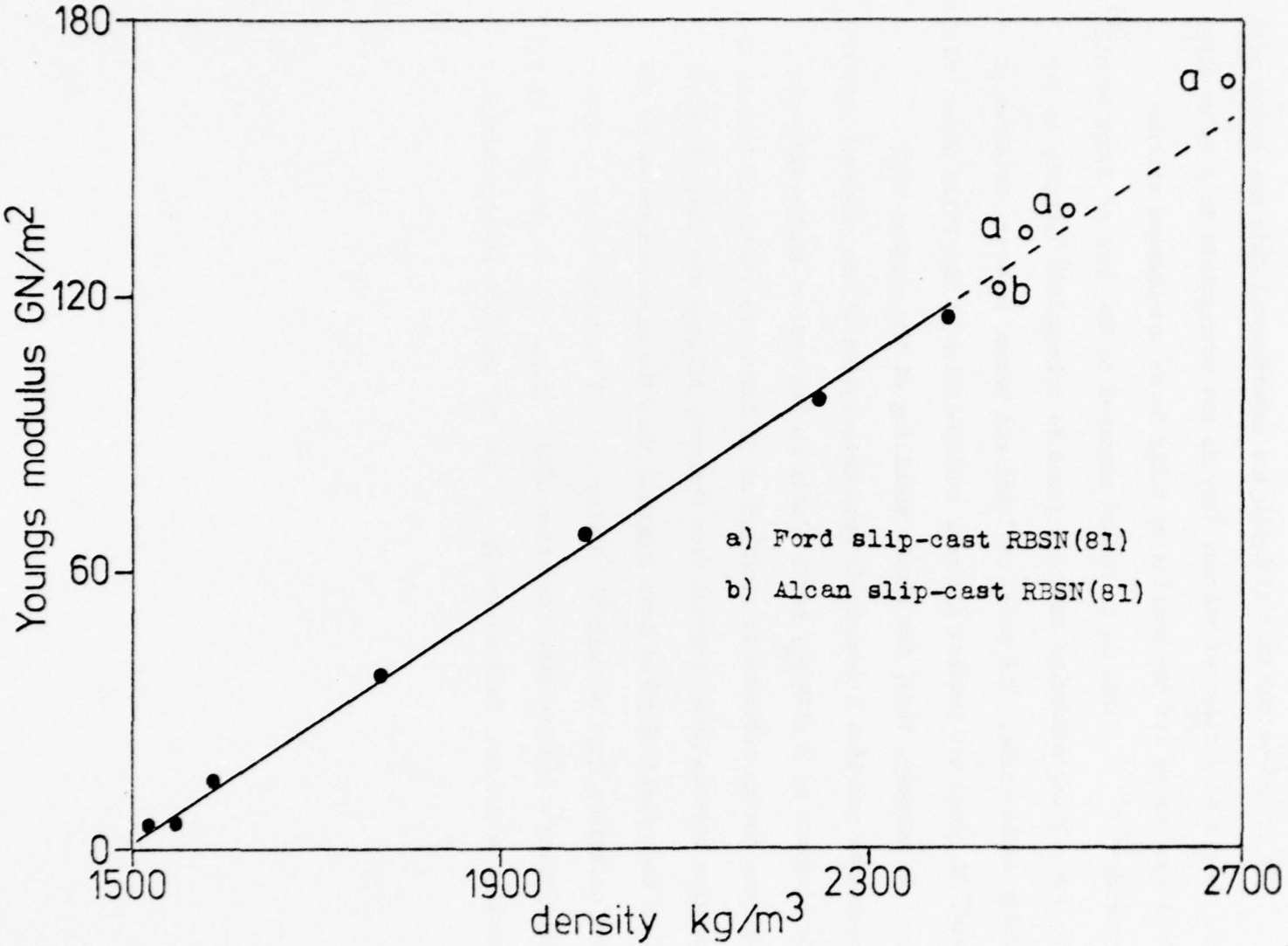


Fig.36. Dynamic Young's modulus data for commercial RBSN's compared to the Koch-Light E vs p_n relationship.

5.4 Development of modulus of rupture during the nitridation of silicon powder compacts

Although not a major aspect of the study, rupture modulus measurements (see Section 4.7) were made on the samples prepared for the determination of E in order to confirm that the RBSN materials under investigation were of a similar strength (σ_f) to those reported in the literature. The σ_f values for each type of powder compact were plotted against the nitrided density of the samples and provided an indication of any large difference in strength between the RBSN's produced.

5.4.1 Washed Monsanto silicon powder

The relationship between σ_f and ρ_n for isostatically pressed compacts of acid-washed Monsanto powder (< 45 μm, $\rho_g = 1500$ kgm^{-3}) nitrided at 1370°C in nitrogen at 50 torr is shown in Fig. 37. The graph indicates that σ_f is linearly dependent on ρ_n over most of the density range, a departure from linearity being observed at low values of ρ_n.

5.4.2 Unwashed Monsanto silicon powder

Isostatically pressed compacts ($\rho_g = 1500$ kgm^{-3}) were nitrided in nitrogen at 50 torr at 1370°C, the dependence of σ_f on ρ_n being shown in Fig. 38. The form of the relationship was the same as for the compacts of washed Monsanto powder but the values of σ_f were slightly higher at all values of ρ_n, as shown in Fig. 40.

5.4.3 Koch-Light 99.9% silicon powder

Rupture modulus data for isostatically pressed compacts (1490 kgm^{-3}) nitrided at 1370°C in nitrogen at 760 torr are shown as a function of ρ_n in Fig. 39. Values of σ_f for this material were consistently lower than those determined for both Monsanto materials.

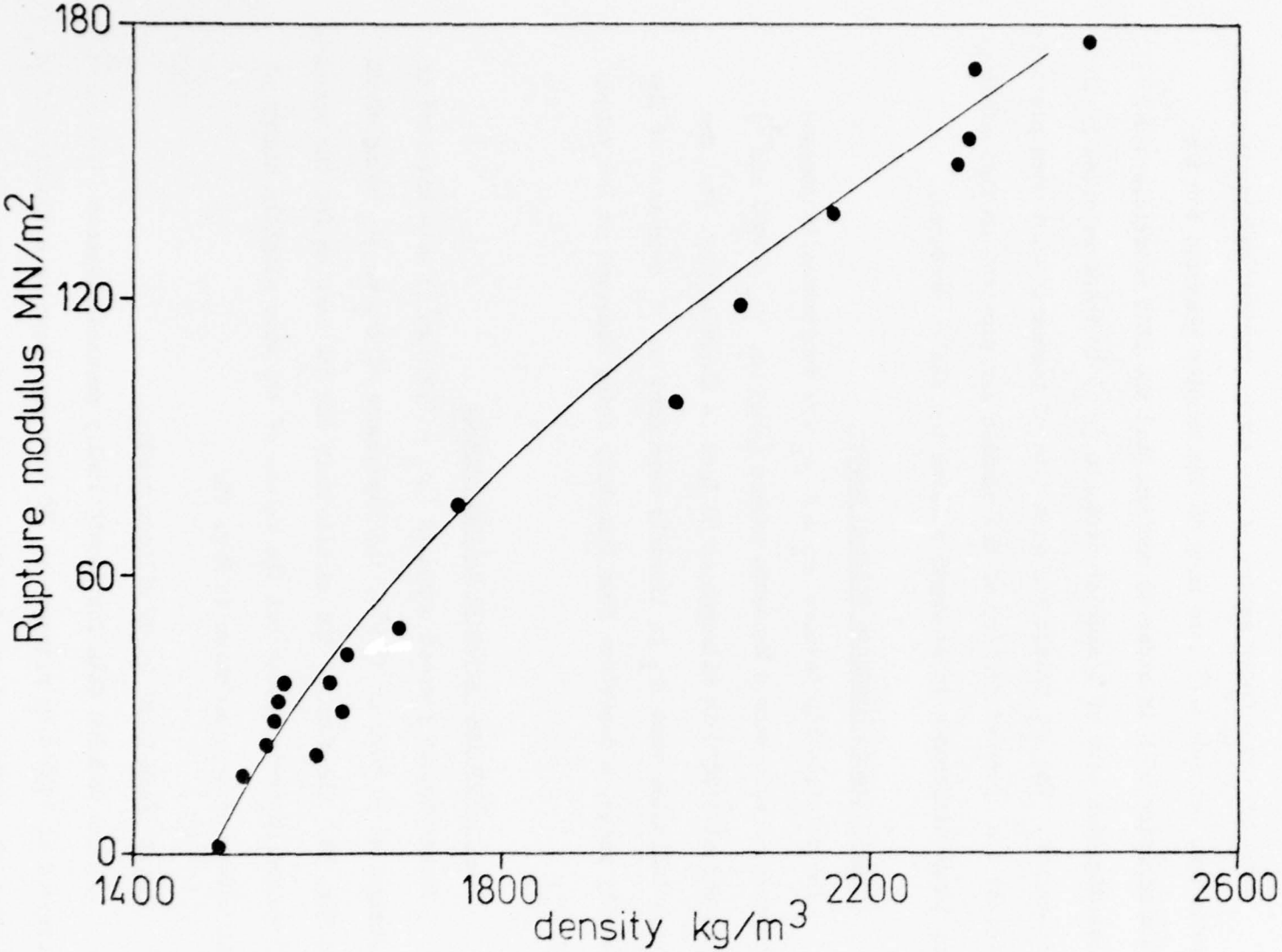


Fig.37. Rupture modulus vs nitrided density, washed Monsanto.

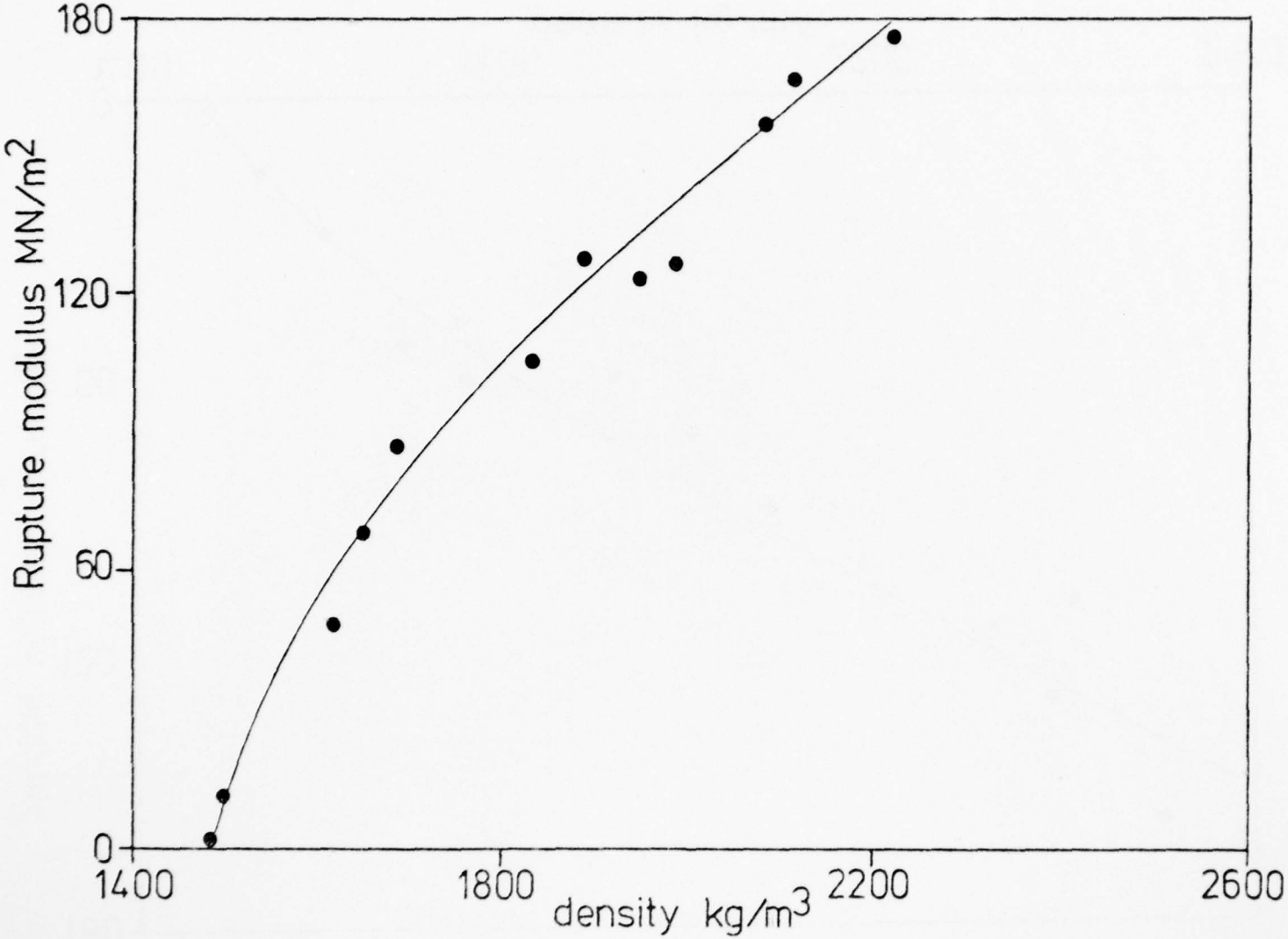


Fig.38. Rupture modulus vs nitrided density, unwashed Monsanto.

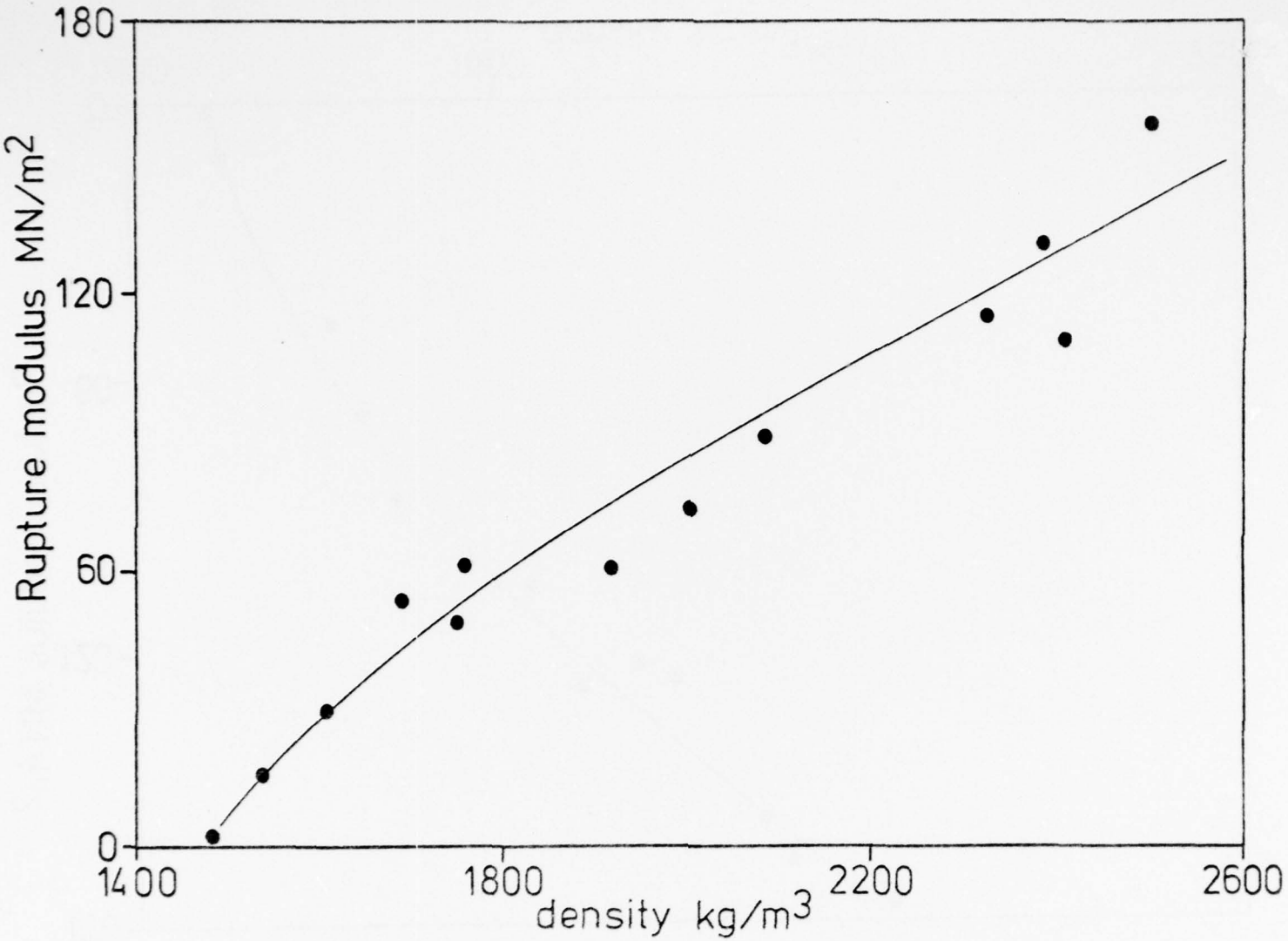


Fig.39. Rupture modulus vs nitrided density, Koch-Light 99.9%.

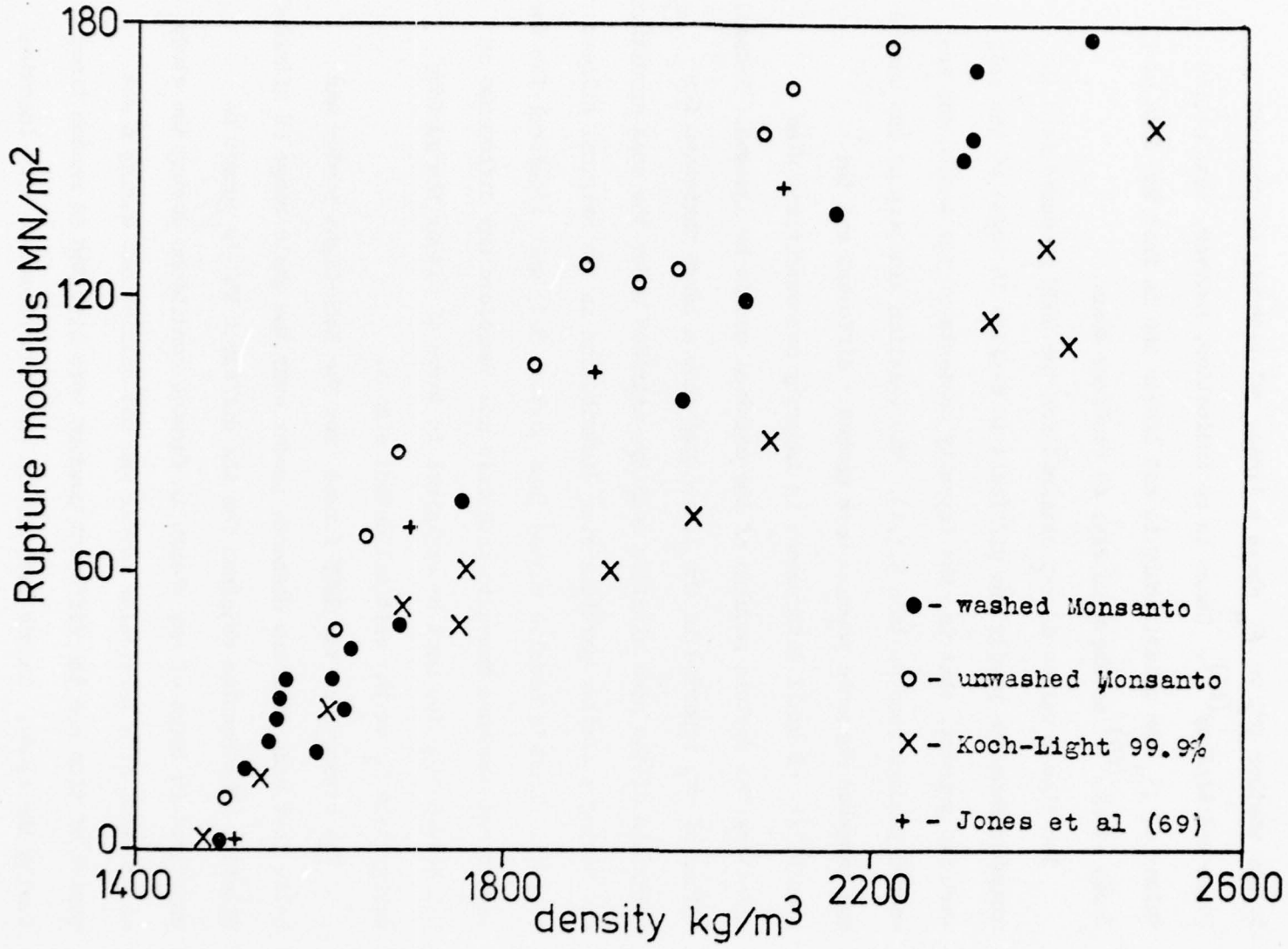


Fig.40. Comparison of rupture modulus data.

5.4.4 Discussion

From the very limited quantity of data available it is not possible to say whether σ_f vs ρ_n obeys a linear relationship as proposed by Jones and Lindley[83]. There is an indication, however, that at low values of ρ_n the relationship is not linear and in fact the data of Jones et al.[69] as shown in Fig. 40 confirms this.

The higher values of σ_f obtained for the RBSN produced from the unwashed Monsanto powder are difficult to explain in terms of the only variable present, that is, the impurity contents of the washed and unwashed powders (see Section 5.1.1). The reaction kinetics of the washed and unwashed Monsanto powders were markedly different and the possibility of small differences in impurity concentrations also affecting the rupture modulus of the material cannot be ignored. Indeed, values of σ_f reported in the literature show a large variation for materials of the same nitrided density, nitrided under the same conditions and having a similar particle size distribution in the original silicon compact. Young's modulus values (see Section 5.4) were identical for the washed and unwashed Monsanto materials and therefore any difference in σ_f between the two must be explained in terms of either the surface energy term γ_i or the critical defect size c.

The strength of the RBSN formed from the Koch-Light powder was below that made from the Monsanto powder over the whole range of nitrided density. The results obtained for the different RBSN's cannot be explained in terms of any change in furnace conditions during the study as the work on a particular powder was not carried out during a set period of time and the different powders were nitrided at random times during the study. Sample preparation and test procedure were identical for all materials.

5.5 Development of microstructure in silicon powder compacts during nitridation

The microstructural studies described here were concerned with the development of interparticle bonding and general microstructural characteristics during the nitridation of compacts of Monsanto and Koch-Light silicon powders. It was originally intended that spherical Monsanto silicon would be used to give a clearer picture of bonding development, but because of the presence of aluminium in some of the silicon spheres this approach was not pursued. The spherical powder, however, did produce many interesting micrographs and a selection of these are shown in Appendix 4.

5.5.1 Washed Monsanto silicon powder

A series of photomicrographs showing the development of microstructure during the nitridation of compacts of this powder in nitrogen at 50 torr is shown in Figs. 41 to 48. The major features of development can be summarised as follows:

1) the formation of a continuous silicon network throughout the compact at an initial stage during which nitride growth is negligible;

2) after the silicon network has formed, the first approximately 7% of conversion to silicon nitride occurs in the neck regions of the silicon network. The nitride morphology is massive and non-porous and bears no resemblance to the whisker formation commonly reported to be the predominant feature of the initial stages of nitridation;

3) after the conversion has exceeded 7%, a more general coverage of the silicon surfaces with silicon nitride occurs and many features of the model of Atkinson et al.[12] are exhibited, as shown in Fig. 46.

Throughout the conversion process, all of the nitride formed was of the massive type and the photomicrographs indicate a seemingly simple process of conversion and densification.

FIG. 41: Acid-washed Monsanto powder, isostatically pressed at 140 MNm^{-2}.

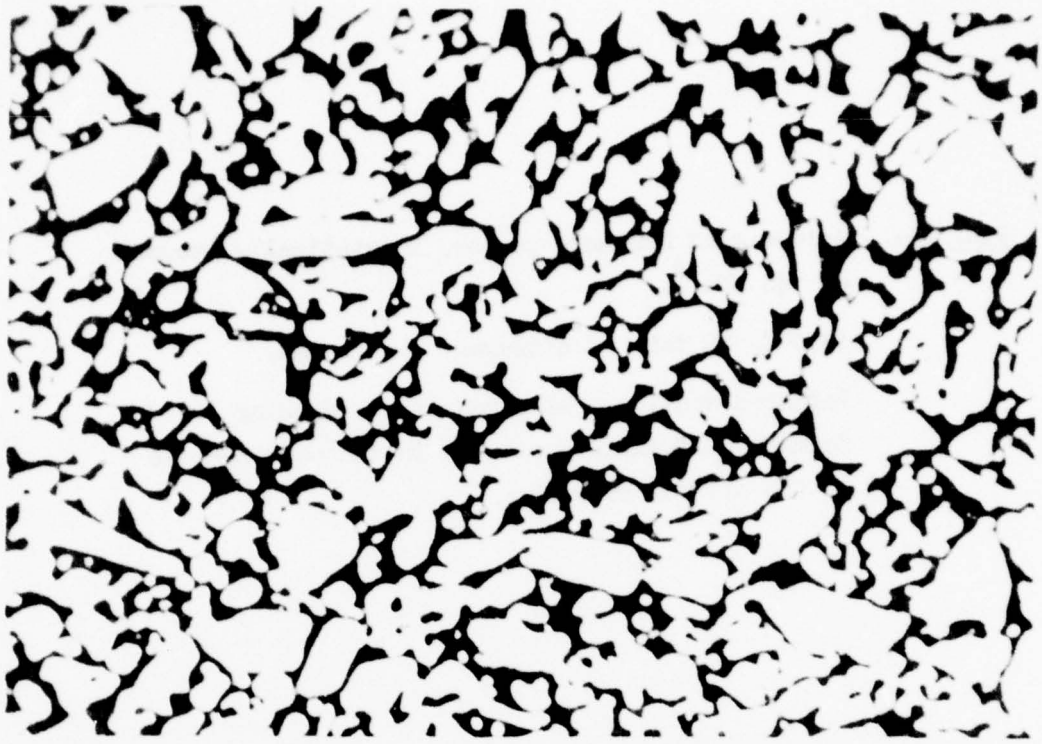
1370°C, 50 torr of nitrogen, 2 minutes.

Polished section, reflected light, showing formation of silicon network.

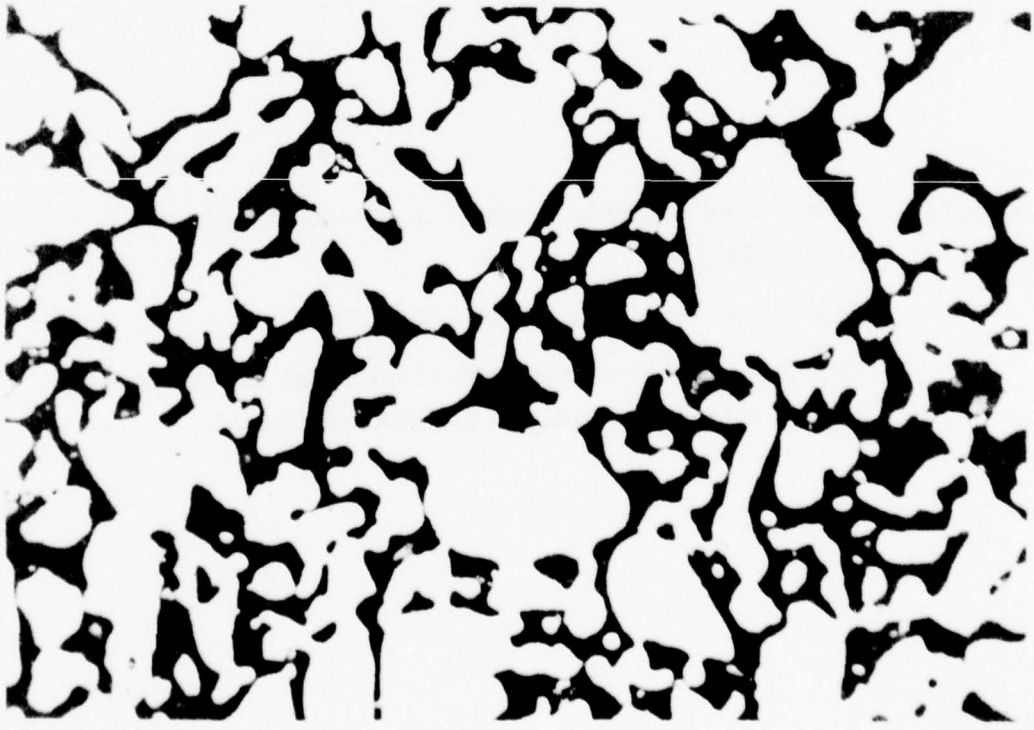
FIG. 42: Acid-washed Monsanto powder, isostatically pressed at 140 MNm^{-2}.

1370°C, 50 torr of nitrogen, 5 minutes.

Polished section, reflected light, showing formation of silicon network.



50μm



50μm

FIG. 43: Acid-washed Monsanto powder, isostatically pressed at 140 MNm^{-2}.

1370°C, 50 torr of nitrogen, 30 minutes.

Polished section, reflected light, showing the formation of silicon nitride in the neck regions of the silicon network.

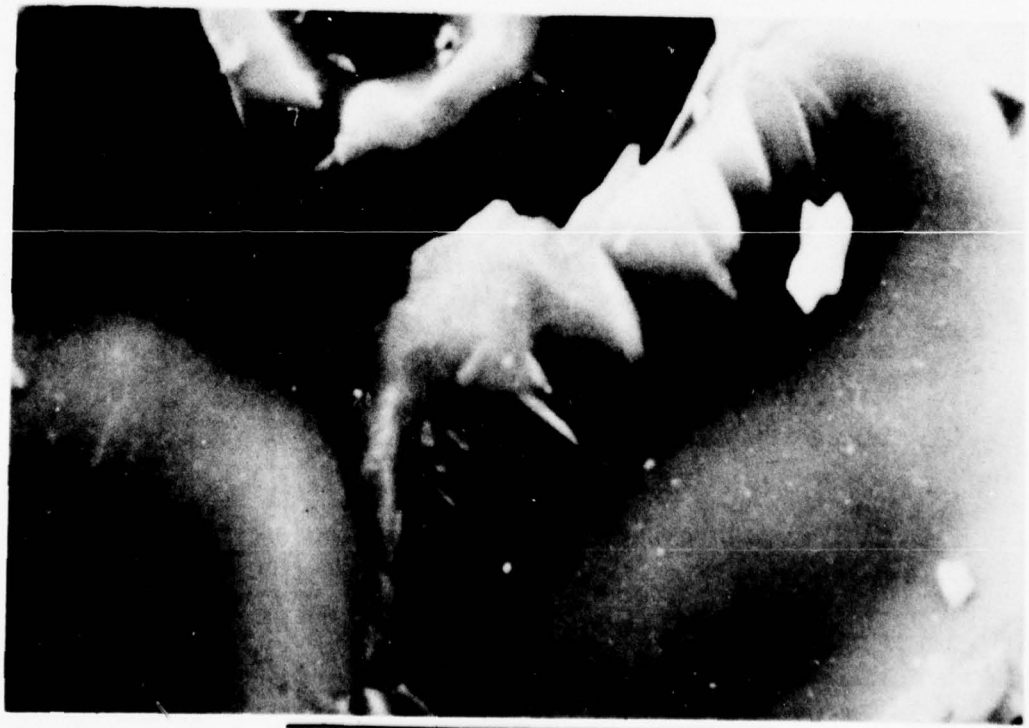
FIG. 44: Acid-washed Monsanto powder, isostatically pressed at 140 MNm^{-2}.

1370°C, 50 torr of nitrogen, 30 minutes.

Scanning electron micrograph showing the morphology of the silicon nitride in the neck regions.



45µm



25µm

FIG. 45: Acid-washed Monsanto powder, isostatically pressed at 140 MNm^{-2}.

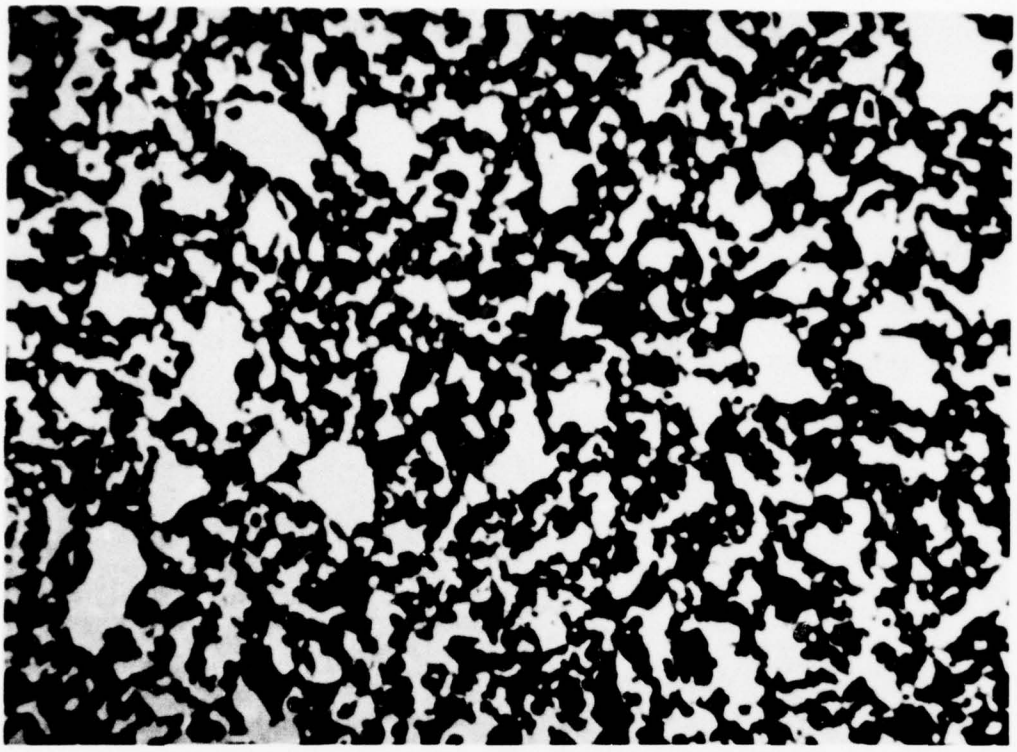
1370°C, 50 torr of nitrogen, 3 hours.

Polished section, reflected light, showing silicon nitride in neck regions and porosity in the silicon. The porosity is formed by the mechanism of Atkinson et al.[12].

FIG. 46: Acid-washed Monsanto powder, isostatically pressed at 140 MNm^{-2}.

1370°C, 50 torr of nitrogen, 7.5 hours.

Polished section, reflected light, showing more general silicon nitride formation. A much greater number of pores can be seen in the silicon than in Fig. 45. The particle marked (A) shows the channel connecting a pore within the particle to the silicon surface.



100μm

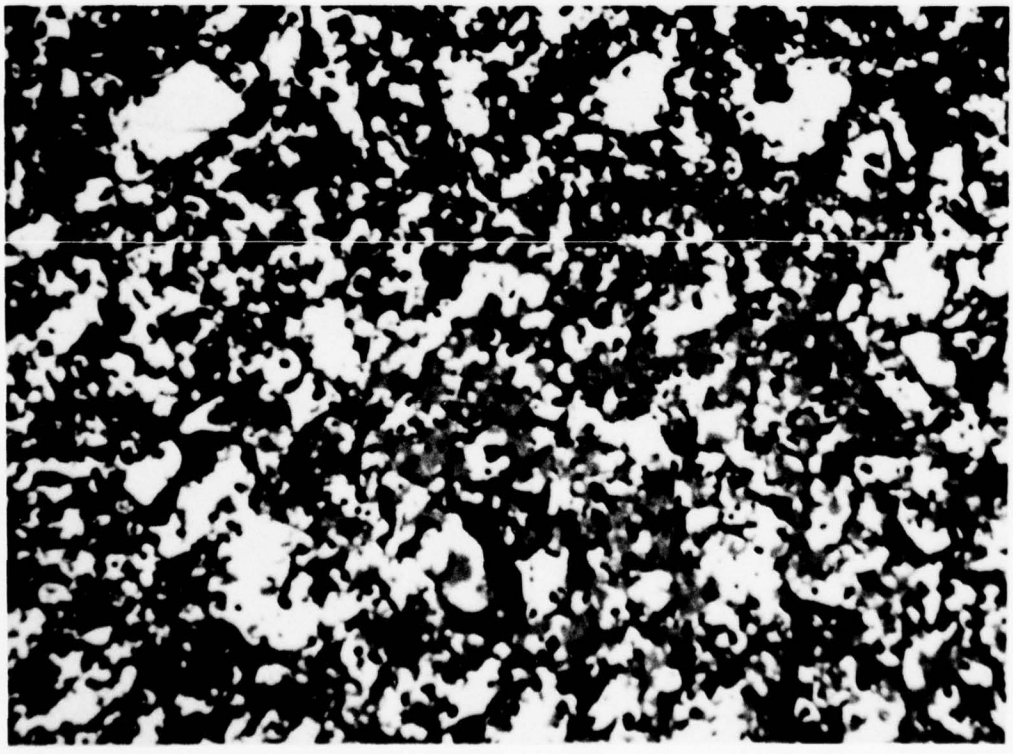


FIG. 47: Acid-washed Monsanto powder, isostatically pressed at 140 MNm^{-2}.

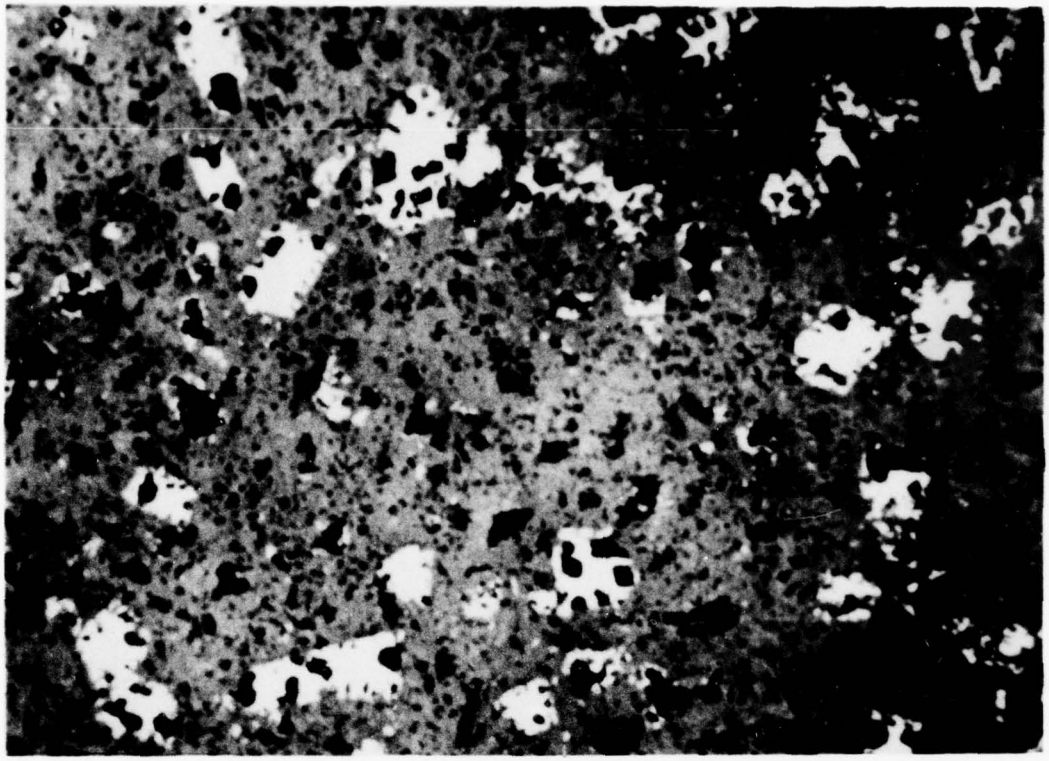
1370°C, 50 torr of nitrogen, 16 hours.

Polished section, reflected light.

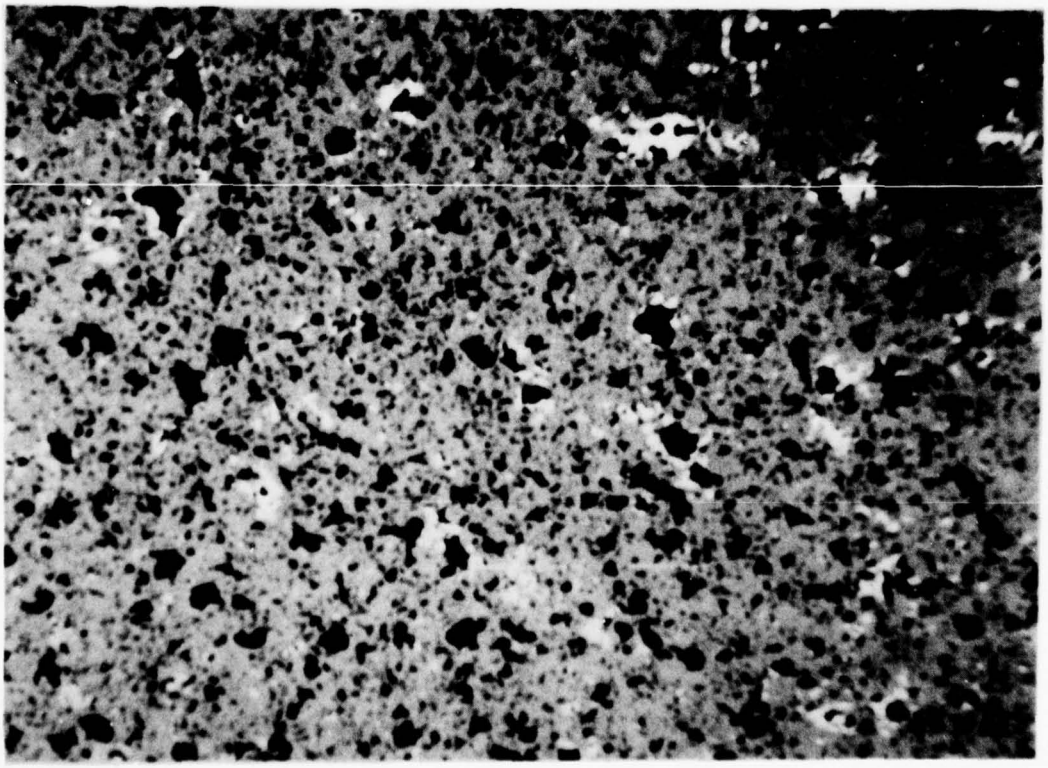
FIG. 48: Acid-washed Monsanto powder, isostatically pressed at 140 MNm^{-2}.

1370°C, 50 torr of nitrogen, 35 hours.

Polished section, reflected light. Fully nitrided compact with residual silicon.



40μm



The proportions of the α- and β-phases present in the material were determined at stages during conversion and the relationship between the α and β content and the nitridation kinetics is shown in Fig. 49. From Fig. 49 it can be seen that initially the rate of α-phase formation is constant and that the rate of β-phase formation begins to decrease at the same time as the rate of α formation increases, the amount of β formation eventually becoming zero. The mean α/β ratio of RBSN produced from this powder at nitrogen pressures of 50-200 torr was consistently determined as ~70/30.

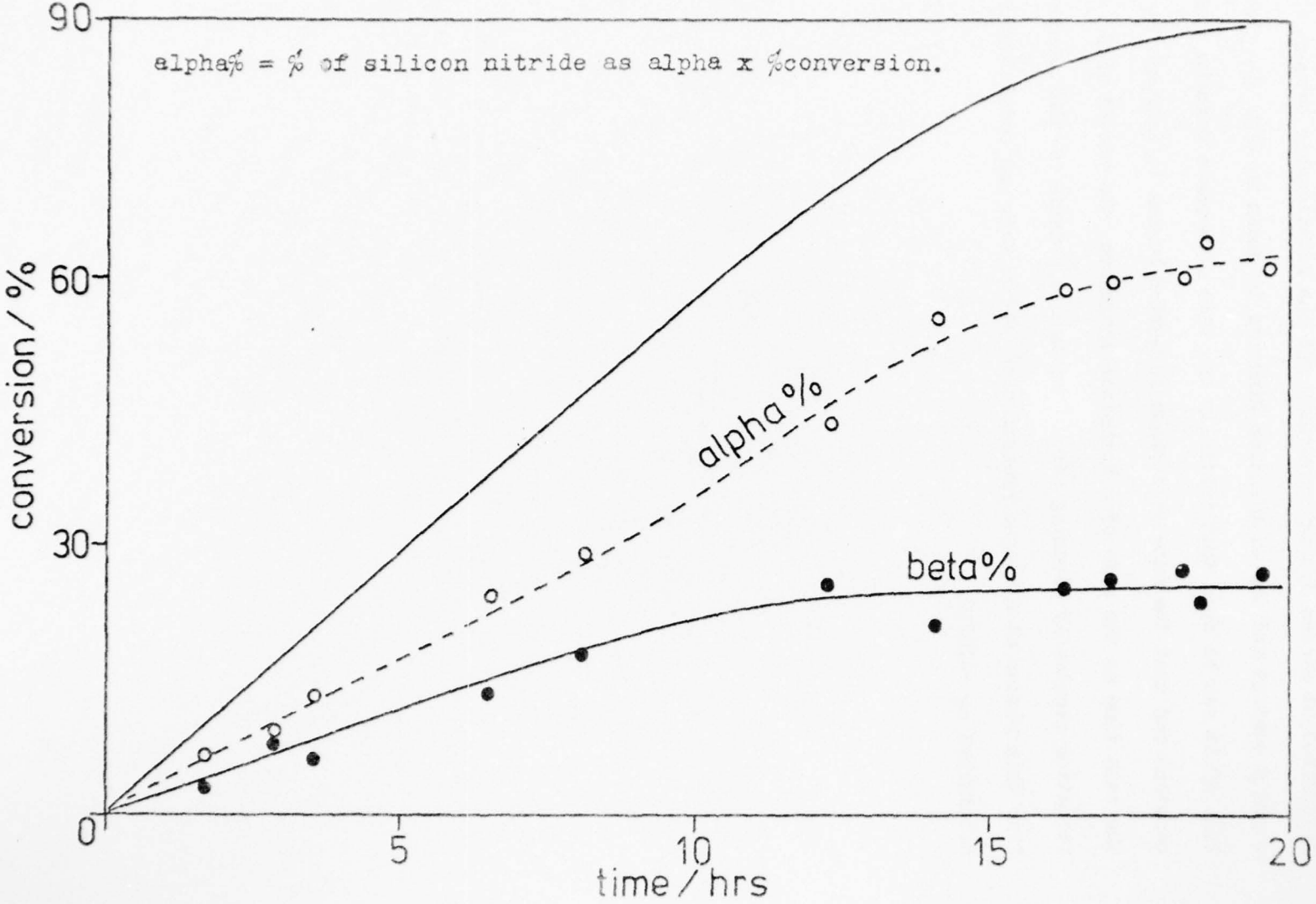


Fig.49. Phase composition of RBSN produced from acid-washed Monsanto powder; alpha and beta-silicon nitride content vs nitriding time.

5.5.2 Unwashed Monsanto silicon powder

Many features of the development of microstructure observed during the nitridation of compacts of this powder in nitrogen at 50 torr were similar to those found for the washed powder, in particular the formation of a silicon network and the subsequent nitride growth in the neck regions of the network. One noticeable difference between the two powders, however, was the growth of silicon nitride inside the silicon particles during the early part of the reaction, as shown in Fig. 50. The nitride inside the particles should not be confused with the nitride visible where the section is taken across a neck region in the sample.

The presence of impurity phases in the silicon powder is shown in Fig. 51 and although the reflectivity of the silicon and the impurity phase is very similar, the presence of such phases was usually indicated by the accompanying cracking of the surrounding silicon.

One other type of nitride morphology observed in this RBSN was the blade-like features shown in Fig. 52; well-formed crystals of silicon nitride can also be seen.

The α and β contents of the nitriding powder compact are described in Fig. 53. For fully nitrided compacts the α/β ratio was approximately the same as that found for compacts of Monsanto washed powder.

FIG. 50: Unwashed Monsanto powder, isostatically pressed at 140 MNm^{-2}.

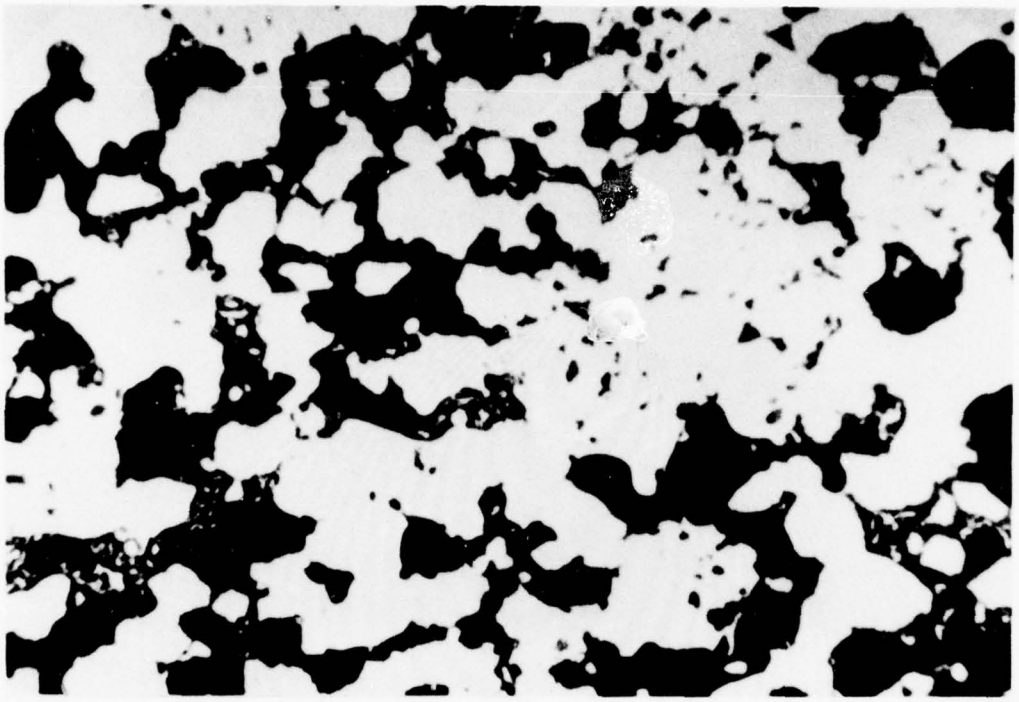
1370°C, 50 torr of nitrogen, 30 minutes.

Polished section, reflected light, showing silicon network and initial nitride formation.

FIG. 51: Unwashed Monsanto powder, isostatically pressed at 140 MNm^{-2}.

1370°C, 50 torr of nitrogen, 15 minutes.

Polished section, reflected light, showing cracking of silicon adjacent to impurity phases.



40μm.



20μm.

FIG. 52: Unwashed Monsanto powder, isostatically pressed at 140 MNm^{-2}.

1370°C, 50 torr of nitrogen, 20 hours.

Scanning electron micrograph showing blades of silicon nitride and well-formed crystals.



30 μm

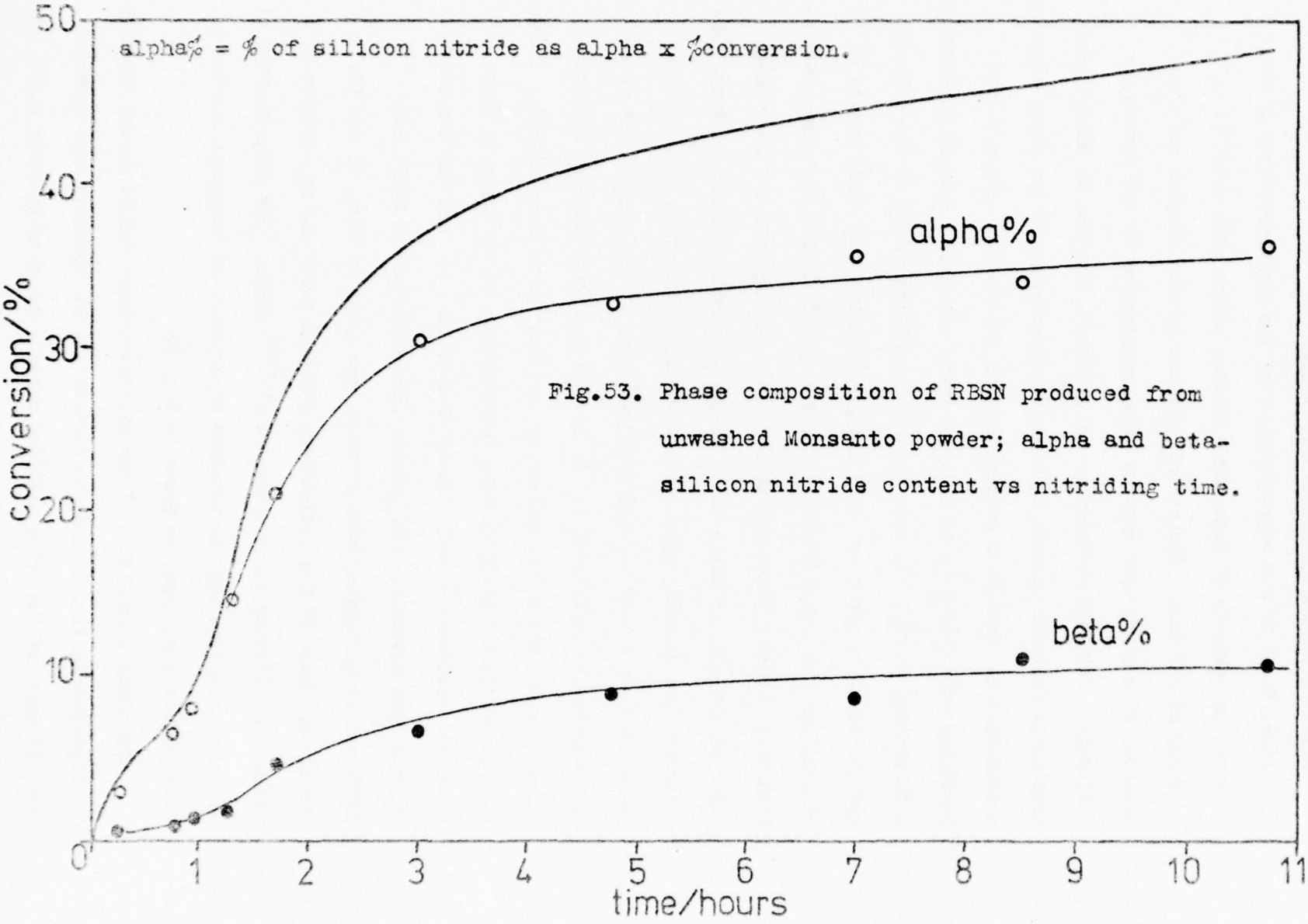


Fig.53. Phase composition of RBSN produced from unwashed Monsanto powder; alpha and beta-silicon nitride content vs nitriding time.

5.5.3 Koch-Light 99.9% silicon powder

Figs. 54 to 60 are representative of the microstructural features observed in compacts of Koch-Light silicon powder when nitrided in nitrogen at 760 torr. The overall picture is very complex and the presence of whisker type growths makes examination by SEM extremely difficult. Polished sections of the material, however, do reveal some persistent features present in the microstructure. In the early stage of nitridation no continuous silicon network was formed, although some particles were joined by an impurity phase material. This is particularly well defined in Fig. 55, even though the reflectivities of the silicon and the impurity phase are very similar. During this early period of nitridation the majority of the silicon nitride formed was associated with this impurity phase and in all cases the impurity was associated with the presence of large holes in the surrounding microstructure. The whiskers formed during this initial period are shown in Fig. 56, and these may form a bond between some particles of the compact but it was not possible to confirm this. As nitridation proceeded the developing microstructure was characterized by two types of silicon nitride; large non-porous areas containing some residual silicon or impurity phase material, particularly well illustrated in Fig. 57, and the presence of whisker type material. The whisker-like features exhibited many different morphologies, some of which are shown in Figs. 56 and 58. During the whole of the nitridation reaction there was no evidence of a mechanism following the Atkinson et al.[12] model. One other feature of the microstructure was the presence of crystals of hexagonal section in some silicon particles, as shown in Fig. 59.

The phase composition of the silicon nitride formed during conversion is described in Fig. 61 and, in contrast to the Monsanto type material, the α/β ratio of the fully nitrided ceramic was approximately 20/80, with the α content being formed entirely during the initial 10% of the reaction.

FIG. 54: Koch-Light 99.9% powder, isostatically pressed at 140 MNm^{-2}.

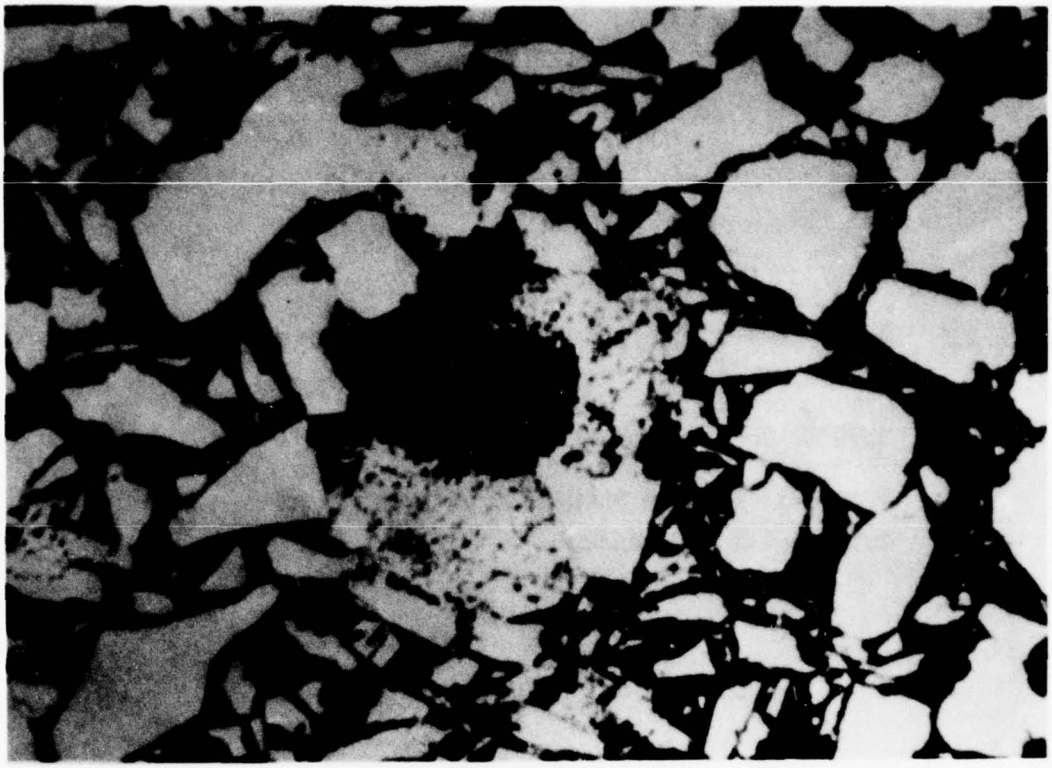
1370°C, 760 torr of nitrogen, 10 minutes.

Polished section, reflected light, showing a large void caused by impurity phase melt-out.

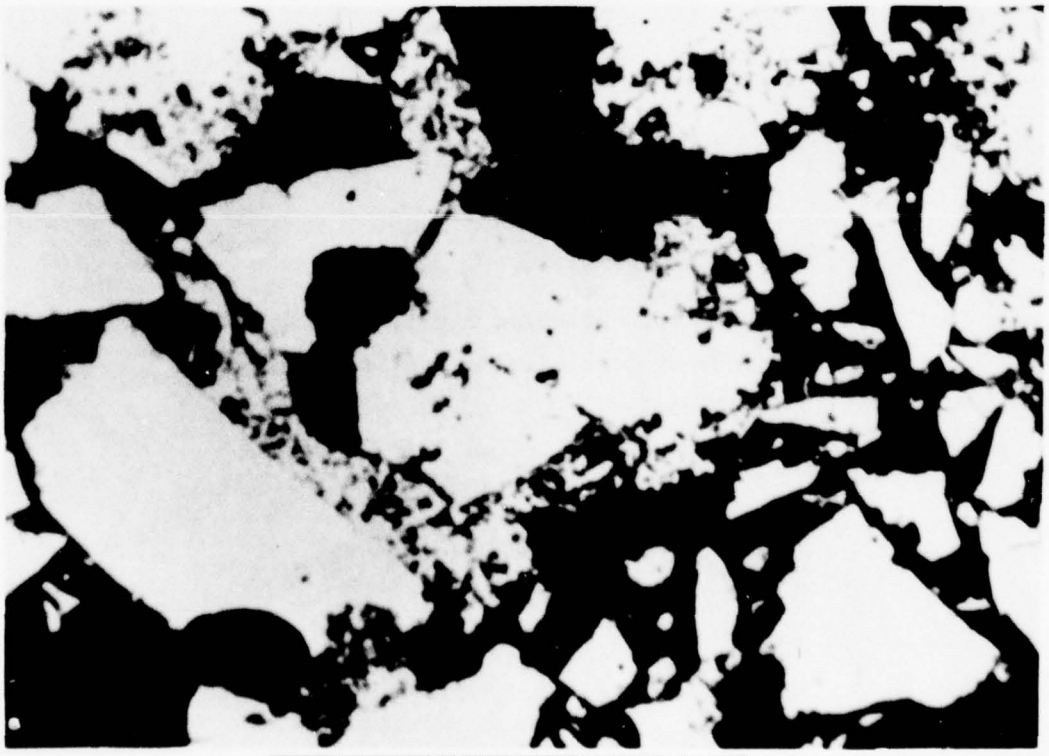
FIG. 55: Koch-Light 99.9% powder, isostatically pressed at 140 MNm^{-2}.

1370°C, 760 torr of nitrogen, 10 minutes.

Polished section, reflected light, showing an impurity phase joining the original silicon particles. Initial nitride formation can be seen to be associated with the impure regions of the compact.



50μm



50μm

FIG. 56: Koch-Light 99.9% powder, isostatically pressed at 140 MNm^{-2}.

1370°C, 760 torr of nitrogen, 1 hour.

Scanning electron micrograph showing whisker-type reaction product.

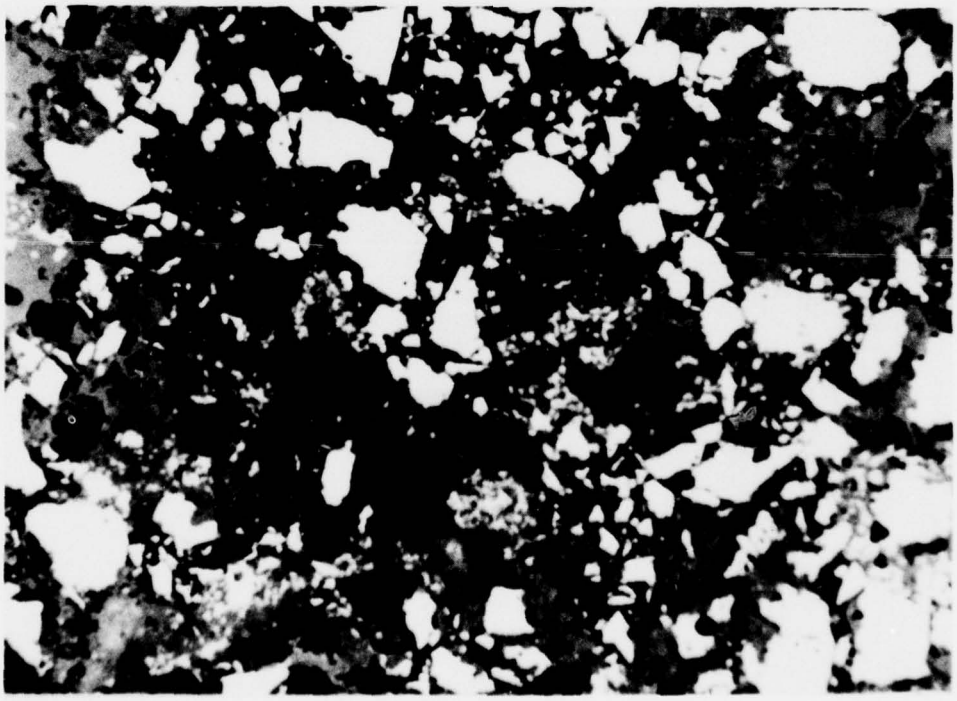
FIG. 57: Koch-Light 99.9% powder, isostatically pressed at 140 MNm^{-2}.

1370°C, 760 torr of nitrogen, 3 hours.

Polished section, reflected light, showing areas of non-porous silicon nitride containing some residual silicon.



20 μm.

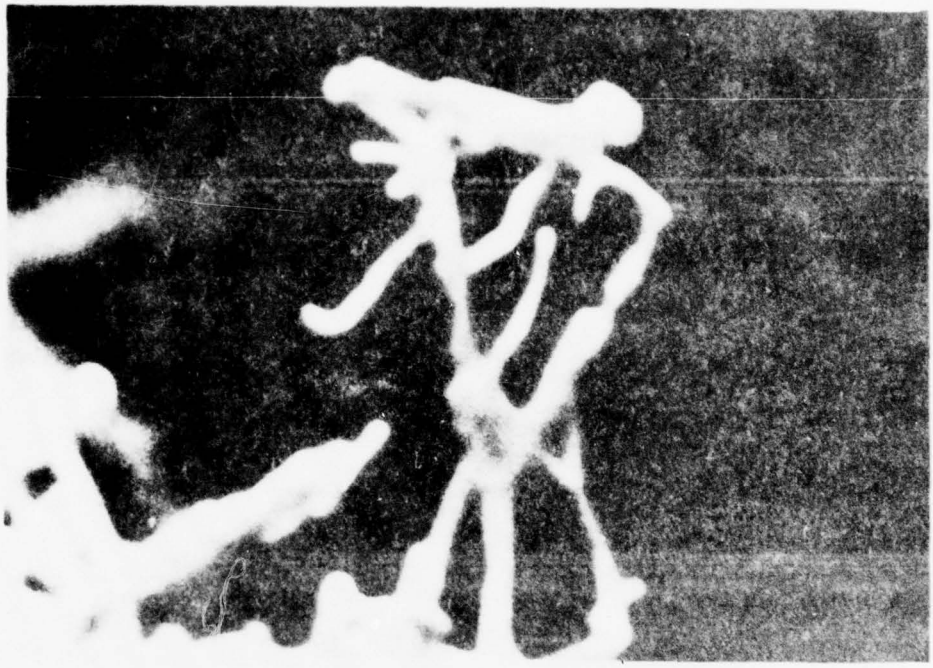


50 μm.

FIG. 58: Koch-Light 99.9% powder, isostatically pressed at 140 MNm^{-2}.

1370°C, 760 torr of nitrogen, 5 hours.

Scanning electron micrograph showing whisker morphology.



10 μm

FIG. 59: Koch-Light 99.9% powder, isostatically pressed at 140 MNm^{-2}.

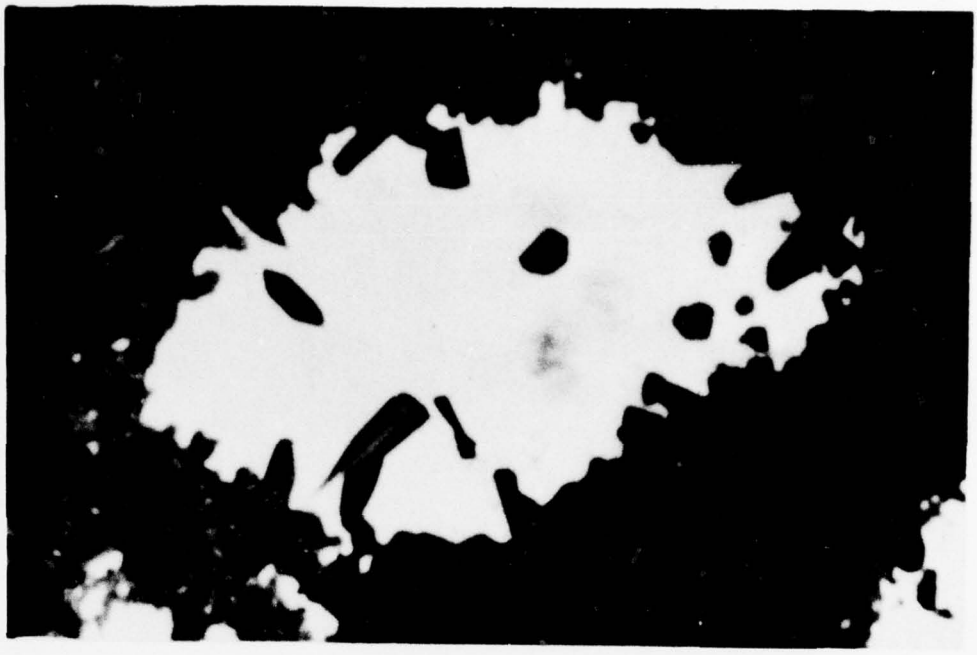
1370°C, 760 torr of nitrogen, 5 hours.

Polished section, reflected light, showing crystals of hexagonal section in a silicon particle. Whisker-type material can be seen on the outside of the particle.

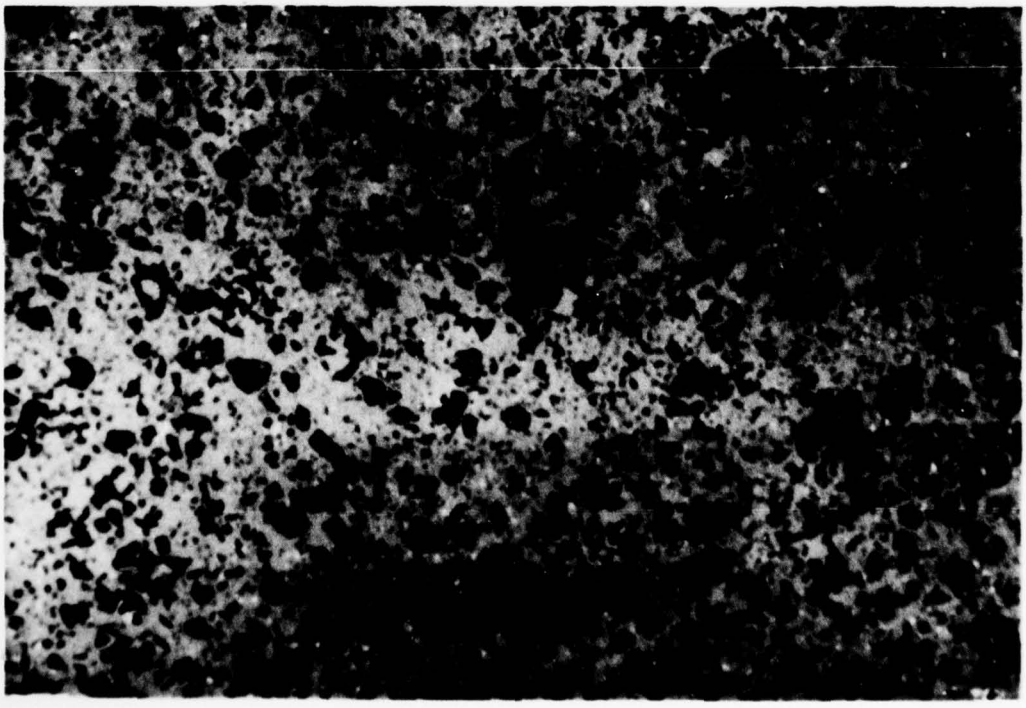
FIG. 60: Koch-Light 99.9% silicon powder, isostatically pressed at 140 MNm^{-2}.

1370°C, 760 torr of nitrogen, 67 hours.

Polished section, reflected light, showing fully nitrided material.



20 μm.



100 μm.

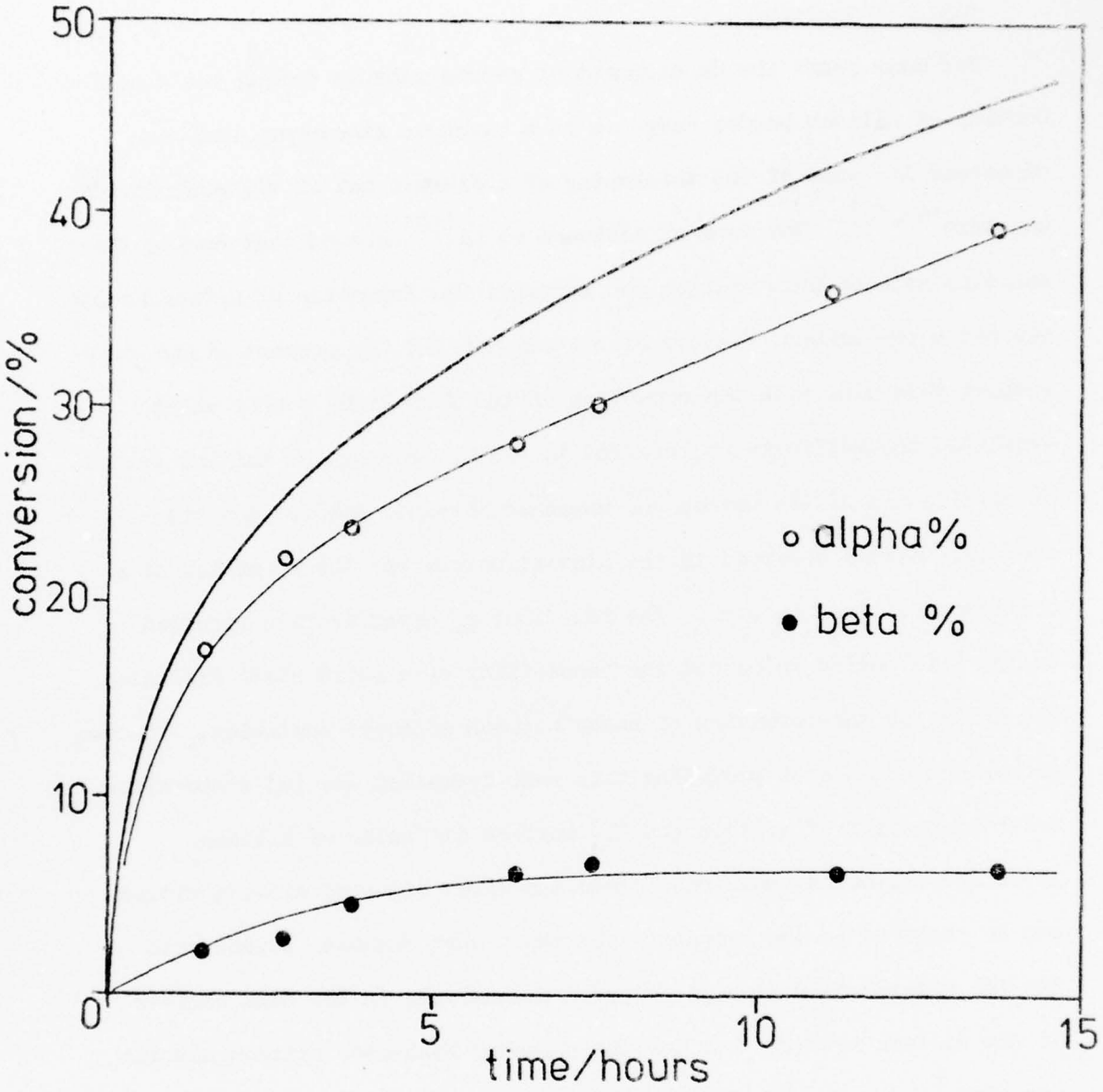


Fig.61. Phase composition of RBSN produced from Koch-Light 99.9% powder; alpha and beta-silicon nitride content vs time.

alpha% = % of silicon nitride as alpha x % conversion.

5.5.4 Discussion

For many years the development of microstructure during the reaction-bonding of silicon powder compacts in a nitrogen atmosphere has been discussed in terms of the thickening of a fibrous mat of silicon nitride whiskers[63,69]. The work of Atkinson et al.[12] showed that during the reaction between pure silicon and nitrogen the formation of a fibrous mat was not a predominant feature of nitridation and the present study would support this view with the exception of the Koch-Light powder which exhibited the mat features referred to above. During the initial period of nitridation of the washed and unwashed Monsanto powders the predominant feature observed in the microstructure was the formation of a continuous silicon network. The fact that no densification occurred during this period rules out the possibility of a solid-state diffusion mechanism for the formation of necks between adjacent particles. The two mechanisms capable of providing this neck formation are (a) evaporation and condensation of silicon and (b) surface diffusion of silicon. After the silicon network has formed, the first signs of silicon nitride can be observed in the compact. For the washed Monsanto powder this initial nitride formation is observed exclusively in the neck regions of the silicon network, but for the unwashed Monsanto, silicon nitride can also be seen inside the silicon particles when a cross-section of the compact is examined. The nitride in the neck regions shows a marked similarity to that formed by the "chemical vapour deposition" of silicon nitride[31], surface topography being the same and the deposits all appearing to be fully dense. The dense nature of the deposits can be gauged from Fig. 62 which shows the results of microhardness measurements on various types of silicon nitride and it can be seen that the Monsanto neck region nitride is even harder than hot-pressed silicon nitride. All crystalline deposits of silicon nitride formed by CVD have been found

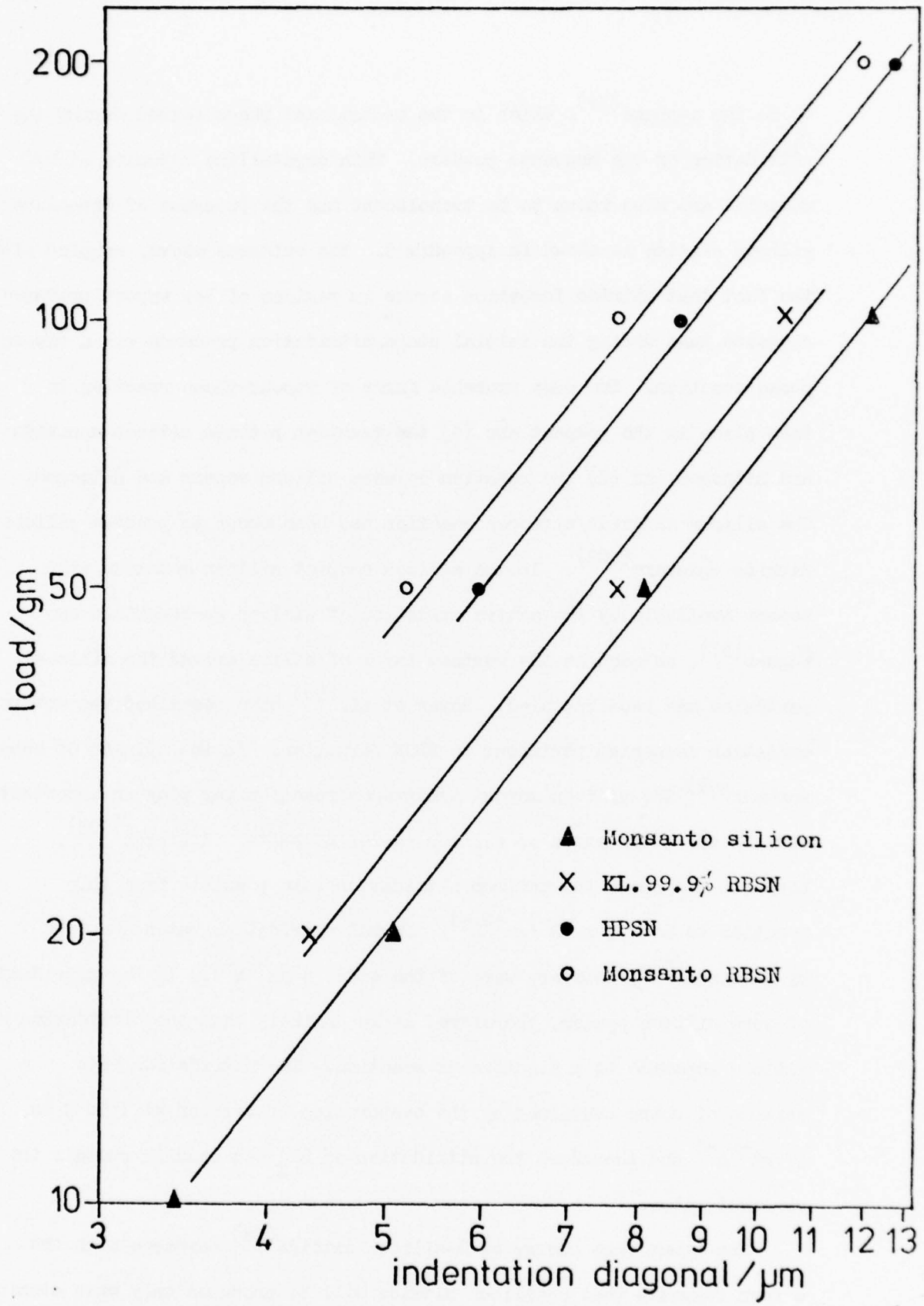


Fig.62. Microhardness data for various silicon nitrides.

to be the α-phase[31], which is the predominant phase formed during the nitridation of the Monsanto powders. Thin crystalline deposits of CVD material are also known to be translucent and the presence of translucent silicon nitride is shown in Appendix 5. The evidence above, coupled with the fact that nitride formation occurs in regions of low vapour pressure, suggests that during the initial stage, nitridation proceeds via a vapour phase reaction. The most probable forms of vapour-phase reaction to take place in the compact are (1) the reaction between silicon monoxide and nitrogen and (2) the reaction between silicon vapour and nitrogen. The silicon monoxide/nitrogen reaction has been shown to produce silicon nitride whiskers[102]. In the silicon compact silicon monoxide will become available by the active oxidation of silicon as described by Wagner[57], as soon as the surface layer of silica around the silicon particles has been ruptured. Boyer et al.[56] have described the active oxidation mechanism pertinent to RBSN formation. In the opinion of some workers[69] the silicon monoxide/nitrogen reaction may play an important part in the nitridation of silicon powder compacts. Atkinson[103], however, has shown the maximum nitridation rate possible from this reaction to be $1.2 \times 10^{-7} gm^{-2} h^{-1}$. Normal nitridation rates observed by Atkinson[12], however, were of the order $5\ gm^{-2} h^{-1}$. In the nitridation of pure silicon powder, therefore, it is unlikely that the nitridation of silicon monoxide is a significant reaction. The nitridation rate capable of being sustained by the evaporation of silicon at 1350°C is $50\ gm^{-2} h^{-1}$ and therefore the nitridation of Si_g can readily sustain the observed rates.

The lower free energy of β-silicon nitride[28] compared with the α form suggests that β-silicon nitride will be produced only when atomic rearrangement can take place during the nitridation reaction.

If the above is correct then, in the nitridation of the Monsanto powders, the α-phase content will be formed from reaction between silicon vapour (from silicon evaporation) and nitrogen gas. RBSN formed from the Monsanto powders also contain approximately 25% of the β-phase and from observation of the microstructure (Figs. 45-47) it is clear that the nitridation model of Atkinson et al.[12] is occurring in the system. This involves reaction between silicon in the solid state and chemisorbed nitrogen and hence β-silicon nitride would be expected to be formed from this mechanism.

Taking into account everything mentioned above it is possible to formulate a model for the nitridation of pure silicon powder compacts in nitrogen at 50 torr:

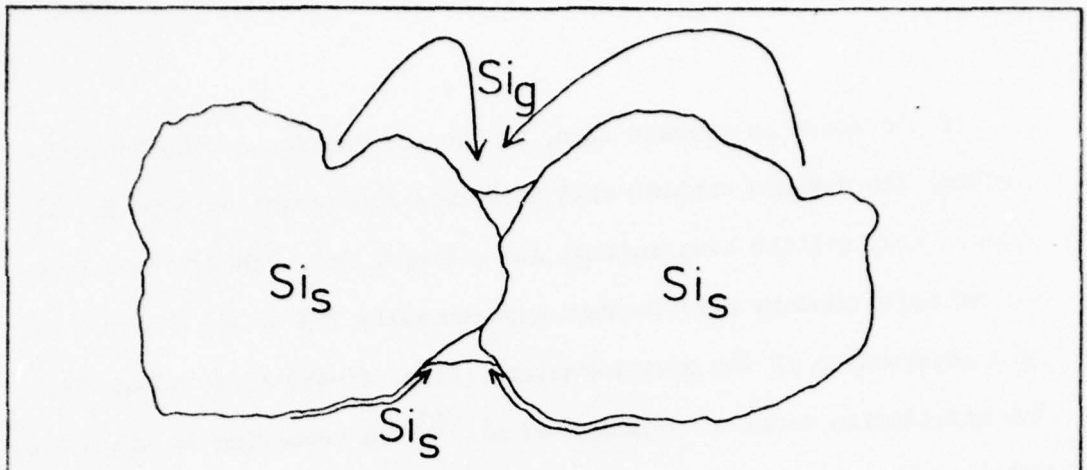
1) The evaporation and condensation of silicon, or surface diffusion of silicon, or both, results in a continuous silicon network throughout the compact (Fig. 63a).

2) The deposition of α-silicon nitride in regions of low vapour pressure occurs as a result of the reaction between silicon and nitrogen in the vapour phase (Fig. 63b).

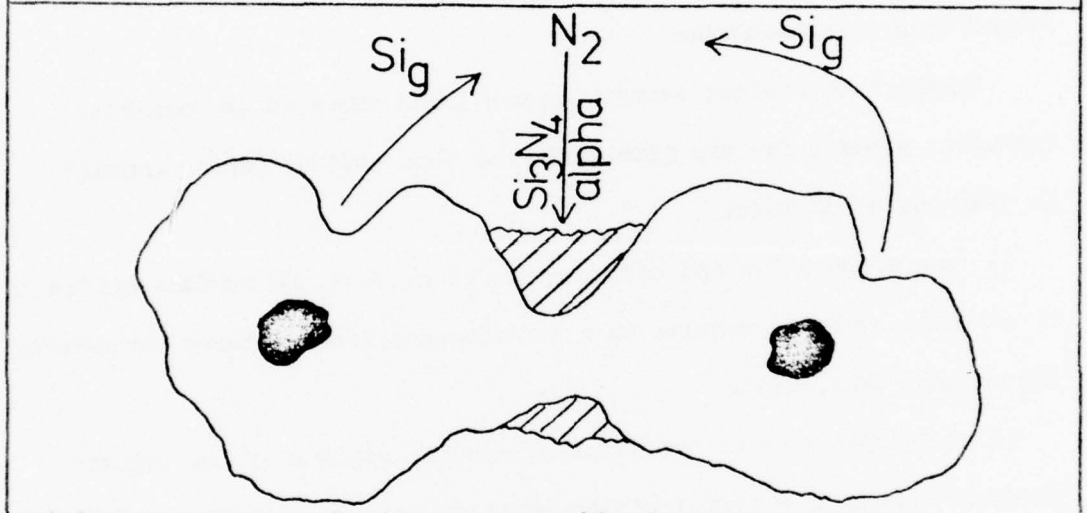
3) As the radius of curvature of the neck regions of the network becomes greater, then more general deposition of α-silicon nitride occurs. β-silicon nitride is formed via the reaction between chemisorbed nitrogen and the silicon surface according to the Atkinson et al.[12] model (Fig. 63c).

4) The reaction proceeds as in (3) until conversion approaches approx. 70% at which stage β-formation ceases; α-formation continues as long as silicon vapour is available for reaction.

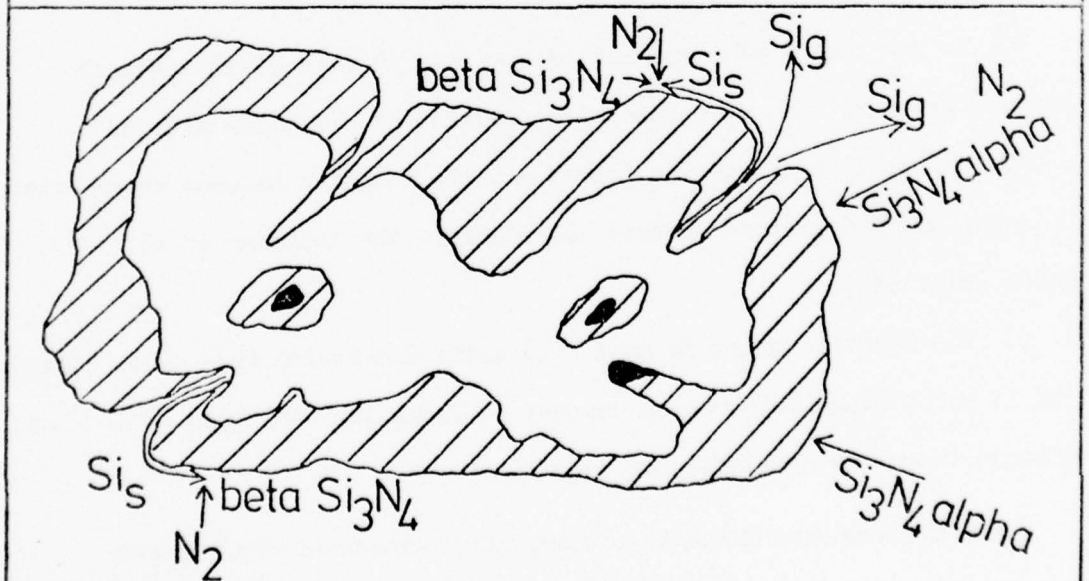
For the unwashed Monsanto powder, microstructural development proceeds in a similar manner to that described above, with the notable exception of the nitride formed inside the silicon particles. In order



(a) formation of silicon network.



(b) deposition of silicon nitride in neck regions.



(c) stage (b) mechanism and mechanism of Atkinson et al(12)

Fig.63. Nitridation model for pure silicon powder in 50 torr of nitrogen at 1370°C.

to gain more information concerning this phenomenon, cross-sections of compacts were etched in boiling 5% NaOH for 5 minutes in order to define the grain structure of the silicon particles. Figs. 64 and 65 clearly show that all of the nitride within the silicon is associated with grain boundaries. The nitride is surrounded by a region exhibiting different etching characteristics to the bulk silicon and some of the nitride exhibits a well-formed crystal habit similar to that commonly observed in the formation of nitride from a liquid phase. This phenomenon requires further investigation but, considering that the only difference between the two Monsanto powders is the impurity content, it would seem that the nitride on the grain boundaries develops because of grain boundary impurities and the diffusion of nitrogen to nitride growth sites.

The presence of blades and well-formed crystals in compacts of the unwashed Monsanto powder, as shown in Fig. 52, must also be associated with the impurity content of the powder.

RBSN formed from the Koch-Light powder showed no microstructural similarity to the Monsanto type material, and the Koch-Light material contained 80% β-silicon nitride compared with 70% α-silicon nitride for the Monsanto compacts. Although a continuous silicon network was not formed during the initial stage of nitridation, some silicon particles were joined by an impurity phase as shown in Fig. 55. The presence of such impurity phase material was always associated with large holes in the surrounding structure; this has also been demonstrated by Arundale and Moulson[104] for silicon compacts containing iron disilicide, $FeSi_2$. The majority of the nitride formed during the early stages was found within the impurity phase, as shown in Fig. 55, continued nitridation in these regions giving rise to the large dense formations of nitride shown in Fig. 57. In the author's opinion the majority of nitride formed during the nitridation of compacts of the Koch-Light powder is produced via the nucleation and growth of silicon nitride in liquid impurity phases

FIG. 64: Unwashed Monsanto silicon powder, isostatically pressed at 140 MNm^{-2}.

1370°C, 50 torr of nitrogen, 20 minutes.

Polished section, etched in 5% NaOH for 3 minutes at 100°C, reflected light.

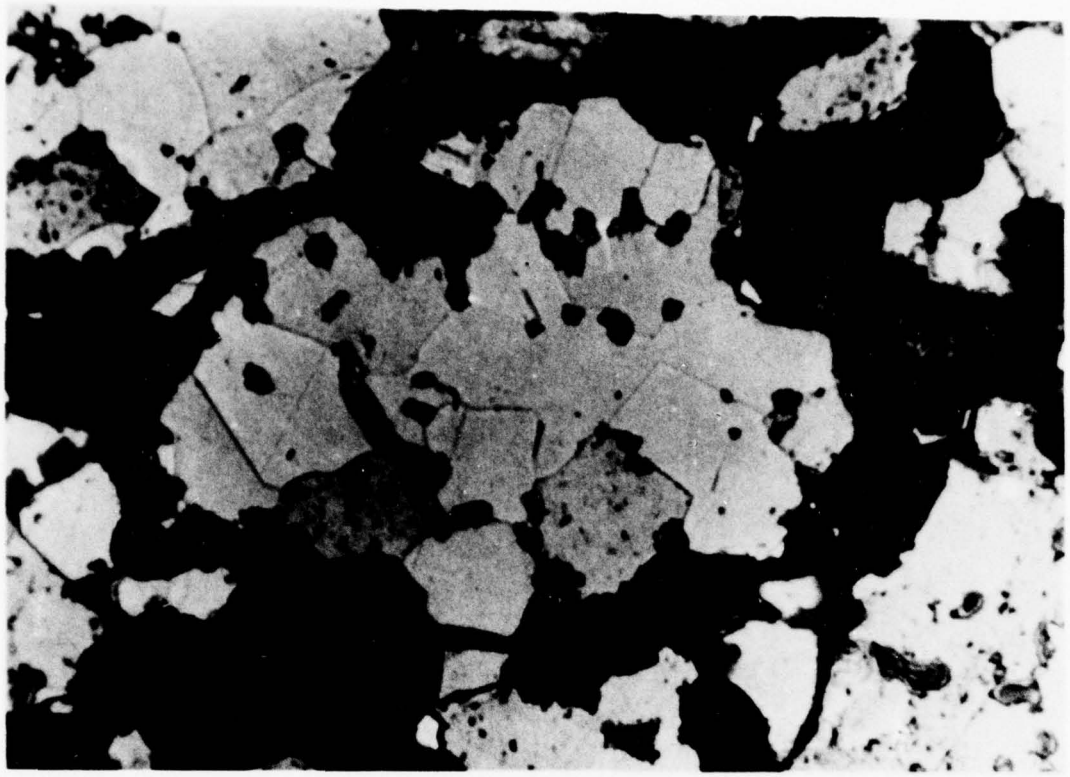
Nucleation of silicon nitride on grain boundaries.

FIG. 65: Unwashed Monsanto silicon powder, isostatically pressed at 140 MNm^{-2}.

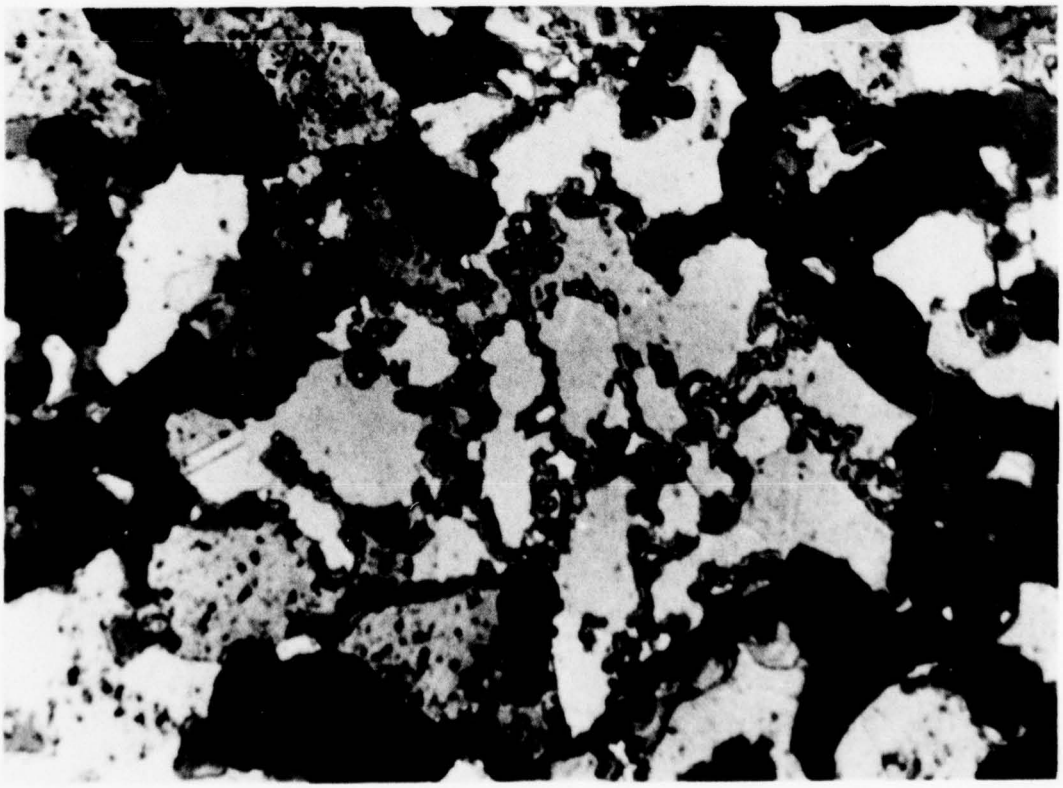
1370°C, 50 torr of nitrogen, 1 hour.

Polished section, etched in 5% NaOH for 3 minutes at 100°C, reflected light.

Growth of silicon nitride along grain boundaries; note the possible existence of a different phase between the silicon and the silicon nitride.



40μm



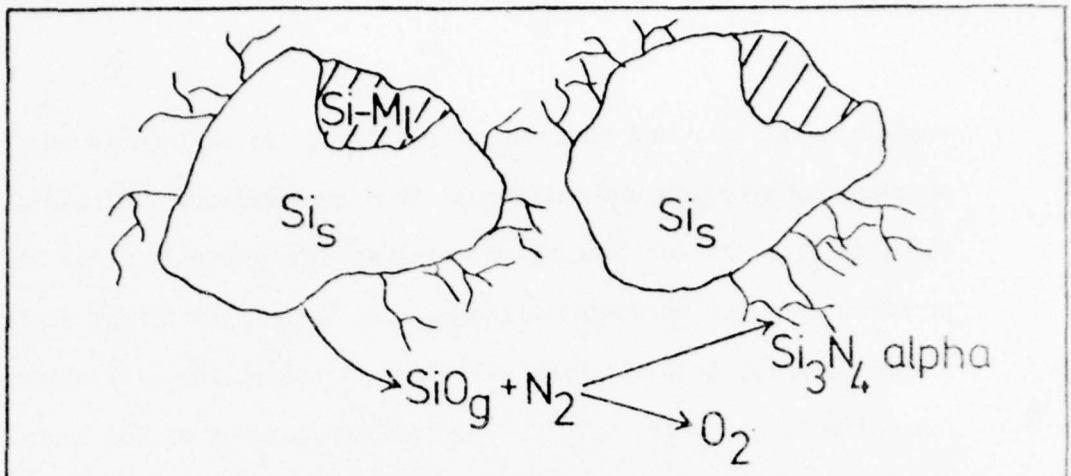
containing silicon and nitrogen in solution. As silicon is removed from solution by reaction with nitrogen, then more silicon will be taken into solution from the surrounding material and the impurity phase will progress into the unreacted silicon. The Koch-Light powder contains 1.45% Al and 0.3% Fe, both of which will form liquid phases with silicon at the nitriding temperature, 1370°C. The α-phase content of the Koch-Light material was formed entirely during the initial 10% of conversion which suggests that vapour-phase reactions play very little part in the formation of silicon nitride in this system. SEM studies of the microstructure show that the α-content may well be associated with the formation of a fibrous reaction product as shown in Fig. 56, the appearance of which also occurs exclusively during the initial stages of the reaction. The relationship between the aluminium content of silicon powder and the large proportion of beta-silicon nitride product has also been noted elsewhere[34].

Although it is possible that many mechanisms of nitridation are taking place during the conversion of compacts of Koch-Light 99.9% silicon to RBSN, the microstructural observations of this present study suggest the following model of nitridation:

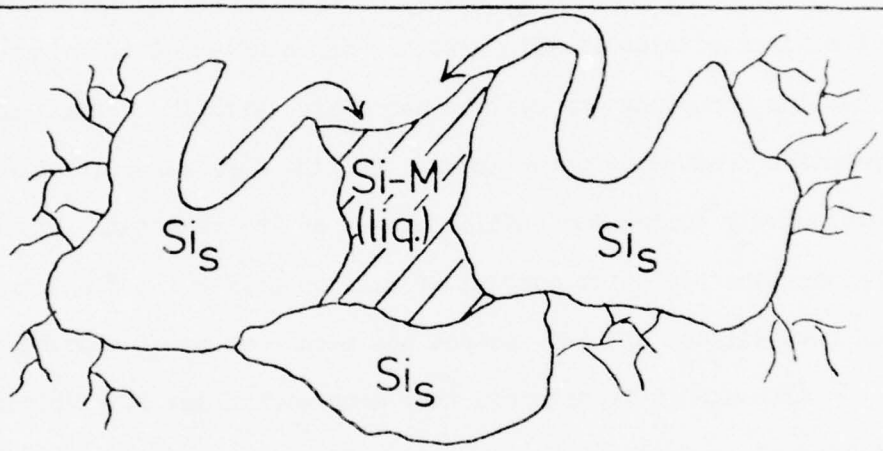
1) The surface layer of SiO_2 on the silicon particles is removed following the mechanism proposed by Boyer et al.[56], the resulting SiO reacts with nitrogen to form whiskers of α-silicon nitride (Fig. 66a).

2) Fe-Si and Al-Si impurity phases melt and flow into the voidage between the silicon particles leaving large holes in the microstructure (Fig. 66b).

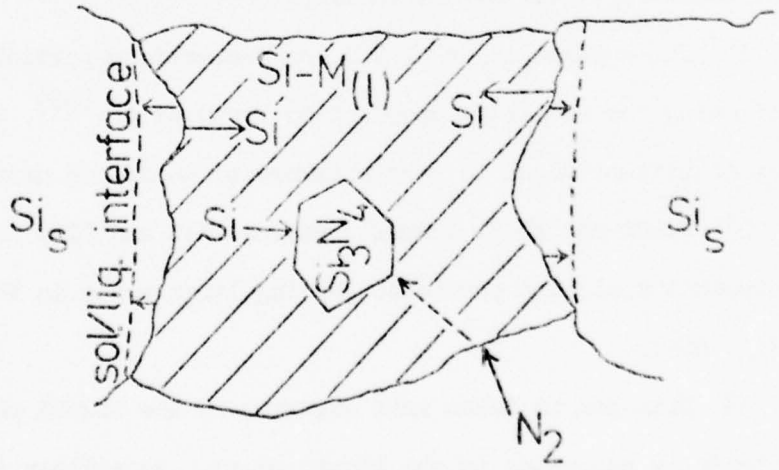
3) Nitrogen is taken into solution in the liquid phases and β-silicon nitride is nucleated in the liquid phase. As silicon is taken out of solution to form solid silicon nitride, the impurity phase/silicon interface moves forward as the silicon content of the liquid phase is maintained. Silicon nitride continues to grow in the liquid phase resulting in large dense areas of β-silicon nitride (Fig. 66c).



(a) formation of fibrous alpha-silicon nitride.



(b) flow of liquid impurity phases.



(c) growth of beta-silicon nitride in liquid phase.

Fig.66. Nitridation model for Koch-Light 99.9% silicon in 760 torr of nitrogen at 1370°C.

6. GENERAL DISCUSSION

The major aim of the present study was to correlate the Young's Modulus of RBSN, at various stages of conversion from a silicon powder compact to a ceramic body, with its microstructure and phase composition. During the course of the study many experimental techniques were employed and they are now briefly analysed.

The use of a dynamic, non-destructive, method for the determination of E was found to give very accurate and reproducible results at all stages of conversion. Some special care, however, was required in the preparation of test-bars from lightly nitrided compacts. The "electrostatic" apparatus can also be used for the measurement of "internal friction", one application of which would be the monitoring of thermal shock damage, since energy losses in the material are proportional to the amount of cracking present in the sample. A non-destructive method has the added advantage that test-bars can undergo further reaction after testing and the resultant change in properties can be determined on the same sample.

Of the methods used for observing the microstructure of RBSN optical microscopical examination of polished sections yielded useful general information. Scanning electron microscopy is a technique for observing growth morphology but unfortunately it cannot distinguish between different phases, particularly between silicon and silicon nitride. The observations made on etched polished sections were shown to be of value in correlating nitride nucleation sites with grain boundaries in the silicon, and it is recommended that in any further studies of the microstructure of RBSN this technique should be fully exploited. Electron-probe microanalysis was not extensively used but from the experience of observations made on polished sections it is likely that such a technique could be of value in determining nitride growth mechanisms, particularly where liquid phase reactions are thought to be occurring.

The friable nature of RBSN at low extents of conversion presented problems with the preparation of polished sections; it is recommended that such samples should not be machined or ground using coarse abrasive; in the present study the coarsest abrasive used was 6 micron diamond spray.

The use of spherical silicon was not as successful as was hoped because of the aluminium contamination which occurred during spheroidisation. The photomicrographs shown in Appendix 4, however, illustrate that the use of such particles does provide a very clear picture of developing microstructure. Another possible disadvantage in the use of spherical powder is the difference in specific surface area when compared to the normal angular powder particles, resulting in a difference in reaction rates in the present case.

The theoretical E/ρ_n relationship derived from Ishai and Cohen's (100) three-phase-composite model accurately predicts the linear slope of the experimentally determined relationships for all of the powders investigated. This suggests that the treatment of RBSN as a three-phase-composite of silicon, silicon nitride and porosity, with all the components affecting the modulus of the material, is essentially correct. The constant deviation from the predicted value of E at any ρ_n, however, implies that the model is not an exact representation of the practical situation. For a material such as partially nitrided RBSN, which has a complex and, as the reaction proceeds, continuously changing microstructure, this is not surprising and one difficulty is probably the correct modelling of the void content of the material. The model considers pores to be an isolated dispersed phase in the composite matrix whereas much of the porosity of RBSN is interconnected, particularly at low values of ρ_n.

For the compacts of Monsanto silicon nitrided at nitrogen pressures below atmospheric, the silicon content was also shown to be inter-

connected at low values of ρ_n. Indeed the development of a continuous silicon network was shown to account for the initial steep rise in E, as demonstrated by the measurements made of the modulus of vacuum-treated silicon compacts which reached a limiting value of 35 GNm^{-2}. Although the theoretical model also predicts an initial steep rise in modulus, this is due to an entirely different reason. For the green silicon compact $C_{SN} = 0$ and hence $E_c = 0$; as silicon nitride is formed the model predicts a steep rise in modulus as it considers the silicon nitride to form a continuous network. Mathematically this is determined by the term $\left[1 - \left(\frac{C_p}{C_p + C_{SN}}\right)^{\frac{2}{3}}\right]$. The model assumes a continuous silicon nitride ($E_{SN} = 310\ GNm^{-2}$) network, whereas in practice a silicon ($E_{SN} = 110\ GNm^{-2}$) network is formed initially, and hence a lower value of E_c, that that predicted by the model, would be expected during this initial stage of nitridation. The experimental data, as shown in Fig. 35, are in accordance with the expected low value of E_c.

Although it has been demonstrated that the silicon network can account for a modulus value of 35 GNm^{-2}, the experimental E/ρ_n relationship does not become linear until a value of 65 GNm^{-2} is attained. This suggests that a different mechanism of strength development is occurring between (a) the formation of a silicon network and (b) the mechanism giving rise to the linear E/ρ_n dependence. From the microstructural observations made at stages between (a) and (b), (Figs. 43, 44), modulus development can be seen to be due to the formation of silicon nitride in the neck regions of the silicon network. As the necks will be the "stiffness-determining" regions of the network, nitride formed here will increase the modulus of the material to a greater extent than at later stages when the nitride formation occurs more generally over the surfaces in the compact.

Even though the difference between the theoretical and experimental

data for the early stages of nitridation can be explained, the fact that a difference still exists at higher conversions is more difficult to explain in terms of the microstructure observed. The most obvious difference between the model and the actual situation, at these later stages of conversion, is the large channels of porosity that exist in the microstructure and which originate during the formation of the silicon network. Such channels will still exist as nitride forms on the silicon surfaces, and will not be eliminated until sufficient nitride has been produced to interconnect across the channels. For RBSN of ρ_n = 2400 kgm^{-3}, formed from a silicon compact of ρ_g = 1500 kgm^{-3}, these channels still exist in the microstructure, as shown in Fig. 67. The inhomogeneity in the structure caused by the channels will reduce the modulus of the material and is a possible reason for the difference between the theoretical and experimental data. At higher nitrided densities it is expected that cross-linking would occur across the channels and the experimental data should approach the theoretical curve of Ishai and Cohen[100].

The Young's Modulus data for the "unwashed" Monsanto silicon compacts showed no significant difference to those of the washed powder and, as the microstructures of the RBSN's, formed from the two Monsanto materials were very similar, it can be concluded that the same mechanisms of strength development are taking place in both instances.

RBSN formed from the Koch-Light 99.9% silicon powder (1370°C, 760 torr of N_2) was of a consistently lower Young's Modulus than the Monsanto material and the E/ρ_n relationship was linear over the whole range of ρ_n investigated. A linear relationship was also observed for the compacts of "unwashed" Monsanto powder nitrided in nitrogen at 760 torr, and the common feature of the microstructure of these materials was the lack of a continuous silicon network during the initial stage of

Fig. 67. Washed Monsanto silicon powder, isostatically pressed at 140 MNm^{-2}.

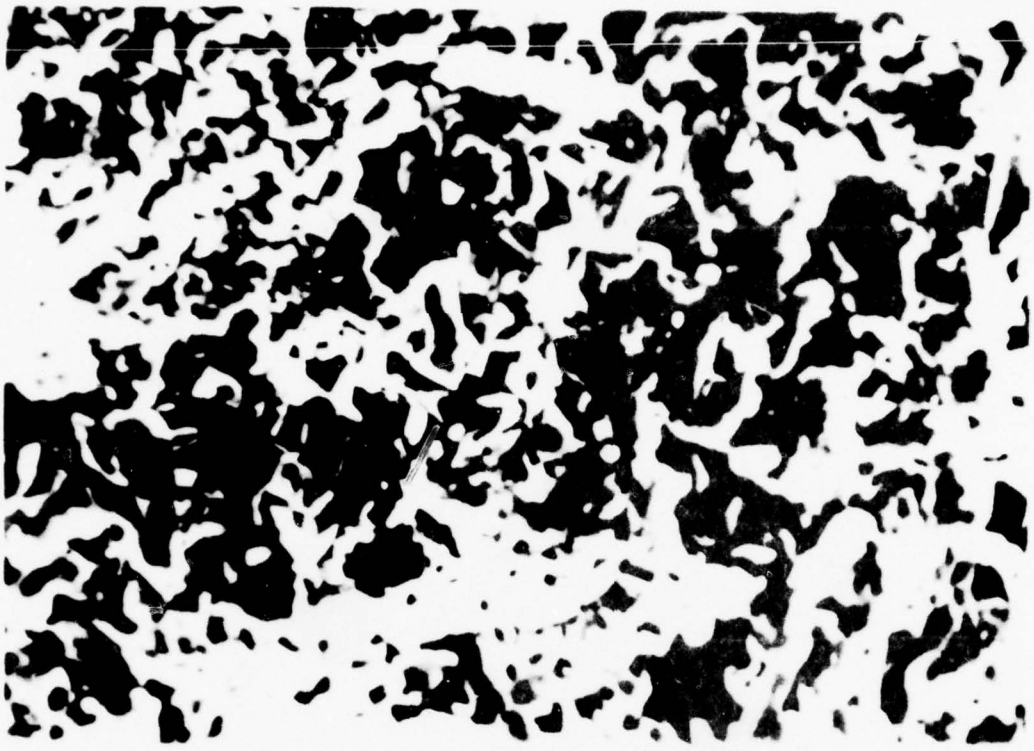
1370°C, 50 torr of N_2, 30 hours.

S.E.M. of fracture surface showing long (200 μm) channel-like void.

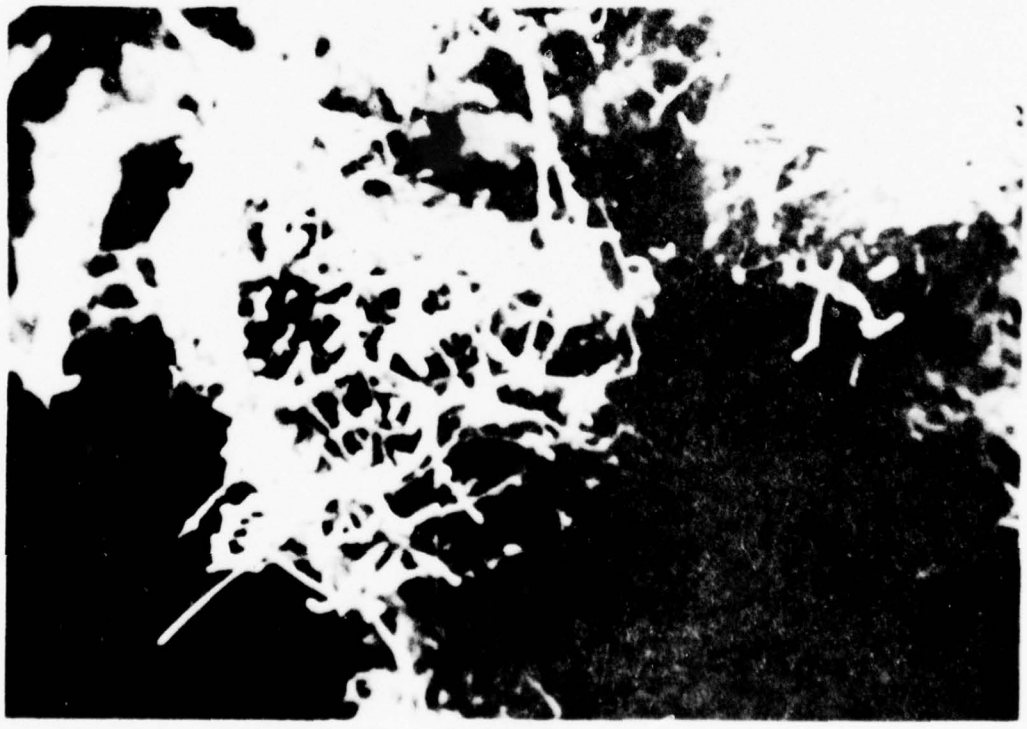
Fig. 68. Koch-Light silicon powder, isostatically pressed at 140 MNm^{-2}.

1370°C, 760 torr of N_2, 8 hours.

S.E.M. of fracture surface showing whisker-type reaction product.



100μm.



20μm.

nitridation. Although the unwashed Monsanto compacts, nitrided in nitrogen at 760 torr initially showed a lower modulus than the compacts nitrided in nitrogen at 50 torr, the modulus values did become coincident as nitridation proceeded. The Koch-Light compacts, however, exhibited a lower modulus value at all values of ρ_n with the modulus value being directly proportional to the amount of nitride present over the whole range of ρ_n. The fact that no steep rise in modulus was observed during the initial stages is consistent with the fact that the formation of a continuous silicon or silicon nitride network was not observed until the later stages of nitridation. The difference between the Young's Modulus of the Monsanto and Koch-Light RBSN's cannot be explained satisfactorily from the microstructural evidence, but it can be concluded that RBSN formed from silicon powders containing iron and aluminium at the 1 wt% level has a lower value of Young's Modulus than RBSN produced from pure silicon powder.

During the early stages of conversion of the Koch-Light silicon compacts no silicon network was formed but a large amount of whisker growth was observed. In view of the low value of the elastic modulus for such compacts the whisker growth cannot be effective in bonding the loose silicon particles in the compact. Also, where no whiskers or silicon network were formed, for example in the case of the "unwashed" Monsanto nitrided in nitrogen at 760 torr, the initial rise in modulus was comparable to the situation where whiskers were present. It seems unlikely, therefore, that whisker growth plays a significant part in modulus development during the first stages, approximately 20%, of the conversion process.

Part of the background to the present study was the work of Atkinson et al.[12] which showed that pure silicon powder of mean particle size 85 microns could not be fully converted to silicon nitride when nitrided at 1350°C in nitrogen at 760 torr, but that 100% conversion

could be obtained at lower pressures of nitrogen because of a change in the nitride growth morphology. The reaction mechanism proposed by Atkinson et al. is described in Section 2.2.2 and involved a surface reaction between chemisorbed nitrogen and silicon. No mention was made, however, of the phase composition of the resultant RBSN. Recent studies[52,53] of the formation of α and β-silicon nitride during the nitriding of commercial type silicon powder in nitrogen at 760 torr suggest that two separate reactions are involved, one forming β and the other forming α. The possibility of two separate reactions must also be considered for low pressure reaction-bonding of high purity silicon powder.

The present concensus of opinion concerning the two phases of silicon nitride is that both are polymorphs of Si_3N_4 with α being a metastable form, the growth of one or the other being determined by kinetic rather than thermodynamic considerations. If α-Si_3N_4 is a metastable form then the reaction mechanism leading to its formation must be one in which atomic rearrangement to the more stable β configuration is not possible. Vapour-phase reactions meet the above condition and it has been suggested[52,53,26] that α formation is associated with silicon-bearing vapour species.

The normal growth morphology postulated for α-silicon nitride has been the whiskers commonly observed in previous studies and which can be produced by the silicon monoxide/nitrogen reaction[32]. It has also been suggested[26] that the presence of α-silicon nitride in RBSN is always accompanied by whiskers. The present study and the work of Guthrie[105], however, show that α can be formed in other than a whisker type morphology and the lack of whiskers in the present study of high-purity silicon makes it probable that silicon monoxide does not play a significant role in reaction-bonding under such conditions. It has also

been argued[103] that the maximum possible flux of oxygen away from the site at which the silicon monoxide is nitrided is not sufficient to sustain the reaction rates commonly observed in the production of RBSN. The most probable silicon species to be involved in alpha formation is silicon vapour, the availability of which, estimated from vapour pressure data[106], is sufficient to explain the observed reaction rates.

The RBSN produced from high-purity silicon had an α-phase content of 70% with the formation rate being linear during the early part of the reaction as shown in Fig. 49. There is an indication in Fig. 49 of a small increase in α formation when the beta-forming reaction ceases. This would be the result of extra nitrogen being available for reaction with silicon vapour; the supply of nitrogen being rate controlling at this stage. The direct nitridation of solid silicon by gaseous nitrogen, as described by Atkinson et al.[12] is seen from the present study to be the β-forming reaction. This reaction effectively stops before the α-forming reaction because surface diffusion distances become too great to sustain the supply of silicon to reaction sites.

In the nitridation of high-purity silicon the reactions involved in the formation of α and β-silicon nitride can, therefore, be summarised as follows:

(a) reaction in the vapour phase between silicon and nitrogen, resulting in α-silicon nitride, and

(b) reaction between chemisorbed nitrogen and surface diffusing silicon, resulting in β-silicon nitride.

Although it is not possible to distinguish between α and β-silicon nitride using optical microscopical methods, reactions (a) and (b) above were found to exhibit certain distinguishing features which enabled the description of developing microstructure given in Section 5.5.4 to be made. The predominant features of microstructural development in

compacts of pure silicon powder nitrided at low pressures of nitrogen and their relationship to the Young's Modulus of the compact (ρ_g = 1500 kgm^{-3}) can now be summarised as follows:

(a) On the introduction of the green silicon compact into the furnace hot-zone, neck formation occurs between powder particles as a result of either surface diffusion or vapour phase transport of silicon. No overall densification of the compact takes place, the pore volume only being redistributed with long channel-like pores developing in the compact. This process, which has also been described by Greskovich and Rosolowski[107], is accompanied by an increase in Young's Modulus of the compact to 35 GNm^{-2}.

(b) α-silicon nitride is deposited in the neck regions of the compact in a dense, massive form, and the Young's Modulus rises to a value of 65 GNm^{-2}. β-formation is negligible during this stage.

(c) α-silicon nitride is deposited more generally over all silicon surfaces in the compact because of the increase in the radius of curvature of the neck regions of the silicon network. β-silicon nitride is concurrently formed by the mechanism described by Atkinson et al.[12], the E/ρ_n relationship now being linear.

(d) β-silicon nitride formation ceases as the surface diffusion of silicon to nitride growth sites becomes limiting. There is a corresponding increase in α formation because more nitrogen is available for reaction in the vapour phase. The E/ρ_n relationship remains linear.

Although some minor differences were observed between the microstructure of "unwashed" and "washed" Monsanto compacts, as described in Section 5.5.2, these were not reflected in the value of Young's Modulus.

It is assumed, therefore, that the basic mechanisms of nitridation and strength development summarized above will also apply to compacts of "unwashed" Monsanto powder.

The microstructure developed in the nitrided Koch-Light compacts would seem to be determined by the large impurity concentration present in the silicon powder. The impurities are also responsible for the high degrees of conversion, obtained in nitrogen at 760 torr, in contrast to those achieved when pure silicon powder of the same particle size is nitrided. The RBSN formed from the Koch-Light powder contained approximately 80% β-silicon nitride and, from the evidence described in Section 5.5.4, it is probable that the majority of the β growth occurs as a result of the reaction between silicon and nitrogen in liquid solution. Furthermore, in the case of the Koch-Light material the α content was found to form predominantly during the initial stages of the reaction, and some of the α phase may be present in a whisker-type morphology.

The rupture modulus data showed the Monsanto RBSN's to be approximately 40% stronger than the Koch-Light RBSN at all values of ρ_n, with the "unwashed" Monsanto compacts having a slightly higher strength than compacts of the "washed" powder. Although the Monsanto RBSN's exhibited a higher value of Young's Modulus than that normally obtained[61,69,81] for RBSN, the rupture modulus of the material was only equivalent to commonly observed strengths in commercial RBSN's of much lower purity. On consideration of the three strength-controlling factors, E, γ_i, and c, it is probable that an increase in critical defect size is the most likely explanation of the relatively low strength values encountered. This view is supported by the microstructural evidence for the existence of large channel-like pores in the Monsanto RBSN.

The low Young's Modulus of the Koch-Light RBSN was reflected in the rupture modulus of the material. The formation of large voids resulting

from the melting and subsequent flow of impurity phases has been demonstrated by Moulson and Arundale[104] and it is probable that the critical defect size in the Koch-Light RBSN is determined by this process.

The present study has demonstrated that the formation of RBSN from pure silicon powder, at low pressures of nitrogen, is a potential route for improving the mechanical properties of the ceramic with the Young's Modulus of the pure material being substantially higher than that of commercial RBSN's. At the present time, however, the rupture modulus of the pure material would seem to be limited, either by fabrication variables or by the formation of large, elongated pores in the structure during silicon network formation. Possible methods of preventing the development of such pores would include the use of a small silicon particle size and the controlled addition of dopants which would inhibit silicon network formation. The work of Boyer[108] suggests that small additions of iron, introduced by washing in an iron salt solution to give a uniform distribution over the silicon surface, may be effective in restricting the extend of silicon network growth.

The correlation achieved between the Young's Modulus data and the theoretical three-phase-model has shown that in any consideration of developing mechanical properties during nitridation, RBSN can be considered as a composite of silicon, silicon nitride and porosity, with all three components influencing the properties of the material. For compacts of pure silicon powder, the inter-relation of the three components of the composite can easily be determined by microscopical methods, whereas for impure materials the important aspects of micro-structural development can easily be masked by secondary reaction products and effects, such as whisker morphologies and impurity phases.

face moves forward as the silicon content of the liquid phase is maintained. Silicon nitride continues to grow in the liquid phase resulting in large dense areas of β-silicon nitride (Fig. 66c).

For a microstructural engineering approach to RBSN optimisation to be successful it is necessary that the microstructure of the material is able to be closely monitored. This is possible for the pure material described in the study and taken in conjunction with the high value of Young's Modulus obtained, low pressure nitridation of pure silicon powder provides a sound basis for further development of the reaction-bonded silicon nitride ceramic.

REFERENCES

1. "Ceramics for High Performance Applications". Proceedings of the Second Army Materials Technology Conference, Hyannis, Mass. November 13-16, 1973. Ed. J.J. Burke, A.E. Gorum, R.N. Katz. Brook Hill Pub. Co., 1974.
2. W. Weibull. J. Appl. Mechs. 18, 293, 1951.
3. R.W. Davidge, J.R. McLaren and G. Tappin. J. Mats. Sci. 8, 1699-1705, 1973.
4. E. Glenny and T.A. Taylor, Powder Met. 1/2, 189, 1958.
5. E. Glenny and T.A. Taylor, Powder Met. 8, 164, 1964.
6. "High Temperature Technology". Ed. Campbell, John Wiley and Sons Inc., New York, 460, 1956.
7. D.J. Godfrey, Metals and Materials, 2, 10, 305, 1968.
8. R.M. Cannon and R.J. Hill, "High Temperature Compounds for Turbine Vanes". N.A.S.A. Report CR-72794.
9. A.N. Holden, S. Mumford and C.R. Booher. "Third Materials Conference, Turbine Applications". October 30-November 1, 1974. Ann Arbor, Mich.
10. G.R. Terwilliger. J. Amer. Ceram. Soc. 57, 48, 1974.
11. M. Mitomo, M. Tsutsumi, E. Bannai, T. Tanaka. J. Amer. Ceram. Soc. 55, 313, 1976.
12. A. Atkinson, A.J. Moulson and E.W. Roberts. J. Amer. Ceram. Soc. 59, 7/8, 285, 1976.
13. E.T. Turkdogan, P.M. Bills and V.A. Tippett. J. Appl. Chem. 8, 296, 1958.
14. D. Hardie and K.H. Jack. Nature 180, 332, 1957.
15. W.D. Forgeng and B.F. Decker, Trans. Met. Soc. of A.I.M.E., June, 1958.
16. S.N. Ruddlesden and P. Popper. Acta Cryst. 11, 465, 1958.
17. P. Grieveson, K.H. Jack and S. Wild. "Special Ceramics" 4, Ed. P. Popper, Brit. Ceram. Res. Assoc., Stoke-on-Trent, 1968, p.237.

38. R.F. Horsley. Ph.D. Thesis, University of Leeds, 1971.

39. A. Atkinson, P.J. Leatt and A.J. Moulson. Proc. Brit. Ceram. Soc. 22, 253, 1973.

40. D.R. Messier and P. Wong, A.M.M.R.C., Watertown, Mass. Technical Report A.M.M.R.C. TR 72-10, 1972.

41. J. Stringer. Acta Met. 8, 758, 1960.

42. J. Stringer. Acta Met. 8, 810, 1960.

43. D.R. Messier and P. Wong. J. Amer. Ceram. Soc. 56, 480, 1973.

44. D.S. Thompson. Ph.D. Thesis, Imperial College, London, 1963.

45. A. Atkinson and A.J. Moulson. S.R.C. Research Grant B/SR/7943, Progress Report No. 4, 1974.

46. A.G. Reeves and R.J. Evans. J. Phys. Chem. Solids, 30, 551, 1969.

47. D.J. Godfrey. Proc. Brit. Ceram. Soc. 25, 325, 1975.

48. B.C.H. Steele and M.A. Williams. J. Mats. Sci. 8, 427, 1973.

49. D.W. Ready and G.C. Kuczynski. J. Amer. Ceram. Soc. 49, 26-29, 1966.

50. R.B. Guthrie and F.L. Riley. J. Mats. Sci. 9, 1363, 1974.

51. Sin-Shon Lin. J. Amer. Ceram. Soc. 58, 271, 1975.

52. D.P. Elias and M.W. Lindley. J. Mats. Sci. 11, 1278, 1976.

53. D. Campos-Loriz and F.L. Riley. J. Mats. Sci. 11, 195-198, 1976.

54. A. Atkinson and A.J. Moulson. Sci. of Ceramics 8, Publ. Brit. Ceram. Soc. 111, 1976.

55. Carborundum Co. Ltd., Brit. Pat. 726,812, 1955.

56. S.M. Boyer, D. Sang and A.J. Moulson, in "Nitrogen Ceramics". Ed. F.L. Riley, NATO Advanced Study Institute. Applied Science Series No. 23, Noordhoff International Publ. BV, 1977, p.297.

57. C. Wagner. J. Appl. Phys. 29, 9, 1295, 1958.

58. K.J. Huttinger. "High Temperatures-High Pressures", 2, 89, 1970.

59. A. Atkinson and A.J. Moulson. S.R.C. Research Grant B/SR/7943, Progress Report No. 5, 1975.

60. K. Niwano and A.J. Moulson. "Slip-casting of silicon powders". Report, Department of Ceramics, University of Leeds, U.K. 1977

18. N.L. Parr and E.R.W. May, Proc. Brit. Ceram. Soc. 7, 81-98, 1967.

19. S. Wild, P. Grieveson and K.H. Jack. "Special Ceramics", 5, Ed. P. Popper, Brit. Ceram. Res. Assoc., Stoke-on-Trent, 1972.

20. T. Maruyama and H. Suzuki. J. Amer. Ceram. Soc., 58, 11/12.

21. A.G. Evans and J.V. Sharp in "Electron Microscopy and Structure of Materials". Eds. G. Thomas, R.M. Fulrath and R.M. Fisher, Univ. of California Press, Berkeley, 1141-1154, 1972.

22. H.F. Priest, F.C. Burns, G.L. Priest and E. Skaar. J. Amer. Ceram. Soc. 56, 7, 395, 1973.

23. I. Kohatsu and J.W. McCauley. Mat. Res. Bull. 9, 917-920, 1974.

24. A.J. Edwards, D.P. Elias, M.W. Lindley, A. Atkinson and A.J. Moulson. J. Mats. Sci. 9, 516, 1974.

25. K. Kato, Z. Inoue, K. Kijima, J. Kawada, H. Tanaka and T. Yamane, J. Amer. Ceram. Soc. 58, 3/4, 90, 1975.

26. K. Blegen, "Special Ceramics", 6. Ed. P. Popper, Brit. Ceram. Res. Assoc., Stoke-on-Trent, 1975, p.223.

27. K. Kijima, K. Kato, Z. Inoue and H. Tanaka. J. Mats. Sci. 10, 2, 362, 1975.

28. C.M.B. Henderson and D. Taylor. Trans. J. Brit. Ceram. Soc. 74, 49, 1975.

29. R.S. Bradley, D.C. Munroe and M. Whitfield. J. Inorg. Nucl. Chem. 28, 1803-1812, 1966.

30. A. Hendry and K.H. Jack. "Special Ceramics", 6, 199, 1975. Ed. P. Popper, Brit. Ceram. Res. Assoc., Stoke-on-Trent.

31. K. Niihara and T. Hirai. J. Mats. Sci. 11, 593-611, 1976.

32. C.C. Evans. Brit. Pat. 1, 121, 293, 1968.

33. A.G. Evans and R.W. Davidge. J. Mats. Sci. 5, 314, 1970.

34. H. Suzuki. Bull. Tokyo Inst. Tech. 54, 19, 163-177, 1963.

35. Proc. Brit. Ceram. Soc. 22, 1973.

36. R.L. Brown, D.J. Godfrey, M.W. Lindley and E.R.W. May. "Special Ceramics" 5, 345-361, 1970, Ed. P. Popper, Brit. Ceram. Res. Assoc.

37. P. Popper and S.N. Ruddlesden. Trans. Brit. Ceram. Soc. 60, 9, 603, 1961.

in the compact.

Even though the difference between the theoretical and experimental

61. B.J. Dalgleish and P.L. Pratt. Proc. Brit. Ceram. Soc. 25, 2, 297, 1975.

62. A.G. Evans and J.V. Sharp. J. Mats. Sci. 6, 10, 1292, 1971.

63. N.L. Parr, G.F. Martin and E.R.W. May. "Special Ceramics", 1960. Ed. P. Popper, Heywood & Co., London, p.102.

64. D.J. Godfrey and M.W. Lindley. Proc. Brit. Ceram. Soc. 22, 229, 1973.

65. T.J. Whalen and A.T. Anderson. J. Amer. Ceram. Soc. 58, 396, 1975.

66. Per Kofstad. "High Temperature Oxidation of Metals". John Wiley and Sons Inc. 1966.

67. G. Pfefferkorn. Z. Wiss. Mikroscopie, 62, 109, 1954.

68. G. Pfefferkorn and J. Vahl. Werkstoffe Korrosion, 14, 1021, 1963.

69. B.F. Jones, K.C. Pitman and M.W. Lindley. J. Mats. Sci. 12, 1977.

70. S.C. Danforth and M.H. Richman. Metallography, 9, 321-332, 1976.

71. E.M. Carr and R.W. Bartlett. Technical Report, AFML-TR-68-197, 1968.

72. A. De S. Jayatilaka, T.F. Page and J.A. Leake. J. Mats. Sci. 9, 514, 1974.

73. A. Atkinson, P.J. Leatt, A.J. Moulson and E.W. Roberts. J. Mats. Sci. 9, 6, 981-4, 1974.

74. J. Bernard, F. Gronlund, J. Oudar and M. Duret. Z. Electrochem. 63, 7, 799-804, 1959.

75. F.M. Ernsberger. Proc. 8th Int. Conf. on Glass, Soc. of Glass Tech., Sheffield, 1969.

76. C.E. Inglis. Inst. Naval Architects Trans. 55, 219, 1913.

77. A.A. Griffith. Phil. Trans. Roy. Soc. (London), 221A, 163, 1920.

78. G.R. Irwin. Hanbuck der Physik 6, 551, Springer, Berlin, 1958.

79. J.T. Barnby and R.A. Taylor. "Special Ceramics" 5. Ed. P. Popper. Brit. Ceram. Res. Assoc., Stoke-on-Trent, 1972.

80. F.F. Lange. J. Amer. Ceram. Soc. 56, 10, 518, 1973.

81. W.A. Fate. J. Appl. Phys. 46, 6, June, 1975.

was the lack of a continuous silicon network during the initial stage of

82. D.S. Thompson and P.L. Pratt. Proc. Brit. Ceram. Soc. 6, 37-47, 1966.

83. B.F. Jones and M.W. Lindley. Powder Met. Int. 8, 32, 1976.

84. Saluh ud Din and P.S. Nicholson. J. Amer. Ceram. Soc. 58, 11/12, 500, 1975.

85. H.L. Marcus, J.M. Harris and F.J. Szalkowiki. "Auger Spectroscopy of Fracture Surfaces of Ceramics", in "Fracture Mechanics of Ceramics", Vol. 1, Plenum Press, London, 1973.

86. J.A. Mangels. J. Amer. Ceram. Soc. 58, 7/8, 354, 1975.

87. B.J. Dalgleish, Ph.D. Thesis, Imperial College, London, 1974.

88. W. Ashcroft. Proc. Brit. Ceram. Soc. 22, June, 1973.

89. P.B. Noakes and P.L. Pratt. "Special Ceramics" 5. Ed. P. Popper, Brit. Ceram. Res. Assoc., Stoke-on-Trent, 1972, p.299.

90. D.E. Lloyd. "Special Ceramics" 4. Ed. P. Popper, Brit. Ceram. Res. Assoc., Stoke-on-Trent, 1968, p.165.

91. J.A. Coppola, R.C. Bradt, D.W. Richerson and R.A. Alliegro, Ceram. Bull. 51, 11, 847, 1972.

92. B.F. Jones and M.W. Lindley. J. Mats. Sci. 10, 967, 1975.

93. M.J. Wahll, J.R. Van Orsdel and R.B. Fischer. Powder Met. 8, 41, 1961.

94. J.M. Ide. Review Sci. Instr. 6, 10, 296-298, 1935.

95. D. Bancroft and R.B. Jacobs. Review Sci. Instr. 9, 279, 1938.

96. W.R. Davis. Trans. Brit. Ceram. Soc. 67, 11, 515-541, 1968.

97. R.E. Booker and F.H. Sagar. Ultrasonics, Oct-Dec. 1963.

98. B. Paul. Trans. Met. Soc. of AIME, 218, 36-41, 1960.

99. O. Ishai. Mag. Concrete Res. 17, 52, 148-150, 1965.

100. L.J. Cohen and O. Ishai. J. Comp. Matls. 1, 390, 1967.

101. Silicon Semiconductor Technology. W.R. Runyon, McGraw-Hill, London, 1965.

102. C.C. Evans. Brit. Pat. 1, 121, 293, 1968.

103. A. Atkinson and A.J. Moulson.S.R.C. Research Grant, B/SR/7943, Progress Report No. 5, 1975.

104. P. Arundale and A.J. Moulson. J. Mats. Sci. 12, 2138, 1977.

105. R.B. Guthrie, Ph.D. Thesis, University of Leeds, 1975.

106. Yu. M. Shashkov. "Metallurgy of Semiconductors", p.3. Consultants Bureau, New York, 1961.

107. C. Greskovich and J.H. Rosolowski. J. Amer. Ceram. Soc. 59, 7/8, 336-343, 1976.

108. S.M. Boyer. Ph.D. Thesis, Department of Ceramics, University of Leeds, 1978

APPENDIX 1

Dynamic Characteristics of Real Materials

Elastic moduli can be determined to an accuracy of 0.1% or better by resonant frequency measurements. The resulting adiabatic values are related to the isothermal moduli, determined in static tests, by a theoretical equation which shows that isothermal moduli should be the smaller, typically by approx. 0.3%, depending on the material. In practice the experimental error in static determinations is usually greater than 1% and sometimes static elastic moduli are determined in a manner which permits plastic strain to be included; the resulting low values should not be considered true elastic moduli.

In a perfectly elastic material, i.e. a Hookean solid, stress is strictly proportional to strain and in cyclic stressing there is no energy loss. In all real materials, however, strains are found to be accompanied by the loss of some energy in the form of heat. Therefore the ratio of stress to strain under isothermal conditions (E_i) will not be the same as under adiabatic conditions (E_a). This difference was shown by Kelvin, and is given by:

$$\frac{E_a}{E_i} = \frac{1}{1-E_i\,\alpha^2} \cdot \frac{T}{\rho s}$$

where α, ρ, s and T are, respectively, the coefficient of linear expansion, the density, the specific heat, and the absolute temperature.

In fact real materials show a greater difference between E_a and E_i than can be explained by Kelvin's equation, and it is necessary to invoke the occurrence of heat generating processes other than adiabatic compression and expansion. Such processes are irreversible "frictional" effects. The presence of frictional effects implies that where a material is subject to time dependent stressing, the strain will lag behind the applied stress. In the particular case where the stress is applied

sinusoidally, the strain will lag the stress by a constant angle θ.

This situation can be described mathematically with the aid of a complex compliance, $\underline{K} = K_o e^{-j\theta}$.

Using $\underline{K}$, we have $\underline{\sigma} = \sigma_o e^{jwt}$

$$\underline{\varepsilon} = \underline{K}\,\underline{\sigma}$$

$$\therefore \quad \underline{\varepsilon} = K_o \sigma_o e^{j(wt - \theta)}$$

Consider a stress σ applied longitudinally to a bar of length 'l', and c.s.a. 'a'. If the stress σ produces an elongation 'x', then the work done:

$$wd = \sigma.a.x.$$

$$\therefore \quad dw = \sigma.a.dx.$$

$$= \sigma.a.l.\frac{dx}{l}$$

$$\therefore \quad dw = \sigma.v.d\,\varepsilon.$$

$$\therefore \quad \frac{dw}{v} = \sigma.d\,\varepsilon.$$

If: $\sigma = \sigma_o \sin wt$

$$\varepsilon = \varepsilon_o \sin (wt - \theta)$$

$$\therefore \quad d\varepsilon = w\varepsilon_o \cos (wt - \theta)\,dt$$

$$\therefore \quad \frac{dw}{v} = \sigma_o w \varepsilon_o \sin wt \cos (wt - \theta)\,dt$$

$$\int \frac{dw}{v} = \sigma_o w \varepsilon_o \int_o^T \sin wt\,(\cos wt \cos\theta + \sin wt \sin\theta)dt$$

$$= \sigma_o w \varepsilon_o \left[\int_o^T \cos\theta . \tfrac{1}{2} \sin 2wt.dt + \int_o^T \sin\theta \sin^2 wt.dt \right]$$

$$= \sigma_o w \varepsilon_o \sin\theta \int_o^T \tfrac{1}{2}(1 - \cos 2wt)dt$$

$$= \tfrac{1}{2}\sigma_o w \varepsilon_o \sin\theta . T$$

$\therefore$ Energy loss per unit volume in 1 cycle, E =

$$\tfrac{1}{2}\sigma_o w \varepsilon_o \sin\theta . \frac{2\pi}{w}$$

$$\therefore \quad \underline{E = K\sigma_o^{\,2} \pi \sin\theta .}$$

If energy dissipation is occurring in a system then $\theta \neq 0$, and the situation can be described with the aid of $\underline{K}$.

Consider the longitudinal forced vibration of a rod of length 'l', clamped at one end.

If the rod were perfectly elastic it would have a natural fundamental angular frequency w_o, given by:

$$w_o = \frac{\pi c}{2l}$$

where c is the velocity of longitudinal waves in the material. For a perfectly elastic material, $c^2 = \frac{1}{K\rho}$, and for a material characterised by $\underline{K}$,

$$\underline{c}^2 = \frac{1}{\underline{K}\rho} = \frac{1}{K_o \rho} e^{j\theta}$$

$$\therefore \qquad \underline{w_o} = \frac{\pi}{2l} \cdot \underline{c} = w_o e^{\frac{1}{2}j\theta} .$$

It can be shown that the "amplitude per unit stress", A_w, at the free end is given by:

$$A_w = \frac{c\,\underline{K}}{w} \tan . \frac{wl}{\underline{c}} = \frac{c\,\underline{K}}{w} \tan . \left[\frac{\pi}{2} \cdot \frac{w}{\underline{w_o}} \right]$$

Note: that for w close to w_o, i.e. close to the resonance condition for materials exhibiting a small loss:

$$A_w \doteq \frac{c\,\underline{K}}{w} \left[\frac{\pi}{2} \left(1 - \frac{w}{\underline{w_o}}\right) \right] \cdots 1$$

$$= \frac{1}{\rho w l} \cdot \frac{1}{\underline{w_o} - w}$$

If $\underline{w_o} = w_r + jw_i$

Then $A_w = \frac{1}{\rho w l} \frac{1}{(w_r - w) + j w_i}$

$$= \frac{1}{\rho w l} \frac{(w_r - w) - j w_i}{(w_r - w)^2 + w_i^2}$$

and $/A_w/^2 = \frac{1}{(\rho w l)^2} \frac{1}{(w_r - w)^2 + w_i^2}$

The rod will go into resonance at $w = w_r$,

when $/A_M/^2 = \frac{1}{(\rho w l)^2} \frac{1}{w_i^2}$

Experimentally one observes $\frac{/A_M/^2}{/A_w/^2}$ at w values close to w_r, and it is convenient to observe values of w when the ratio is 2.

$$\frac{/A_M/^2}{/A_w/^2} = \frac{(w_r - w)^2 + w_i^2}{w_i^2}$$

which = 2, when $w = w_r \pm w_i$

Hence a measurement of the bandwidth Δw, when $\frac{/A_M/^2}{/A_w/^2}$

gives $\frac{\Delta w}{w_r} = \frac{2w_i}{w_r} = 2 \tan \frac{\theta}{2}$

which approximates to θ.

APPENDIX 2

Theory of Electrostatic Drive and Detection

The two electrodes incorporated in the specimen mounting rig are biased with a positive voltage w.r.t. earth; this bias voltage is usually of the order of 300V. This produces an electrostatic field which exerts a pull on the ends of the earthed specimen. The voltage from the drive amplifier is fed to the driver electrode so that an alternating pull, at the oscillator frequency, is exerted on that end of the specimen. The detector electrode together with the earthed end-face of the specimen acts as a capacitor microphone, so that at the resonant frequency a small alternating voltage will be produced across this capacitor.

Factors Affecting Sensitivity

a) End-face Displacement Amplitude

The displacement amplitude (A) of the end-face of a supported bar subjected to a simusoidally varying attractive force of given magnitude and frequency depends directly on the length of the bar (L), its resonance magnification factor (Q), and inversely on Young's modulus (E), and the square of the order of the harmonic generated (N).

$$A = \frac{\xi V_1^2 LQ}{2\pi^2 N^2 d_1^2 E}$$

where $\xi = 8.85 \times 10^{-12}$ Fm^{-1}. The force of attraction on the end-face depends on the square of the applied field, i.e. on $\frac{V_1^2}{d_1}$, where V_1 is the driving voltage, and d_1 is the spacing between electrode and specimen end.

b) Output Voltage

The voltage (V) appearing at the output electrode depends on the magnitude of the applied bias voltage (V_o) and on the ratio of displacement amplitude to mean electrode spacing, i.e. $\frac{A}{d_2}$.

$$\text{and } V = \frac{\mathcal{E}}{2\pi^2} \cdot \left(\frac{V_1}{d_1}\right)^2 \frac{L.Q}{E.N^2} \frac{V_o}{d_2}$$

Sources of Error

a) $E = 4 \times 10^{-3}\, n^2 l^2 \rho \ \text{Nm}^{-2}$.

The above formula is only correct for long thin wires. Correction factors have been tabulated by Bancroft, but these factors are very small and can be ignored for all practical purposes.

b) Clamping pressure on the specimen has no effect.

c) Small displacements in the centre clamping have no significant effect, approximately 1 part in 20,000 for a displacement of 2×10^{-3}m.

d) Effects of the silver coating are so small that they can be ignored.

e) The main source of error lies in the determination of density.

Calibration of Apparatus

Results obtained from the "electrostatic" apparatus were checked by using "standards" of perspex and fully-dense alumina. The longitudinal resonant frequency of the "standards" had previously been determined at The British Ceramic Research Association, Stoke-on-Trent.

APPENDIX 3

Relationship between volume fractions of silicon nitride, silicon and porosity with green and nitrided densities.

ρ_g = initial green compact density

ρ_n = nitrided density

V = compact volume

$(M_{Si})_o$ = original silicon mass

ΔM = mass of original silicon converted to nitride

ρ_{Si} = 2330 kg m^{-3}

ρ_{SN} = 3200 kg m^{-3}.

A green density of 1500 kg m^{-3} yields a nitrided density of 2500 kg m^{-3} on conversion of 100%.

$$\therefore \quad \frac{M_{Si}}{V} = \frac{3}{5}\frac{M_{SN}}{V}$$

$$\therefore \quad M_{SN} = \frac{5}{3} M_{Si}$$

At any stage of conversion:

$$\rho_n = \left[\frac{(M_{Si})_o - \Delta M + 5/3\Delta M}{V}\right] = \frac{(M_{Si})_o + 2/3\,\Delta M}{V}$$

$$\therefore \quad \rho_n = \rho_g + \frac{2/3\Delta M}{V}$$

$$\therefore \quad \Delta M = 3/2(\rho_n - \rho_g)V \qquad \ldots\ldots\ldots (1)$$

Initial porosity volume $(V_p)_o = V - (V_{Si})_o$

$$\therefore \quad \frac{(V_p)_o}{V} = 1 - \frac{(V_{Si})_o}{V}$$

$$= 1 - \frac{(M_{Si})_o\,\rho_g}{\rho_{Si}(M_{Si})_o}$$

$$\therefore \quad (V_p)_o = V\left(1 - \frac{\rho_g}{\rho_{Si}}\right)$$

Intermediate porosity $V_p = (V_p)_o$ + vol. of Si converted to SN − vol. of SN.

$$\therefore\ V_p = (V_p)_o + \frac{\Delta M}{\rho_{Si}} - 1.23\ \frac{\Delta M}{\rho_{Si}}$$

where the volume expansion on converting Si to SN is assumed to be 23%.

$$\therefore\ V_p = (V_p)_o - 0.23\ \frac{\Delta M}{\rho_{Si}}$$

$$\therefore\ V_p = V(1 - \frac{\rho_g}{\rho_{Si}}) - 0.23\ \frac{\Delta M}{\rho_{Si}}$$

$$\therefore\ \frac{V_p}{V} = (1 - \frac{\rho_g}{\rho_{Si}}) - 0.23\ \frac{\Delta M}{\rho_{Si} V}$$

From (1) $\frac{\Delta M}{V} = \frac{3}{2}(\rho_n - \rho_g)$

$$\therefore\ \frac{V_p}{V} = 1 - \frac{\rho_g}{\rho_{Si}} - 0.23 \cdot \frac{3}{2} \cdot \frac{\rho_n - \rho_g}{\rho_{Si}}$$

$$\therefore\ \frac{V_p}{V} = 1 - 0.281\ \rho_g - 0.148\ \rho_n$$

$\therefore$ Intermediate porosity concentration $\underline{C_p = 1 - 0.281\ \rho_g - 0.148\ \rho_n}$

Intermediate Si volume, $V_{Si} = (V_{Si})_o - \frac{\Delta M}{\rho_{Si}}$

$$= \frac{(M_{Si})_o}{\rho_{Si}} - \frac{\Delta M}{\rho_{Si}}$$

$$= \frac{\rho_g \cdot V}{\rho_{Si}} - \frac{\Delta M}{\rho_{Si}}$$

$$\therefore\ \frac{V_{Si}}{V} = \frac{\rho_g}{\rho_{Si}} - \frac{1}{\rho_{Si}} \cdot \frac{\Delta M}{V}$$

$$= \frac{\rho_g}{\rho_{Si}} - \frac{1}{\rho_{Si}} \cdot \frac{3}{2}(\rho_n - \rho_g)$$

$$\therefore C_{Si} = \frac{5\rho_g - 3\rho_n}{2\rho_{Si}}$$

$$\underline{C_{Si} = 1.070\rho_g - 0.643\rho_n.}$$

Intermediate SN volume concentration $C_{SN} = 1 - C_{Si} - C_p$

$$\therefore \underline{C_{SN} = 0.791(\rho_n - \rho_g).}$$

APPENDIX 4

Scanning electron micrographs of spherical Monsanto silicon nitrided in nitrogen at 50 torr and 1370°C.

Particle size, 53 - 65 μm.

a) 10 minutes. Silicon network formation and thermal etching characteristics.

b) 20 minutes. Silicon network formation and grain boundary reaction product.

c) As in (b).

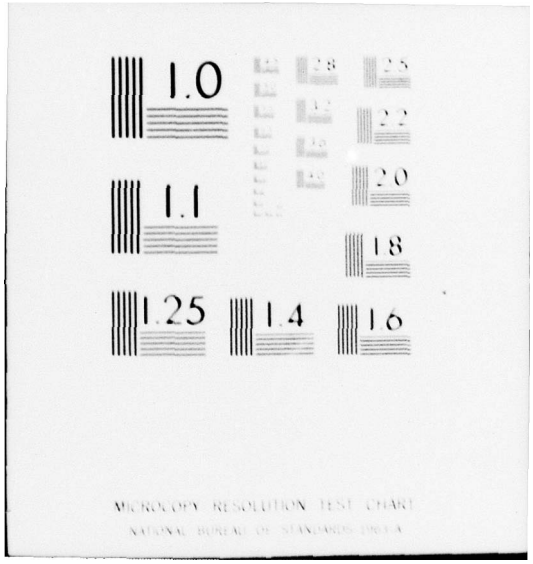
AD-A057 559 HOULDSWORTH SCHOOL OF APPLIED SCIENCE LEEDS (ENGLAND)--ETC F/G 11/2
THE DEVELOPMENT OF THE MECHANICAL STRENGTH OF REACTION-BONDED S--ETC(U)
APR 78 A J MOULSON, P LONGLAND DA-ERO-75-G-078

UNCLASSIFIED NL

3 OF 3
AD
A057 559



END
DATE FILMED
9-78
DDC


1.0
1.1
1.25
1.4
1.6
2.2
2.0
1.8
MICROCOPY RESOLUTION TEST CHART
NATIONAL BUREAU OF STANDARDS 1963-A



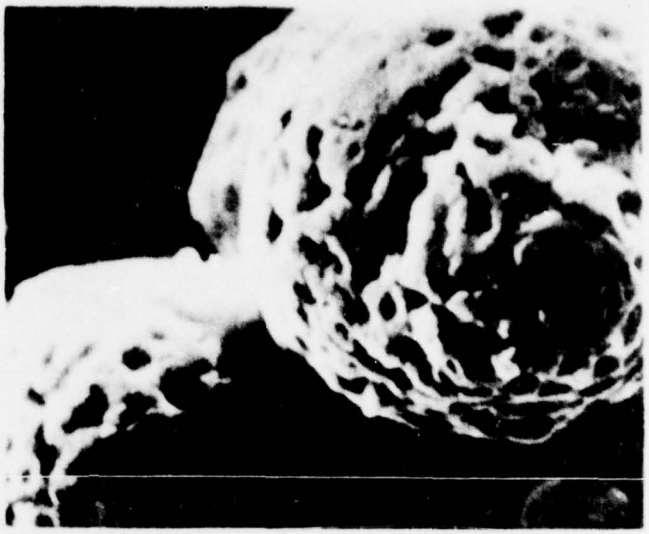




d) 20 minutes. Neck formation and pitting of silicon surface.

e) 45 minutes. Inhomogeneous microstructure over a small area of the sample.

f) 45 minutes. Exudations from silicon.







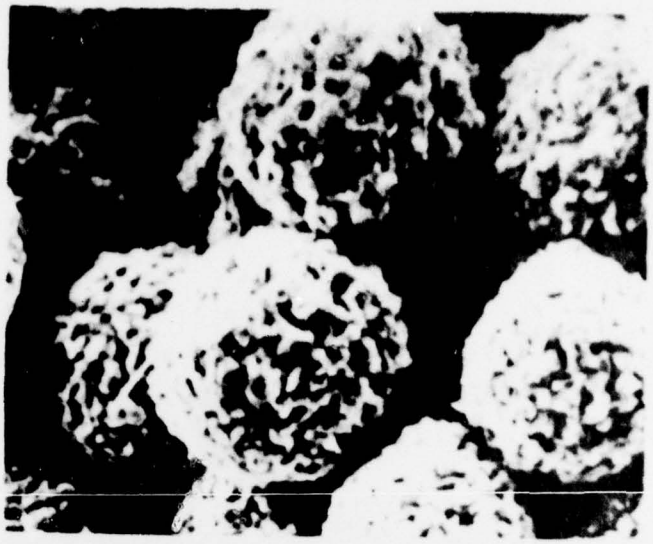
g) 4 hours. Nitride morphology.

h) As (g).

i) 4 hours. Two types of reaction product:

(a) Translucent material

(b) "Chunky" deposits.







j) 15 minutes. Aluminium contaminated region. Note whisker morphology and lack of silicon network.

k) As (j).



